Università degli Studi di Palermo

AREA QUALITÀ, PROGRAMMAZIONE
E SUPPORTO STRATEGICO
SETTORE STRATEGIA PER LA RICERCA
U. O. DOTTORATI

Doctoral Course in Civil, Environmental and Materials Engineering
Department of Engineering
ICAR/08

AN INNOVATIVE MOMENT RESISTING STEEL CONNECTION: OPTIMAL DESIGN FORMULATIONS, PRACTICAL APPLICATIONS AND EXPERIMENTAL TESTS

PhD Candidate
Santo Vazzano

Coordinator
Prof. Antonina Pirrotta

Supervisor
Prof. Luigi Palizzolo

CICLO XXXIV
A.A. 2021/2022

INDEX

INTRODUCTION

Earthquakes, such as those in Mexico City (1985), Northridge (1994), and Kobe (1994), have firmly tested civil buildings and infrastructures' safety and performances. Each event, characterized by unique forces and unpredictable levels of ground acceleration, which are dependent upon the type of soil and on the type of structures, is an indicator of the critical aspects of structural design in use. By examining the consequences of these earthquakes on buildings, case by case, the specific issues in their design have been discovered, and by observing these effects many lessons can be learnt.

Focussing, specifically on the Northridge earthquake, in 1994, the catastrophic consequences provoked a change in building codes and civil engineering standards. During this event many steel structures experienced an unexpected problem. The connections between these structures were mainly formed by welding the wings and the web of the I-shaped beam elements constituting the frames directly to the columns. In some other cases, the connections consisted of a mix of bolted joints (only the web or only the wings) and welded parts. Following this event, many buildings developed fractures within the joints, making them unusable and economically disadvantageous to repair. To fix the problem, the international technical codes introduced a series of prescriptions, belonging to the wider field of capacity design, to protect the connections as crucial elements of the structures. For instance, the codes allow the designer to adopt the strategy of reducing the strength of a specific beam portion just before its coupling with the column. The goal is to allow the onset of plastic deformations outside the joints, and preferably at the ends of the beam elements rather than in the columns.

A commonly adopted strategy that follows this idea is the “dogbone”, introduced in the last decade of 20th-century. The dogbone joint reduces the strength of a specific beam portion by cutting off part of the wings. This cut can take different shapes, but the most common is the parabolic cut. This strategy is relatively simple to adopt and to design, since it can be implemented during the manufacturing phase without involving other more complex strategies or precautionary actions.

This simple cut removes a significant portion of the wings, resulting in a decrease in the beam's flexural stiffness. This means that the strength reduction and the stiffness loss are strictly related to each other. One of the topics that will be discussed is the possibility of independently designing and fixing these two quantities within the same beam element.

Furthermore, this device can be used in cases involving the creation of a breach in historical masonry walls. In this case, technical codes usually prescribe using only the in-plane stiffness of the involved elements as a parameter to evaluate the efficacy of the operation. Therefore, the stiffness of the opened panel, which is now equipped with the steel frames, can be maintained at the same level as with the panel one in its pre-intervention condition. In this way, the prescriptions set out in the building codes are satisfied. In this way, however, the significant increment of the global resistance incurred as a consequence of the panel-frame coupling is not considered. In such a situation, it could be helpful to separately, and independently, design elements with a specific strength and stiffness. This feature cannot commonly be realised with standard design techniques and standard steel frames.

The thesis focuses on the investigation of an innovative steel connection device with unique kinematical and mechanical characteristics.

The proposed device is known as the *Limited Resistance Plastic Device* (LRPD); it is composed of three consecutive I-shaped portions, which are symmetrical on three orthogonal planes, where the thickness of the external portions is greater than that of the inner one. These devices are embedded within two end-plates that serve as interface links with the beam on one side and the column on the other.

The good functioning of this device is based on its design phase, which is developed by means of a suitably defined optimization problem, as will be explained in detail in the following chapters. The solution of this problem is accomplished through the use of nonlinear programming algorithms, which rely on the search for the minimum value of a pre-assigned objective function while guaranteeing a series of boundaries/constraints which are chosen to obtain desired features from the resulting device (such as the limit resistance or the flexural stiffness). All of the aspects regarding the optimal problem for designing the proposed device will be deeply analysed in subsequent chapters.

In literature other solutions and techniques have been proposed in recent decades, and some of the most significant and well known will also be briefly discussed in the subwequent chapters. The main point of reference, however, will be the dogbone, which represents the principal competitor to the proposed device. Many comparisons between the structural performances of the dogbone and the proposed LRPD will be performed and analysed as the thesis progresses.

The goal of the research presented in this doctoral thesis is to study the reliability and usability of the proposed device by enhancing the theoretical model and validating it by numerical and experimental tests. This was accomplished first through an extensive simulation campaign using the finite element method (FEM), as well as through an evolution of the optimal

problem in which various improvements were proposed to account for specific aspects of the device's structural performance.

Finally, an experimental campaign was carried out to obtain preliminary results which will allow the validation of the analytical model. The obtained results confirmed the LRPDs expected behaviour, demonstrating its dependability and efficacy.

This thesis will demonstrate that the LRPD can be a reliable solution in place of other reduced beam section (RBS) techniques, as well as in situations where the flexural stiffness and limit strength must be independently fixed. The future developments section of the thesis will focus on the technological aspects that have not been addressed in the text and on the expansion of the experimental campaign along with improvements which could be made to the experimental model.

CHAPTER 1 – MRFS AND CONNECTIONS

Since the late 19th century and, more significantly, throughout the 20th century, steel-framed structures have significantly contributed to the advancement and the enhancement of structural design and, more generally, the field of civile engineering. Thanks to their great reliability, the performance expected from buildings and infrastructure assets progressively increased, leading to higher safety levels for the structures as technological progress moved forward.

The most common type of steel structure is constituted of steel frames in which the constituent beam elements are characterized by low thickness cross-sections in various shapes. The aforementioned features permit good structural behaviour to be obtained for assets with relatively low weights, at the price of more flexible and deformable structures.

Different national and international standards regulate the design and the safety checks for these structures, more specifically, some are devoted to the connections between the steel elements. These connections, as mentioned, represent a central element for the structural performance. Their duty consists of acting as link between the different monodimensional elements (beams and columns), and hence, they must be capable of transmitting forces and displacements/rotations with the desired degree of constraint.

While in reinforced concrete structures the joints of the structure are commonly schematized as fully restrained, in steel-framed structure there is a huge variability in the characterisation of the joints connection type in their static models, making these joints an important matter to consider. In order to understand if it is possible to adopt a simple hinge-type connection, or a restrained-type connection, some consideration must be aimed at the understanding of the transmission of the vertical and of the lateral loads.

Regarding the lateral loads, in particular, it is necessary to identify the parts of the structure devoted to transmitting these loads to the ground.

This is important because this choice has an impact on the costs, on the design efforts and on the spatial results. For example, in terms of costs, for steel buildings often it is convenient to equip the frames with braces, but this can negatively impact the space inside the frame, causing obstructions. This impact may be undesirable also due to the resulting effect on the appearance of the building. Even though, it remains a valid technique considering the efficacy on reducing the lateral displacements and improving the seismic response. In addition, with lateral bracing systems it is also possible to have lighter beams and columns, due to the decrease of the internal forces thanks to the tie-rod effect. Putting it in terms of connections, a lateral braced system can have less limiting connections, for example, the tie itself is usually pinned to the joints. The columns and the beams can also have different static schemes.

The most common case is that of portal framed strctures which are single storey industrial facilities. In this case the space inside is totally free of any obstructions and can be used for the purpose the structure was made. The disadvantage of this design is that beam elements must be stronger. This has clear consequences also on the connections, where a lot of attention must be paid in order to avoid unstable static systems. Indeed, in this case, the connections must guarantee higher performances, and, thusly, their realization will be more complex and expensive. In addition, lateral displacements are limited only by the flexural stiffness of the columns (and partially by the degree of constraint represented by the beams connected).

Also, the type of connection to the base foundation has an influence on the structure. Pinned base columns are useful (and in some cases mandatory) when the ground is not consistent or is characterized by low mechanical

properties. Fully restrained base columns, on the other hand, may require bigger, more expensive foundations.

Hence, as stated above, this choice made in the design phase, is crucial to ensure a favourable outcome from the process, and strongly influences the activity of designing the connections.

Regarding connections, it has been underlined that they strongly influence the response of the frame where they are placed, and, consequently the response of the whole structure. A simplified way of seeing a common connection in steel structures is as a hinge equipped with a spring, therefore exhibiting a rotational stiffness.

Clearly, this is just an idealization, in reality these connections are more complex and depend upon a huge number of factors. It is, however, a good approximation and can be adopted to better understand the influence of the connection on the general frame's behaviour. The European technical code[1] contains a simplified method to calculate the rigidity of the simplified rotational spring which idealizes the connection. In this way the coherence of the design can be ensured with the selected connections.

In the present work, as the title suggests, the moment resisting frames (MRF) and their connections are the primary focus. Contrary to what has been previously stated, a moment resisting frame is constituted of beam elements which are rigidly connected to each other. Mechanically this means that the actions are fully transmitted throughout the elements. Kinematically it means that the relative rotations and displacements in the same elements are forbidden.

In conclusion, it appears clear that the choice of the type of connection is not only a technological and manufacturing matter, but also, fundamentally, a design issue that must be considered since the very first idealization process.

[1] EN 1993-1-8:2006, Eurocode 3: Design of Steel Structures Part 1-8: Design of Joints, 2006.

In the following section a brief report of the main aspects of interest for this work will be presented.

1.1 - Steel connections

As discussed, in steel structures the connections have a crucial role in the stability and in the structural integrity of the entire building. They represent the most delicate, and from a certain point of view, the most 'fragile' part of the whole structural system.

There are different types of connections, and they can be distinguished depending on their kinematical and mechanical behaviour, as well as on their type of union. One distinguishing factor can be found in their rotational stiffness: indeed it is possible to distinguish hinge-type joints (like pins), rigid joints (totally fixed), and semi-rigid joints (which present an intermediate behaviour between the other two). Of course, as a consequence of their rotational features, the bending moment transmission throughout the frame is also influenced, permitting the partial-strength capacity or full-strength capacity to be distinguished, depending on which portion of the forces they are able to transmit. In terms of the technology adopted to join the different parts, the connections can be classified in two main categories: bolted joints or welded joints. The welded connections (Figure 1.1), normally, behave similarly to a rigid joint, i.e. more closely to a classical fully restrained end.

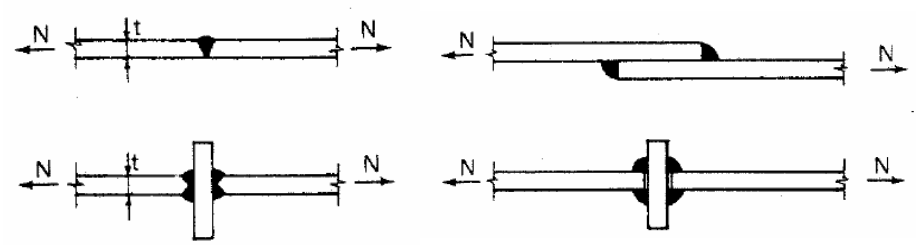

a)


b)

Figure 1.1 – Welded connections; a) Different type of welded union; b) Examples of reticular welded beams.

This type of connection permits an almost complete spreading of the internal forces between the connected elements, avoiding at the same time the presence of relative displacements or rotations. Aside from the good mechanical and kinematical performance, this type of connection requires a specialized manpower for their production, a lot of on-site checks, and consequently they are usually more expensive and burdensome than bolted connections.

Bolted connections (Figure 1.2), on the contrary, show an easier assembly and behave more similarly to an hinge, and therefore they transmit only limited forces allowing relative rotations.

Figure 1.2 – Different types of bolted beam-column connections.

The connections also serve to spread and transmit the forces that develop from the loads, through the ground and, depending on their type and on their geometry, the quantity of the forces transmitted can vary widely. At this juncture, it is useful to provide an example: a hinge-type geometry (typically a poor bolted connection, without weldings) is not indicated as a good choice in situations where it is useful to transmit bending moment. Furthermore, it should be noted that a simple support would never transmit any horizontal forces between the resting and the supporting elements. As stated, the type of connection has a strong influence on the stiffness of the union. These different levels of constraint can be expressed by means of a moment-rotation graph (Figure 1.3).

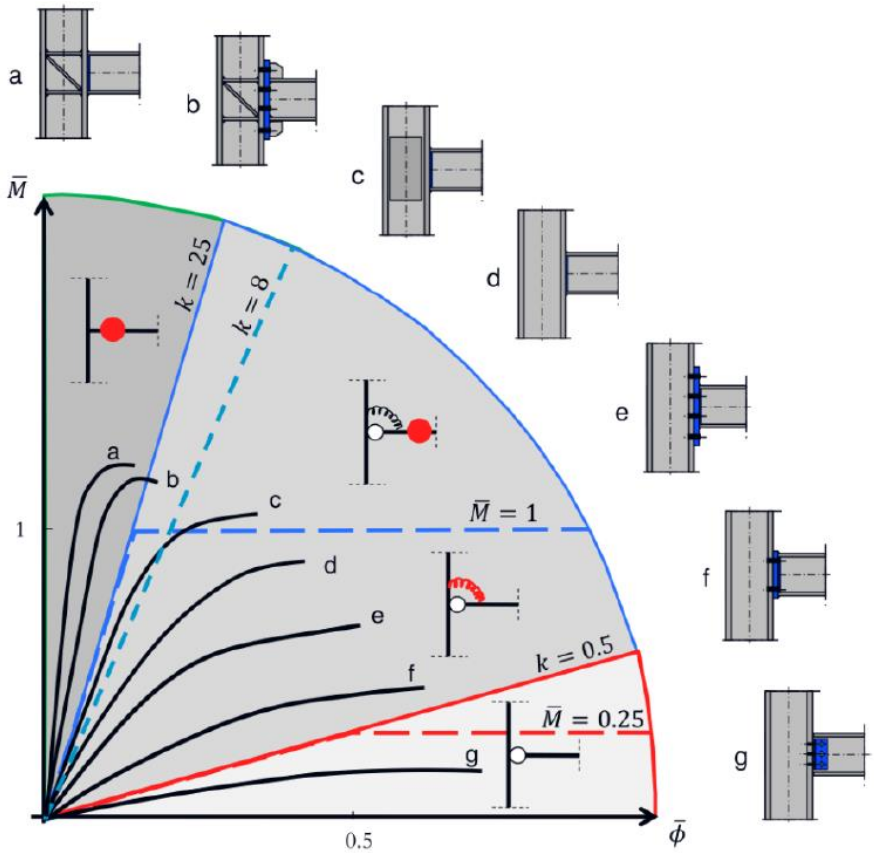

Figure 1.3 – Bending moment – rotation curves for different type of connections.

By observing the ratio between the bending moment and the rotation, it is easy to understand the physical meaning of the flexural stiffness indicator represented by the graph reported above: the greater this ratio, the stiffer the connection. Bolted unions, such as the case in diagrams “e-f-g”, show a low linear branch characterized by a slight inclination, proportional to how poorly constrained the ending plate of the beam is. On the contrary, the linear branch slope of connections “a-b-c-d-e” are more pronounced, and the flexural stiffnessindicator depends on how much the joint has been stiffened. The welding type itself represents a less deformable connection, but in addition it can be equipped with a web stiffener, or additional tissues, or extended ending flanges, which add more degrees of constraints and thus more

stiffness to the whole joint. As is visible, these features deeply influence the limit resistance of the connection, permitting its strength capacity to be fully expressed only in cases “a” to “d”.

The resistance of the joint also depends on the type of union chosen and on the connecting elements. Of course, the material plays an important role, and for this reason the elastic modulus of the connecting elements and the yield stress of the material are usually greater than in those which are commonly adopted for beam elements and for plates. The capacity of the connection, in general terms, can be defined as the capacity of the weaker elements that hold togheter the coupled elements. Thus, by identifying the capacity of all the connecting elements it is easy to identify what is the exact capacity of the connection.

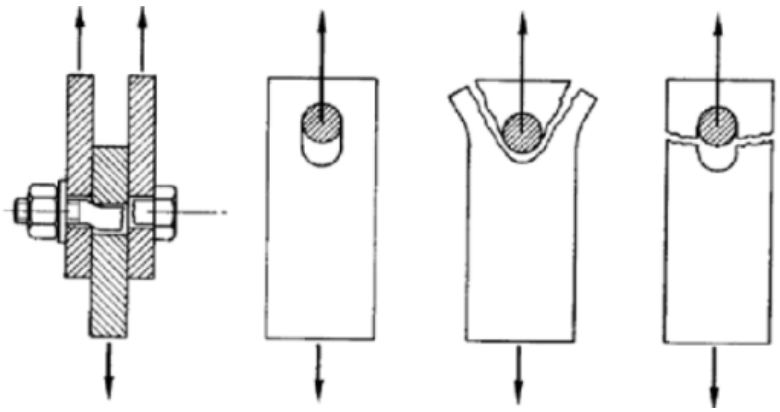

Figure 1.4 – Example of failure mechanism for bolted joined plates.

Again considering a simple example, Figure 1.4 shows three plates which are joined using a bolt, which is composed of a screw head, a screw, and a closing nut. The connection is subjected only to axial force (of traction in this case), therefore, other load conditions can be neglected. To evaluate the capacity of the joint, depending on the considered mechanism, different portions of the connection can be involved in the rupture. In the case reported in Figure 1.4, the ruptures are (from left to right): the shear collapse of the

screw, the bearing failure of the plate, the shearout failure of the longitudinal portion of the plate, and the net shear failure of the transversal portion of the plate. Therefore, to determine the capacity following the previously discussed definition, it is sufficient to calculate the limit resistance for all the possible mechanisms and identify the lowest among them.

To briefly conclude, in this section the role and the importance of the connection has been underlined in order to create a background to the considerations which the proposed device will address.

1.2 - Steel frames with masonry

Masonry buildings constitute a large part of existing real estate assets. This has lead generations of engineers to ask themselves how to maintain these kind of properties and how to prevent them from collapsing in the case of rare events, such as earthquakes. These events can compromise the safety of the occupants and the funcionality of the structure. This last aspect, in particular, is crucial for buildings of high strategic importance such as hospitals, schools, government facilities and so on. In this case the masonry structure is not only required to be highly stable for its own sake, but also as a result of its importance, to fulfill essential social functions.

A large part of the real estate assets is composed of unreinforced masonry buildings, where, as the name suggests, the whole structure is constituted of brick walls, and the loads acting upon it are supported entirely by these bidimensional elements. The adjective “unreinforced” suggests that the walls are not supported by other elements, like single beams or frames made of concrete or steel. These elements are only present in reinforced masonry buildings, where their incorporation helps the whole system to withstand forcing actions (whether typical or rare) that occur during its service life.

In some real cases, like for renovation/reorganization of the original blueprint of a masonry structure, it can be necessary to open a breach in an existing wall. This action influences the static configuration of the building. In other words, this breach creates a variation on the original stiffness and on the strength of the structural system.

When the dimensions of the breach are limited, or the building is located in a low seismic area (and thus the seismic actions can be neglected from considerations on the safety of the structure), this variation can be ignored from a static point of view. In other cases, like for structures in seismic areas or for large openings, the loss of strength and stiffness caused by the removal

of a portion of a wall can significantly influence the global behaviour of the building due to the redistribution of the loads that happens when some part of a compressed element it is excised.

The technical codes prescribe some specific strategies to limit this issue such as the incorporation of a frame inside the breach which is bound to the rest of the panel through the use of specific anchoring systems (Figure 1.5).

Figure 1.5 – Typical breach opening intervention with steel frames.

Also, the codes refer to the panel's lateral stiffness as a parameter to take into account while fulfilling this requirement. The stiffness is evaluated before and after the opening is made, and of course it will have significantly different values. This variation, potentially, can have a negative influence on the behaviour of other parts of the structure, and can force the designer to reconsider the safety of the whole building.

Given that the dimensions of the frame are determined by the design of the opening, the only aspect to control in order to modify the stiffness of the opened panel is the choice of the beam element's cross-sections. These must be chosen in order to balance, within a specific tolerance of aproximately 10 -

15%, of the original stiffness of the panel prior to the intervention. However, adopting this strategy, even if in terms of stiffness the behaviour of the elements pre/after intervention is almost unchanged, a huge increase in the limit resistance of the element could be caused, along with a non-negligible alteration of the initial static scheme. The difference mentioned can be observed in Figure 1.6.

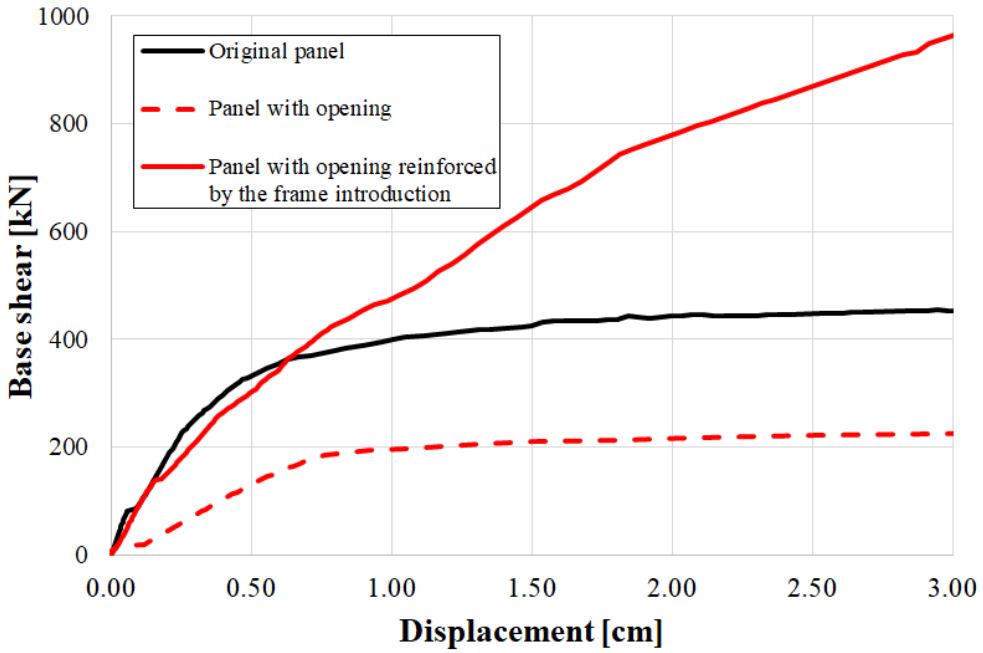

Figure 1.6 – Example of stiffness and strength variation of a masonry panel before and after an opening.

In this figure it can be noted that the stiffness of the opened panel equipped with the reinforcing frame recreates, with good approximation, the stiffness of the original panel, but significantly increases its limit strength. In addition, in the same graph, it is also clear that the opened panel with no reinforcement shows a huge lack both of stiffness and strength compared to the original panel.

As stated, these differences can lead to a variation of the global behaviour in terms of safety and in terms of collapse mechanisms, which must be

reconsidered after the realization of the opening. Usually this does not represent a big problem, but in extreme cases or for some particularly onerous architectural necessity, this can represent a limitation, because it is not always possible to fulfill the safety requirements after modifying the original structure.

When possible, in these cases, it is recommended to operate on a local level, trying to avoid alteration of the preconstituted structural scheme by limiting not only the stiffness variation, but also the limit resistance. This last aspect represents a case in which the incorporation of an LRPD could be a useful addition to the steel fram and will be discussed in the upcoming sections. In particular the problem will be simplified by considering the whole substitution of the panel with an equivalent steel frame equipped with specific devices, instead of considering the interaction between the frame/residual masonry portion. Research into this aspect will be the object of further studies.

1.3 - Codes

The principles previously discussed derive from theoretical assumptions that are transformed into methods and technical prescriptions to be followed in the design and construction of buildings of civil national heritage. The goal is to guarantee an adequate level of safety for human life and to standardise, as much as possible, international techincal codes and over-.national organizations (Eurocodes, FEMA, guidelines etc.).

Most of these codes, which regulate the structural design of civil assets, prescribe the methodology to conduct the assessment of different loading conditions and, afterward, different limit behaviours to be imposed to the structural elements. Usually, two main conditions can be identified: serviceability and ultimate condition. The first condition is characterized by a quasi-static type loads (like gravitional loads and wind forces, as well as low seismic intensity loads); on the other hand, the ultimate condition is the expected state of the building following loading from full intensity seisic actions. Furthermore, the codes prescribe that for serviceability conditions structures must exhibit an elastic or a shakedown behaviour, and that under limit conditions the asset will not collapse or suffer from significant, irreversible damage.

The magnitude of the forcing action considered for each structure is variable, and it depends on the importance that the relevant structure is seen to possesses. As such, high forces are considered in the analysis of essential structures, and lower ones for more common civil buildings. A practical consequence of this is that, for example, generally an hospital will be designed to withstand an earthquake with high energy content (e.g. higher than 7-8 magnitude), while a mono-family house will accept a significant amount of damage during the same event. These smaller buildings, however, are still expected to conform minimum requirements for the preservation of

human life, resisting the event at least long enough to allow the safe evacuation of the occupants.

Modern technical structural codes are based on semi-probabilistic methods. In these methods some quantities are considered “deterministic” while others are considered to be “stochastic”. It is clear that in the first case an approximation is made. This simplification is necessary due to the complexity of modelling reality. For random parameters, the magnitudes of the loads can be evaluated and discussed by utilizing methods from probabilistic calculus.

With regards to seismic actions, in order to have relatively cheap structures which also meet the prerequisite level of safety discussed, a techinque suggested is to make the structures “dissipative” by means of specific construction techniques and dimensioning of specific elements. By doing this engineers and designers are permitted to consider lower input seismic forces in their analysis, allowing them to minimize the strucural mass of, and therefore the costs of, the building.

This complex system of techincal prescriptions is known as capacity design. Some examples of capacity design strategies are: an increase in the overlapping of steel bars in reinforced concrete structures, the study of the ductility features of the section, the presence of refined portions of beam stirrups, and so on. Other examples, generally, referred to as tridimensional frame structures, include the beam-column hierarchy, which is aimed at avoiding the brittle failure mechanism within the building such as the soft flor mechanism (Figure 1.7).

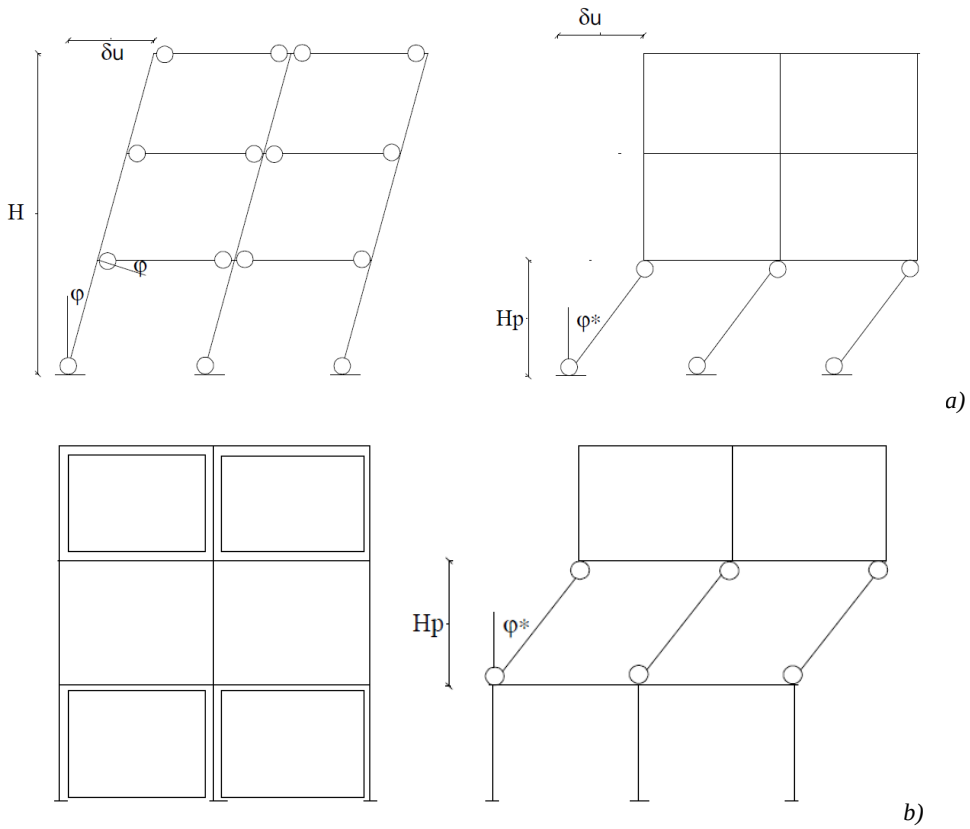

Figure 1.7 – Soft floor mechanisms; a) mechanism caused by weak beam-strong column hierarchy; b) mechanism caused by differential lateral stiffness of the different storeys.

As can be seen in the figure above, this mechanism can happen when the beams and columns in the strcture have similar strength properties. This causes the plastic hinges to develop, not only at the base of the column and at the ends of the beams, but also at the top of the column and in some cases these hinges will be located entirely on one floor. In this case due to the higher forces acting on the specific floor and due to this comparable strength the plasticization focuses on this single storey and cause its collapse (Figure 1.8).

Figure 1.8 – Soft floor mechanisms examples.

In some other cases the soft floor mechanism develops as a result of the variable lateral stiffness of the different structural levels, caused by different walls distribution/characteristic. This can potentially lead to the localized failure of the relevant storey.

The capacity design method addresses this issue by assigning an augmented strength to the columns through overdimensioning. Italian code[2] (Par. 7.5.4.2) suggests the following equation for the overdimensioning of these structural elements:

$$\sum M_{C,pl,Rd} \geq \gamma_{Rd} \cdot \sum M_{b,pl,Rd} \qquad (1)$$

where $M_{C,pl,Rd}$ and $M_{b,pl,Rd}$ are the column's and the beam's plastic bending moments respectively. $\sum M_{C,pl,Rd}$ represents the total sum of the plastic

[2] Norme tecniche per le costruzioni 2018 – Par. 7.5.4.2.

bending moments of all the columns that converge in the joint. Analogously, $\sum M_{b,pl,Rd}$ is the total sum of the plastic bending moments of all the beams that converge in the same joint. γ_{Rd} is a coefficient that depends on the desired ductility level and on the type of structure considered (in the range 1.1 - 1.6).

The regulations regarding the connections can be different depending on the type of structures and on the type of union. The codes contain a series of safety checks to be conducted on the joint in order to verify if it is able to withstand the forces considered during the design process. For instance, in steel structures, as discussed before, the connections have a non-negligible importance and influence on the overall behaviour and efficacy, and must possess adequate strength and suitable stiffness features. With regards to the bolted union, commonly, the checks consist of evaluating if the sum of the bolts can afford specific loading conditions (in terms of shear and axial forces), and also in evaluating if the joining plates are adequate to avoid unpredicted stamping or flexural issues. Regarding the capacity design regulations, for example, a prescription regards the strength of the connection. In this case, regardless of the type of connection, it is intuitive to think that commonly the weak point of a structure can be represented by the union itself, even though their sizing and the related safety controls are accomplished and regulated by means of suitable coefficients. This statement is particularly true when the safety check requirements are less strict, and substantially depends on the safety coefficients adopted while designing and verifying those elements. As is well known, these coefficients depend on a huge variety of factors and parameters which are strictly correlated to the type of elements joined to the material. In this regard, also in the Italian code cited before, a prescription is reported which is useful to quantify this safety gap through the following relation:

$$R_{j,d} \geq 1{,}1 \cdot \gamma_{ov} \cdot R_{pl,Rd} \qquad (2)$$

where $R_{j,d}$ represents the design capacity of the connection, $R_{pl,Rd}$ is the limit strength of the connected beam elements, and γ_{ov} is a factor that takes into account the material type. Through the fulfillment of this relation it is possible to assign a sufficient over-strength to the joint to avoid collapse. If failure occurs it will be located in the other connected elements (characterized by a more ductile behaviour), in place of the connection itself. The same can be said for the foundation attachment: the over-strength must always be assigned to the joint but in this case must be more resistant than the ground beam.

Regarding the reduced beam section (RBS), the Italian code does not present any references, and thus it is not a method/technique which is suggested to solve the issues discussed above. An example of a standard which regulates them is found in the American code[3]. This is owed to the significant consequences of the recent earthquakes which they have endured, and on the simplicity of using this techinque compared to others. In FEMA they are included in the category of prequalified connections. These connections must follow a series of geometrical rules and constraints that - if respected - allow the performances of the union to be known prior to conducting further analysis. The philosophy behind this strategy can appear similar to the Italian code, where a series of requirements must be followed in order to be in compliance with the law, but the rules to follow are strict and the general geometry is pre-assigned. These prescriptions, on the other hand, require a specific performance for the union, and the method used to ensure compliance is decided upon the designer. Hence, even if the RBS technique is not officially presented in the Italian regulations, it can be adopted if the

[3] FEMA-355D, State of the Art Report on Connection Performance. Par. 3.5.

performance requirements are fulfilled. In the following section some examples in which these principles are applied will be presented.

CHAPTER 2 – RBS in MRF state of art

The field of steel structural design hasn't experienced huge variations in the techniques or in the methodologies in recent decades. While it is true that the design approaches and the ideas behind the conception of the many international codes has been refreshed to adapt to the rare events that unavoidably arise over a structure's lifetime.

In the recent past, the Northridge (1994) and Kobe (1995) earthquakes revealed some critical aspects of steel frame structures, so much so that structures designed prior to 1994 are sometimes referred to as "pre-Northridge" in literature. During these events, a lot of buildings were subjected to several damages, mainly due to shortcomings in the codes in force during that period, such as the basic quality controls which were conducted and poor connection of the welding materials. In many cases the damage consisted of fractures along the weldings in the beam-to-column connections. If this type of flaw involves a large part of the joints which make up the building, the repair cost can be excessive, and the structure may be deomissioned.

These events taught structural designers an important lesson: structures should have an adequate strength, stiffness and ductility, considered at both the local level (the single section or connection) and on a global level (the whole structure). In this way it is possibile to guarantee the seismic performance to the building, and hence ensuring an acceptable level of damage.

Another good strategy, to obtain the desired behaviour in terms of global ductility and collapsing pattern, is to allow a specific portion of the structure to develop plastic deformations. Plastic phenomena unavoidably occur when a structure is subjected to limit conditions such as earthquakes and extreme accidents (explosions, impacts, etc.), hence, by identifying a-priori a specific

portion which will suffer from plastic deformations, the brittle mechanisms that can be harmful for occupants and for the dynamics of the building can be avoided. In the following section, some of the major techniques already present in literature will be reported, preparing the ground for the introduction of the LRPD. Some of these techinques will be discussed in greater detail than others, because of their different impacts on research and professional areas.

2.1 - Dogbone

The first technique analyzed in this chapter represents the most well-known and the most widely adopted around the world. It was proposed and tested in various scientific works including: Iwankiw and Carter (1996), Plumier (1997), Shen, (2000) etc. For MRFs, the behaviour of the system must involve an elastic behaviour until a certain limit, and when this limit is crossed by the weaker element, plastic behaviour will be ovserved. Thus, in the most simple case, considering that a typical frame is composed mainly by two different cross-sections, the weaker element corresponds to the beams. These are, usually, constituted of high depth I-shape cross-sections (in order to support the commonly high-span overstructure). Therefore, the weaker element of the structure from a flexural point of view is sufficiently rigid, and potentially, as a consequence, the collapse mechanism can be driven to different elements, such as the connections.

Even if the connections, as stated before, are designed to be moment resisting, they represent a discontinuity in the structure and their rupture is an extremely undesirable scenario. Commonly, the solution proposed by the technical codes is to assign an over-resistance to the columns to prevent their

failure, but this can lead to an over-sizing of the elements and therefore to an increase of the structural mass and associated costs.

In the wake of the mentioned problems, and after some well known post-Northridge damages, André Plumier presented a new device[4] in 1992 with the aim of improving the behaviour of MRF structures.

The solution imagined by Plumier consists of inducing a plastic hinge to develop in the beam at a certain distance from the connection. The techinque is based on the removal of a portion of the beam's wings, thus reducing the relevant strength (Figure 2.1).

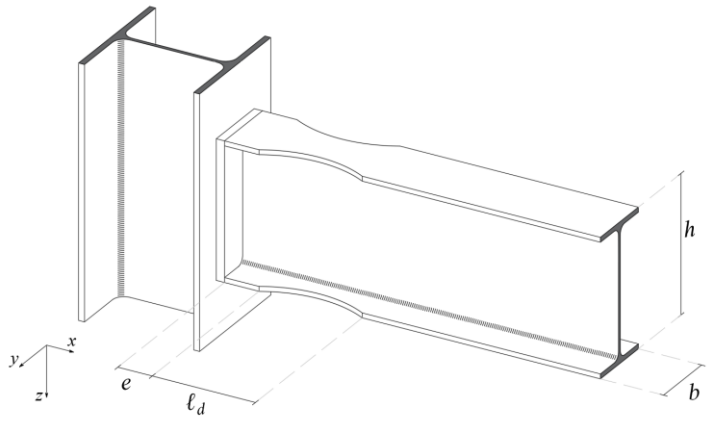

a)

b)

Figure 2.1 – a) Sketch of a typical beam-to-column connection with dogobone; b) Steel joint equipped with dogbone.

[4] The Dogbone Back to the Future. André Plumiere (1992).

As is visibile in the figures above, the dogbone does not cause any significative geometric variation in the normal tridimensional frame structure. The beams are manufactured (by cutting preexisting beams) and assembled on the construction site. The effect of this strategy is comparable to reinforcing the connection. Both of these strategies prevent the brittle failure of the joint, but the dobgbone shows some advantages with respect to the reinforcement; for example, the flange reduction of a specific cross-section by simply cutting a portion of it, is easier and cheaper than improving the stiffness and the strength of a connection by adding more weldings or increasing the joint dimensions. Moreover using a lower resistance portion can help to reduce the demand for continuity plates, the reinforcement of panel zones and the capacity design requirements (strong column – weak beam hierarchy).

On the other hand, this technique has some drawbacks. Removing a portion of the flange does not only affect the strength of the section but also its stiffness. The natural consequence of this is that a frame equipped with this kind of device shows an increased deformability, and hence higher storey drift and displacements. Usually, this variation in the global stiffness of the frame is almost negligible, but it is taken into account by the American techincal code, which also suggest different ways of calculating it. In Figure 2.2 different types of cut are reported, where in the different cases is possible to observe that these shapes have an influence on the cut manufacturing and on the reduced portion volume, e.g. the smoother the cut the lower the possibility of experiencing stress concentration phenomena.

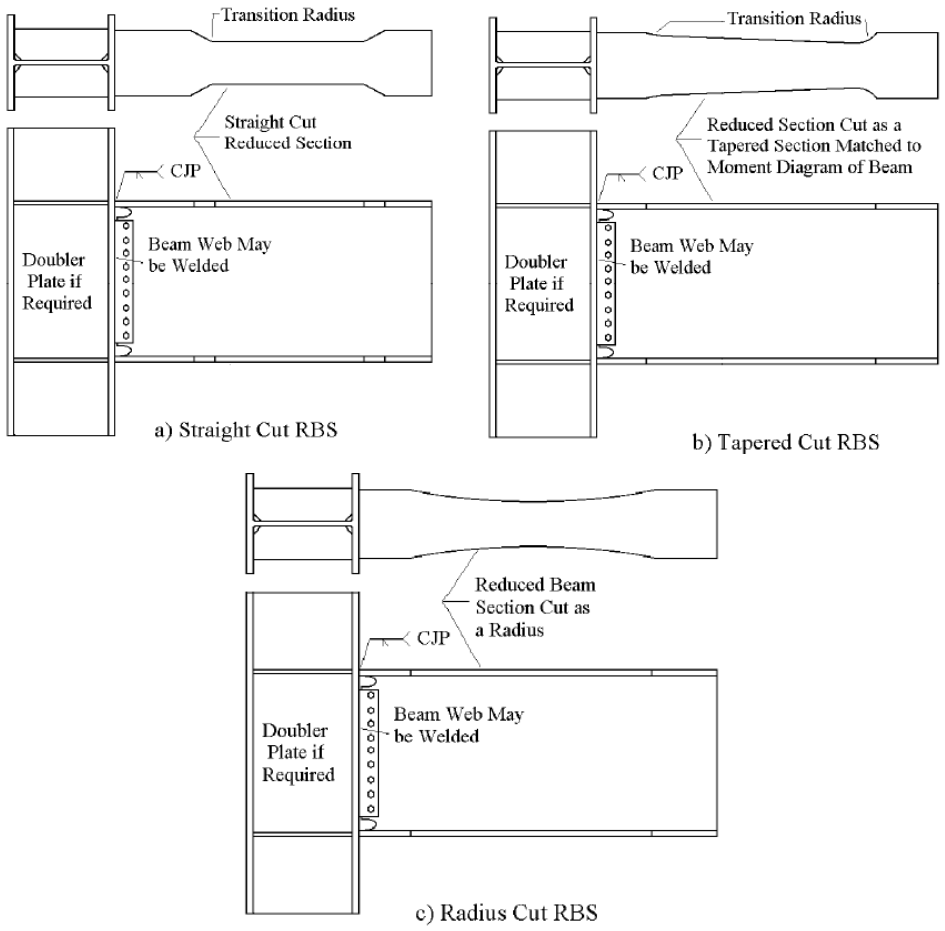

Figure 2.2 – Different approaches of wings reduction.

The side-effect of this apparently minor alteration is that the designer can be forced to increase the beam sizes in order to meet the stiffness requirements that the codes impose. This is particularly true for multi-storey buildings. Despite these disadvantages, RBS strategies such as the dogbone represented a reliable and economical alternative to the commonly used joint technologies in different countries, after the Northridge earthquake.

The FEMA 350 code dedicates a section to reduced beam sections, specifically in paragraph 3.5.5. The regulations that must be respected when designing the dogbone are contained in this paragraph, with specification on the requirements to make this type of connection “prequalified”. This

technique's biggest disadvantage is described at the beginning of paragraph 3.5.5: "*when this type of connection is used, the elastic drift calculations should consider the effect of the flange reduction. In lieu of specific calculations, a drift increase of 9% may be applied for flange reductions ranging to 50% of the beam flange width, with linear interpolation for lesser values of beam flange reduction".*

Therefore, the designer is able to understand, a-priori, if this increased interstorey drift is suitable with the assumptions already made in the design process, and if the dogbone is an advantageous technical choice. Moreover, it indicates the augmented lateral deformability allowing an initial assessment of the structures safety to be ascertained.

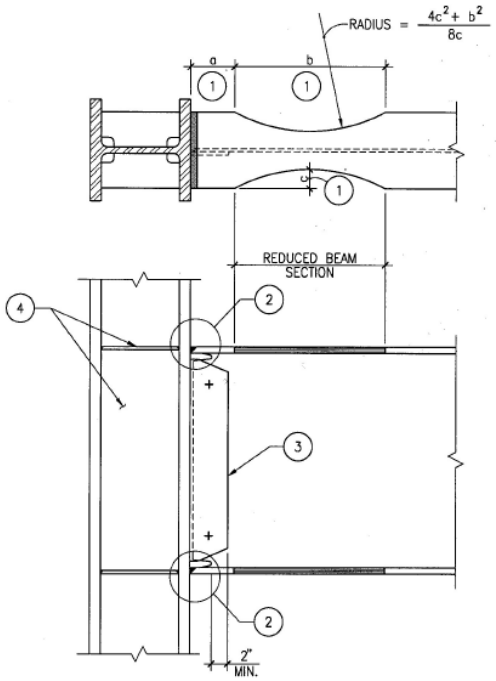

Figure 2.3 – Example reported in FEMA 350 in order to specificy the requirements and the characteristics required from the dogbone.

Referring to Figure 2.3, the code prescribes a series of regulations which must be followed, such as:

- a hinge location distance not lower than $d_c/2 + a + b/2$, where d_c is the column depth, and a and b are visible in Figure 2.3;
- flange thickness up to 2.5 cm maximum;
- standardized steel (such as A572, Grade 50, etc.).

The list above contains only few of the points indicated by the code, which sends the reader to different sections in order to fulfill the requirements in terms of column parameters, beam-column interaction, web panel and connection details, etc.

The quantities indicated at the first point can be calculated as a percentage of the beam flange width (b_f) and of the beam depth (d_b) as follows:

$$a \cong (0.5 \text{ to } 0.75) b_f \quad (3)$$

$$b \cong (0.65 \text{ to } 0.85) d_b \quad (4)$$

In addition the cut depth (c) must also be fixed as a portion of the base width, and after this the reduced cross-section will be characterized by a lowered limit bending moment to take into account when sizing the web connection (which can be bolted or welded). By following the requirements of this paragraph, the structure equipped with dogbones can be in compliance with the FEMA regulations, obtaining the desired effect of protecting the connections from brittle failure. Furthermore, a specific portion of the beam, located at a suitable distance from the column/beam interface, can be selected to develop the plastic hinge.

After its proposal, several authors investigated the features and the contribution of the dogbone in moment resisting frames. The focus was on the behaviour of modified MRFs under cyclic loads[5] and in their influence on the seismic performance of steel frames[6].

[5] Assessment of reduced beam section (RBS) moment connections subjected to cyclic loading. Sofias et al. (2020).

[6] Seismic performance of steel frames with reduced beam section connections. Jin et al. (2004).

2.2 - FUSEIS Project

Different international research organisations have widely studied strategies to increase earthquake resistance for steel frames, putting a lot of effort into the discovery of new possible solutions for improving the behaviour of MRFs and carrying out several experimental analyses. One example is a project funded by the European Union, named INNOSEIS – Valorization of Innovative Anti-Seismic Devices[7], which aims to evaluate and compare different technological solutions to reduce the seismic vulnerability of buildings. In the context of this project numerous strategies and techniques were evaluated. The closest, in terms of funcionality and features to the LRPD, is the strategy developed in the FUSEIS project (which stands for "Dissipative Devices for Seismic Resistant Steel Frames"). The device developed within this project is the "bolted fuses union"[8], a dissipative beam-to-column connection. This device consists of joining the elements through a set of bolted steel plates, both at the web and at the lower flange of the I-shaped cross-section (Fig. 2.4).

[7] See: http://innoseis.ntua.gr/.
[8] Hysteretic behaviour of dissipative bolted fuses for earthquake resistant steel frames. Calado et al. (2013).

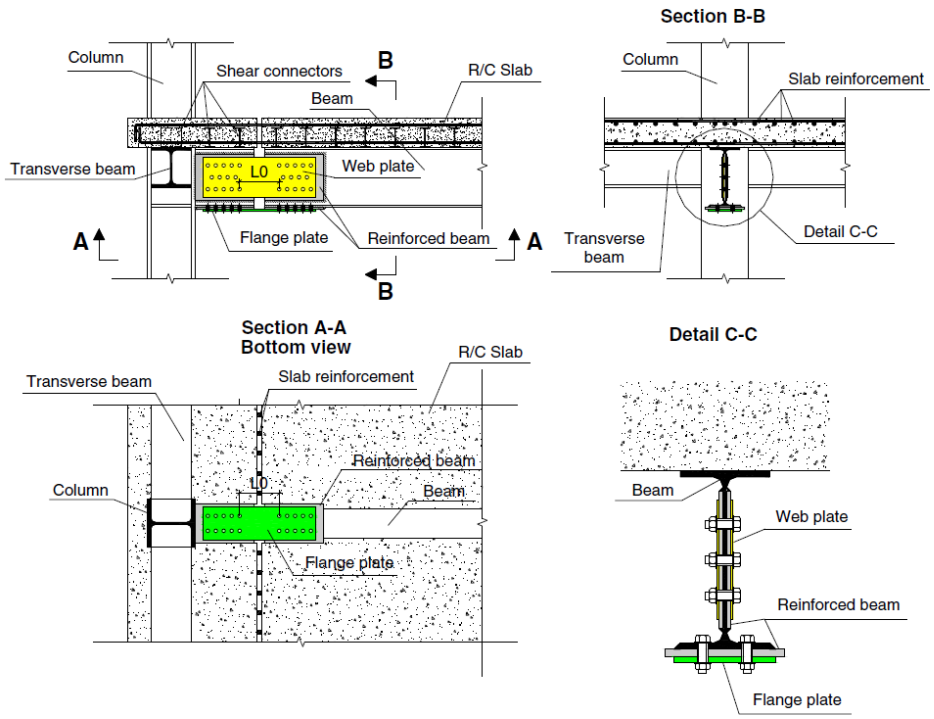

Figure 2.4 – Example of a typical bolted fuse device.

In this way the plastic deformations occur principally in the plate elements, and thanks to its shape and to its joining technology, they are able to dissipate more energy with respect to the normal connection configuration. Moreover, by accomplishing this concentration of the plastic phenomena in this specific cross-section, it is possible to experience forcing actions of a relatively lower magnitude in the remaining portions of the frame, keeping them far from their ultimate conditions.

To accomplish this, the resistance of the joint of bolted plates must exhibit a lower limit value with respect to that of the connected beam. Hence, when reaching its yield value, it will experience plastic deformation and thus dissipate the input energy of the earthquake. The crucial value in this sscenario is the “capacity ratio”, defined as the ratio between the bending moment of the fuse and the one of the beam. This idea is similar to the dogbone technique. In that case, however, the approach is simplified by

considering the reduction of the resistance by reducing the width, and not as mechanical parameter. The dogbone connection type allows an important advantage to this technique to be guaranteed, i.e. the possibility to easily substitute the damaged portion of the frame after a significant seismic event, moreover with relatively low-efforts and low specialized manpower.

In the cited reference, the authors proposed two approaches to predict and estimate the final behaviour of the FUSEIS equipped beam: a resistance and a stiffness model. The resistance model is based on simplifying the calculation by neglecting the contribution of the web plate in the bending behaviour of the element, leading to the section shown in Figure 2.5a. The resisting moment is computed by performing an elastic-plastic analysis with uniaxal $\sigma - \varepsilon$ constitutive relationships for the different materials for the plates. For the compressed flange plate, the authors developed a modified relationship in order to take into account the magnitude of the acting axial force. The stiffness model, on the other hand, is based on the component method of EN 1993-1-8[9], where for each component (upper and lower rebars, web and flange plates) the stiffness contribution was quantified, and, differently from the resistance model, the contribution of the web is taken into account. Therefore, for each of the cited elements an axial stiffness was defined, in addition to a further spring which simulates the bolts.

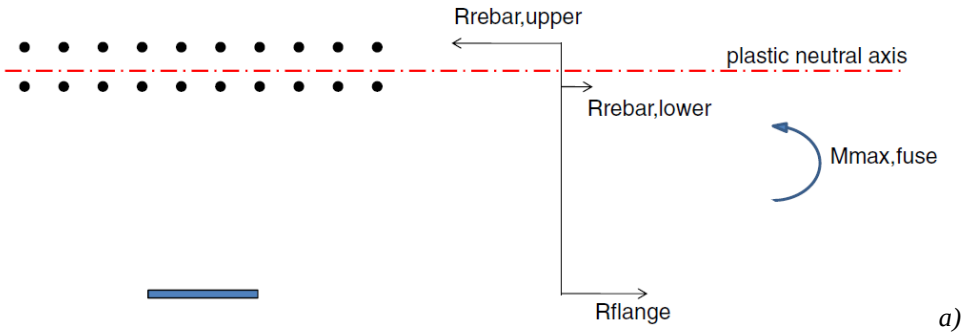

a)

[9] EN 1993-1-8. Eurocode 3: design of steel structures - part 1-8: design of joints (2004).

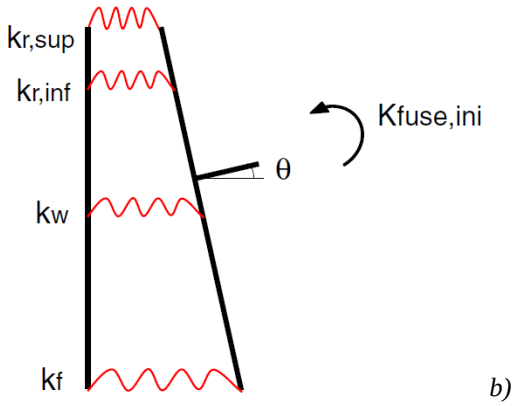

Figure 2.5 – Simplified models of FUSEIS bolted device proposed by Calado et al. (2013); a) resistance model; b) stiffness model.

The two models were used to predict in a simplified way the limit behaviour of the connection. By comparing the results with the revelant experimental analyses carried out and reported in the cited work it was possible to observe that the use of these models provided good results, maintaining a good level of accuracy.

A very similar device, was also developed inside the above mentioned project. This device is known as the dissipative welded fuses connection[10]. As the name suggests, the plates that substitute a specific portion of the beam are welded to the two ends (Fig. 2.6).

[10] Hysteretic behavior of dissipative welded fuses for earthquake resistant composite steel and concrete frames. Calado et al. (2013).

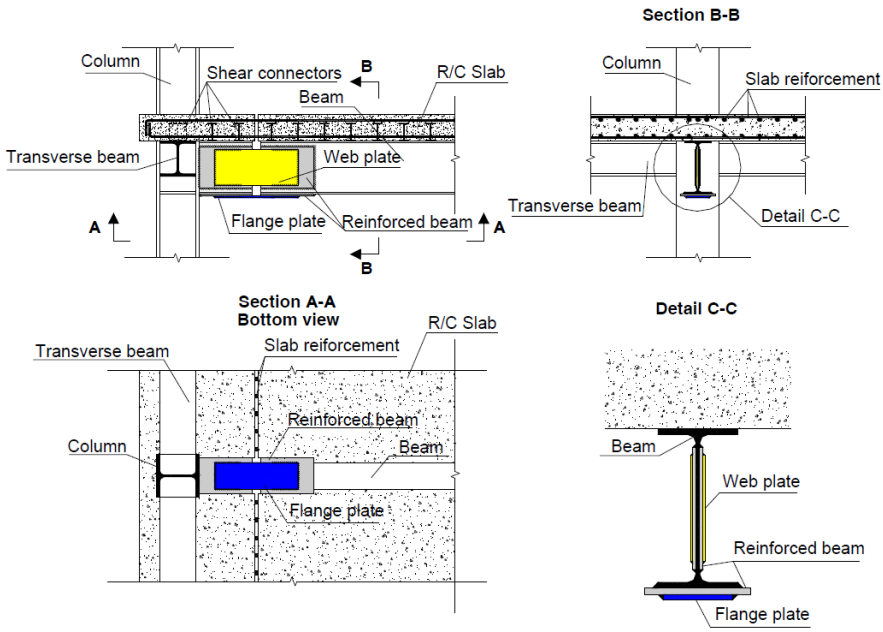

Figure 2.6 – Example of a typical welded fuse device.

The dissipative welded fuses connection functions very similarly to the bolted connection strategt; the plates located at the beam's boundaries are the elements devoted to developing their non-linear behaviour, while the two ends and the remaining parts of the beam must continue to behave linearly. Furthermore, in this case, the device is significantly harder to replace. In fact, the welded connections are known to be complex to install and check. It can, therefore, be easily imagined that in a post-earthquake scenario where these plates are plasticized, a rapid and low-cost substitution may not be achievable. For the welded fuses connection the schematic model are the same as those presented for the bolted connection (Figure 2.5)

The contribution of the two techniques cited, in terms of the structural performance improvement, is to identify a specific location for the onset of plastic deformations. In addition, the possibility to protect the irreplaceable parts of the beam-column coupling is also a good feature that permits the usability and the life of a structural system to be enhanced. Moreover, in

terms of dissipative behaviour both the welded and the bolted FUSEIS devices demonstrated a good behaviour, to be attributed to the plastic deformations and to the buckling of the single plates.

2.3 - Double reduced beam section

As the name suggests the dobule reduced beam section (DRBS) consists of an enhancement to the normal idea of an RBS through the addition of a second reduced beam portion next to the standard reduced section. In essence, the dogbone technique is doubled, with the presence of an additional reduced section following the first, with suitable characteristics and at a specific distance. This strategy has been recently proposed in literature by Morshedi et al. (2017)[11], where the basic assumption is that thanks to the doubling of the plastic hinge developing region it is possible to enhance the rotational and dissipative features of the connections, postponing the onset of plastic deformation in the system. Therefore, the DRBS is simply represented as a doubled dogobone (Figure 2.7). The base mechanism of this strategy is that the presence of a second hinge site permits the development of a secondary stress distribution pattern in addition to the one already present for the normal RBS.

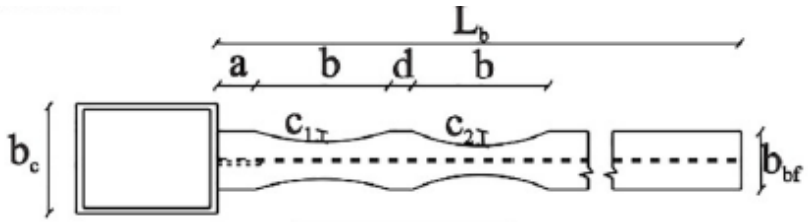

Figure 2.7 – Top view of the double reduced beam section (DRBS).

Thus, as the yielding stresses are reached progressively within the two reduced sections, the total dissipated energy is increased with respect to the use of one single dogbone. Moreover, developing a double hinge in a short distance makes the D-RBS act as a local fuse, helping the spread of plastic deformations.

[11] Double reduced beam section connection. Morshedi et al. (2017).

It is important to note that this second reduced portion must be dimensioned in order to allow the best post elastic behaviour possible, and the reason can be found by looking at Figure 2.8.

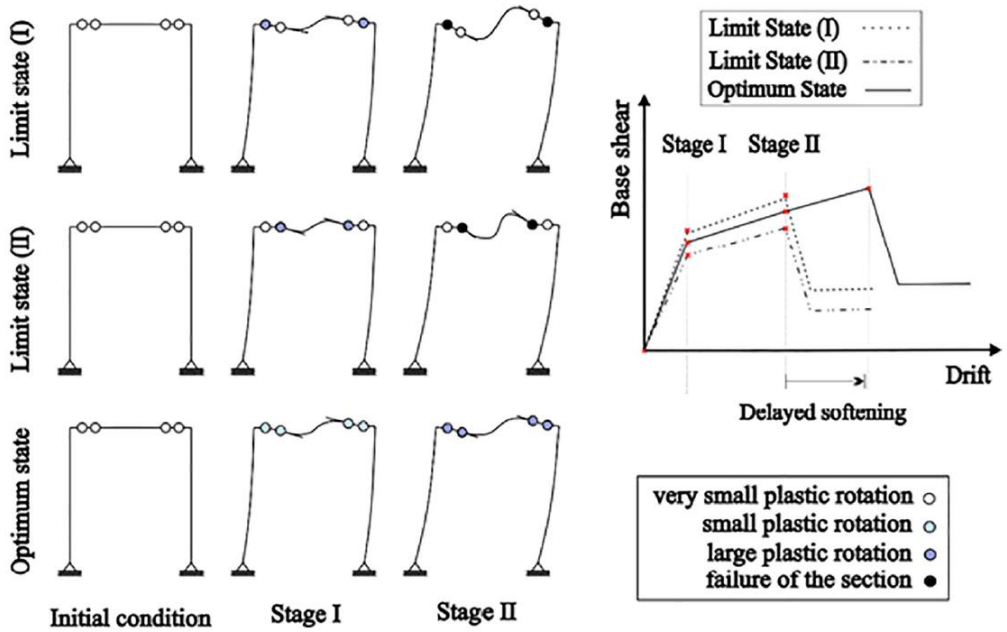

Figure 2.8 – Different failure mechanisms for DRBS equipped steel portals.

The correct strength reduction of the two portions can lead to two different situations for the post-elastic behaviour of the structure: if the two regions are equally weakened, or the first is weaker, sudden collapse will occur when its limit resistance is reached without utilizing the second one; on the other hand, if the second one is over-reduced this unhealthy effect will occur in the second section. Therefore, the cut depth of the two reduced portions must be selected in order to have the second portion slighlty weaker than the first. This difference, and the distance of the second cut, are the crucial parameters for this technique. The cited authors, starting from the codes' prescriptions regarding the normal RBS connections, investigated this aspect through extensive numerical studies, and selected the best recommended proportion for these variables.

The advantages of this technique are different. Generally, it helps in reducing the maximum plastic strain in correspondence of the reduced cross-section. Further, it postpones the ultimate conditions of the reduced portions from being reached. Using this technique, the web local buckling or torsional phenomena which usually occurs is avoided. As mentioned, enlarging the region subjected to plastic hinge developments, increases the amount of the energy absorption with respect to a common RBS.

On the other hand, the DRBS carries with it the same side effect of the dogbone, i.e. the increasing of the flexural stiffness of the elements involved along with the difficult and expensive post-damage substitution.

2.4 - Drilled flanges RBS

Trimming the flanges of one portion of the beam elements it is not the only way to obatin a reduced beam section. In fact, the required resistance reduction can be achieved by drilling the flanges and realizing suitably distributed holes, creating a so-called drilled flanges connection (DF).

This techinque has been recently proposed by some authors[12] and consists of the realization of different couples of doubly symmetric holes at a specific distance from the fixed end of the beam (Figure 2.9).

[12] Modified moment resisting connection for ductile steel frames (numerical and experimental investigation). Farrohki et al. (2009).

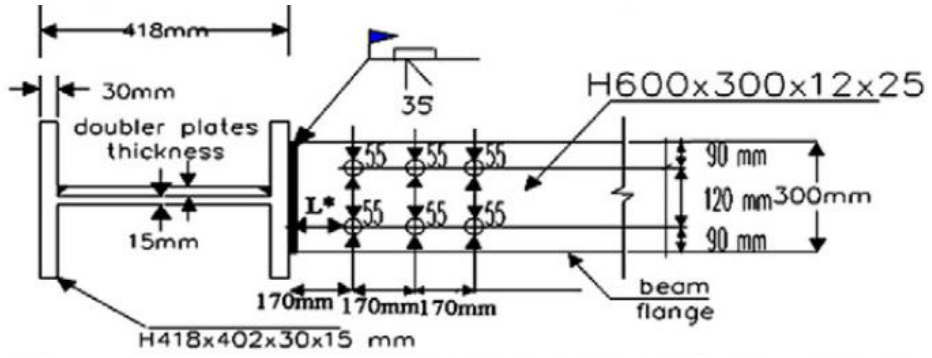

Figure 2.9 – Example of drilled RBS.

The number, the position and the diamater of the holes can be variable. The idea behind investigating different methods to obtain the strength reduction in an RBS is that commonly they suffer from some drawbacks, such the stress concentration that can occur at the beam web, the bad torsional behaviour, or the weakness in terms of out of plane bending moment resistance. The use of the holes instead of reducing the base width moves the biggest issue, i.e. the web concentration stress, from the web to the wings of the cross-section, permitting a better spread of the plastic strains.

In literature different studies[13] have been conducted in order to optimize the performance of this type of RBS, trying holes in different locations and of different sizes. These studies were validated by means of FEM models to determine the post-elastic behaviour and the collapse mechanism of the drilled flanges connection, and it has been compared to the common moment resisting connection and to the classic RBS. The DF connections showed a good aptitude to prevent brittle failures in the welded portions of the union.

[13] Optimum drilled flange moment resisting connections for seismic regions. Atashzaban et al. (2015).

2.5 - Heat-treated RBS

A novelty in the field of reduced beam section technologies is the one proposed by Morrison et al.[14] (2015). It consists of a weakened portion at a specific distance from the fixed end of the beam by means of thermal treatment (Figure 2.10).

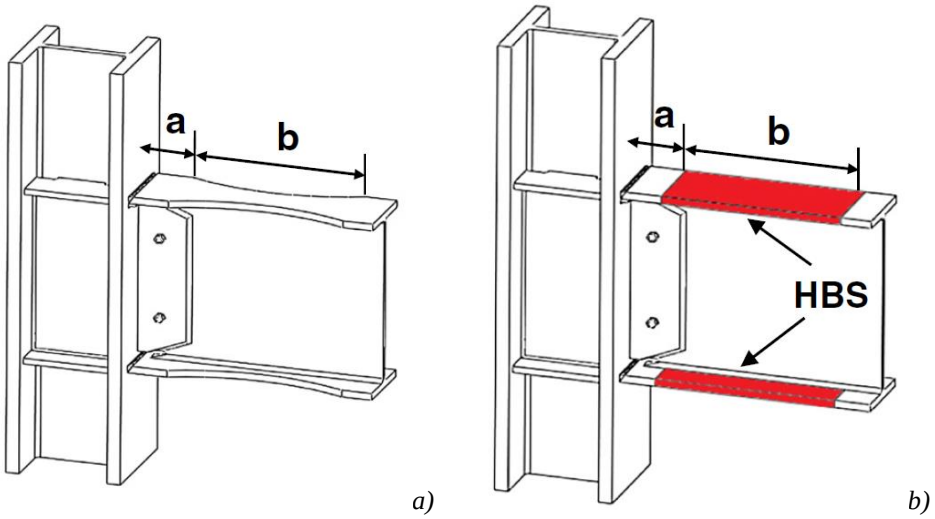

a) *b)*

Figure 2.10 – a) Common dogbone; b) Heat-treated portions for HBS.

This type of RBS is called "heat-treated beam section", and for its functionality relies upon the modifications that occur at a microscopic level within the steel after being subjected to high temperatures and a slow cooling process. The heat treatment proposed by the authors is shown in Figure 2.11a, and the relevant stress-strain diagram that emphasizes the strength reduction is reported in Figure 2.11b.

[14] An innovative seismic performance enhancement technique for steel building moment resisting connections. Morrison et al. (2015).

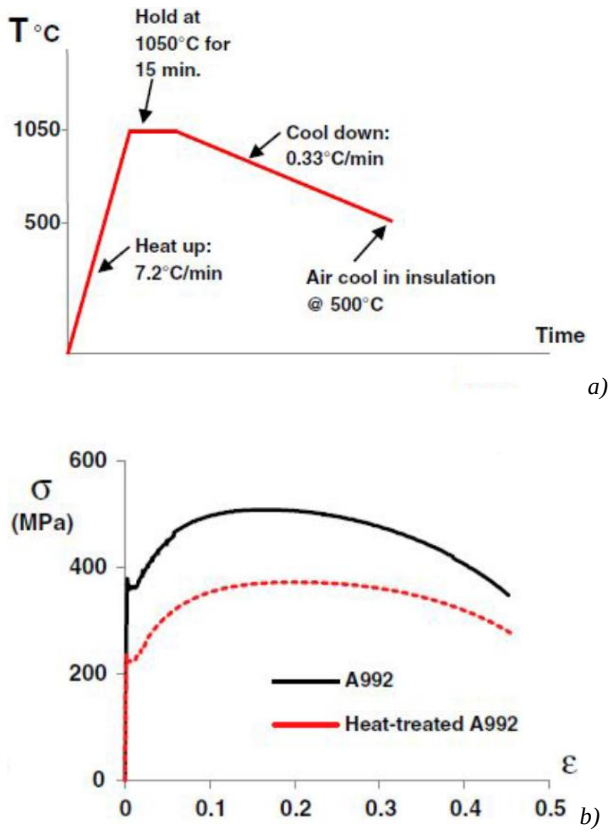

Figure 2.11 – a) Heat treatment process; b) Heat-treated portions for HBS.

The added feature of the HBS, compared to a common RBS, is that the reduction of the resistance is not obtained through shape alteration, as is the case for every other RBS technique, but through a material modification. In this way the elastic/plastic resistance modulus and the inertial properties of the cross-sections are preserved, and thus the stiffness of the beam is the same as a non-treated beam portion. The consequence of this fact is that the overall deformability of the frame where this type of methodology is applied, is not affected by any variation, and thus they preserve the normal behaviour they would have in a non-treated scenario.

2.6 - Reduced web section

As widely argued, the transfer of the onset of plastic deformation from the beam-column interface to a specific beam portion can be accomplished through a reduction of the wings. Until now, in almost every one of the cases presented, this was obtained by modifying the flanges of the structures in different ways. Some authors[15] investigated the possibility of obtaining this resistance reduction by modifying the web of the I-shaped profile instead of the wings, proposing a device named the "reduced web sections" (RWS). As visible in Figure 2.12 the web opening is rectangular, and the edges of the opening are stiffened by welding small L-shaped plates in order to prevent local buckling phenomenon.

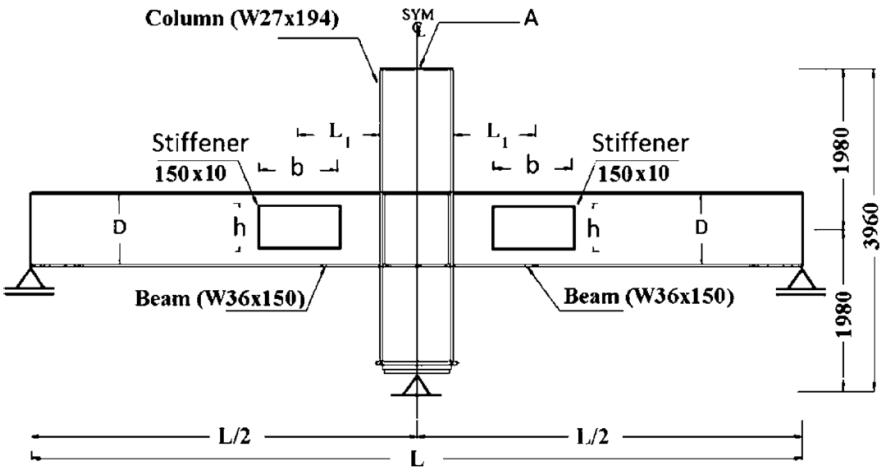

Figure 2.12 – Common RWS model.

The size, shape, number of stiffeners, and distance from the fixed end, are all variables that need to be suitably chosen by means of parametric studies and model calibrations. For instance, in the cited literature, the range indicated for the opening height is between 65% and 85% of the original

[15] Seismic performance of the accordion-web RBS connection. Mirghaderi et al. (2010).

height: lower values than this would cause a non-optimal spreading of plastic strains, while higher values would cause an over-reduction of the section strength (especially in terms of shear capacity). Another prescription indicated regards setting the distance between the medium point of the opening and the column interface at least equal to the height of the cross-section. Other prescriptions that different researchers have studied permitted the RWS to properly fulfill at its role of hosting the plastic deformations of the structures, while the remaining portions remained in the elastic field.

2.7 - RBS with replaceable fuses

With respect to the LRPD presented in this thesis, the most comparable strategy is likely the RBS with replaceable fuses. Almost all of the methodologies previously discussed involve the presence of a specific alteration of the original beam element in order to improve its behaviour in specific loading conditions. The natural consequence is that after an event which acts upon the beam, and hence the RBS device, that pushes an element over its elastic limit, the whole element need to be substituted. After a seismic event it is likely that this substitution would be necessary considering the fundamental purpose of the RBS is to allow the propagation of plastic strains develop across the beam element. It is easy to realize that the task of substituting a plasticized beam element installed inside a tridimensional steel frame building is a complex task, involving high costs and long manufacturing processes.

Following what has been previously discussed, some authors[16] presented a method to benefit from the dogbone features while permitting an easy substitution of the deformed portion, creating a fuse including a reduced beam section, called RBS-F (Figure 2.13a). A variation which was also proposed regards the way of obatining the strength reduction by changing the subject of the weakening: instead of trimming a flange portions, as in the dogbone, in this case the reduced size is the depth of the cross-section (RDS-F, creating a reduced depth section fuse, visible in Figure 2.13b).

[16] Experimental evaluation of rigid connection with reduced section and replaceable fuse. Moradi Garoosi et al. (2018).

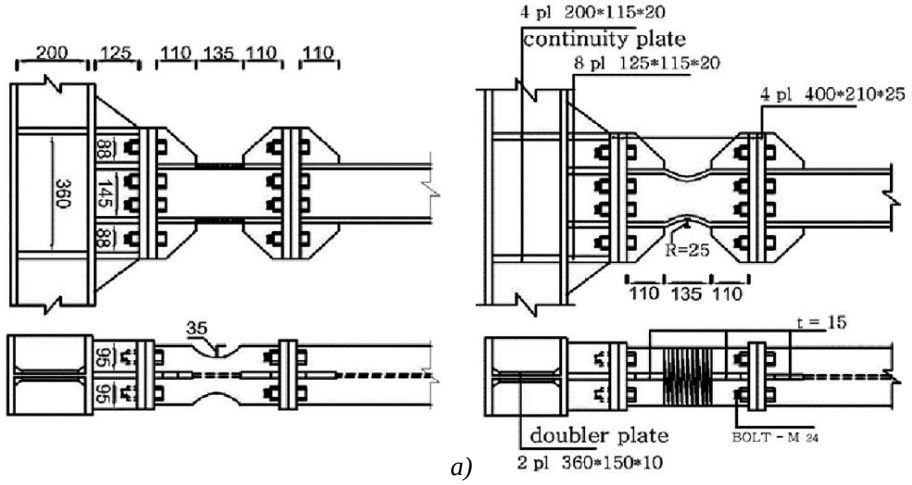

Figure 2.13 – a) Common RBS-F sample; b) common RDS-F sample.

As is visible, the idea is to place the RBS device within two ending plates bolted to the remaining portions of the structure: the column at one end and the beam at the other. Through experimental and numerical analyses these devices have been tested, showing some useful improvement in the seismic behaviour of the structural joint. In detail, both the RBS-F and the RDS-F help to postpone the initiation of damage in the global structure compared to an ordinary bolted plate connection, and moreover they help in reducing the maximum strain experienced by the connection (hence improving the joint protection).

CHAPTER 3 – LRPD

3.1 - Basic idea and introduction

The peviously discussed RBS techniques were useful to locally reduce the strength of steel beam elements in moment resisting frames, and their use has been widely investigated in the available literature. These techniques show some common features that limit their use and their efficacy in certain cases. The most relevant is the strict relationships between the strength reduction and the stiffness variation of the beam in which the RBS device is present. All of the techniques discussed do not provide any solutions to overcome this issue, and therefore the increased deformability is simply taken into account by over dimensioning the remaining part of the structure, or in other cases is simply neglected in favour of simplier and approximated structural outputs. Another common side effect observed is the impossibility to easily substitute the RBS device following damage sustained during an earthquake. The LRPD proposed in this chapter also suffers from this issue. While it is true that a version has been studied in which this problem has been overcome, the research into this device is still ongoing and has not been finalized.

The LRPD represents a novel contribution to the RBS techniques field, and its name stands for Limited Resistance Plastic Device. Since its first appearance in literature[17] the aim was simple: it was a device designed to recreate the advantages offered by a common RBS technique, but with the possibility of independently setting its limit resistance and flexural stiffness.

This last point is the crucial one, because the other techniques mentioned in Chapter 2 do not possess this feature.

The device is covered by a patent at the Italian Ministry of Economic Development and in the International Patent System.

[17] Fixed Strength And Stiffness Hinges For Steel Frames. Benfratello et al. (2017).

As previously stated, the device can be imagined as a steel component which substitutes a specific portion of a beam element. By equipping the beam with the LRPD it is possible to assign new properties to the element, recreating a behaviour that normally is not possible in common beams.

The main ideas behind the LRPD can be summarized as follows:

- it must exhibit a reduced limit resistance in terms of bending moment, compared to the connected beam element;
- it must be able to guarantee a flexural stiffness equal to the original portion of element that has been locally substituted;
- it must ensure the possibility to independently fix the reduced resistance and the flexural stiffness;
- while ensuring the previous requirements are met, the LRPD has to permit a proper and complete development of a plastic hinge;
- it must maintain the original class of the connected beam element (in terms of preventing local buckling, as defined in literature and in the European standard[18], and as above briefly discussed).

Moreover, as its name suggests, the device must also be as smaller as possible in order to be used in the joints themselves. Therefore, the device must possess a volume and a longitudinal length which allow it to meet the features required.

To the latest developments, the research presents a simplified version of the device to make the study of its behaviour and of its performances easier. Therefore, only the axial force and the in-plane bending moment are considered in its design. The effects of shear forces, torsional forces and compound bending moments are not analyzed in this thesis. For the material

[18] UNI ENV 1993-1-1, Design of steel structures. Part 1-1: General rules and rules for buildings.

an elasto-plastic model was adopted, with the aim of simplifying the dissertation and the computations.

Commonly, commercial steel profiles (especially box sections, I-shaped sections, C-shaped sections and so on) can experience instability phenomena. This is more true as the plates composing the profiles are made thinner. Thus, this problem can represent a limitation in the usability and in the functioning of the device. For instance, to guarantee the reduction of its limit resistance it is mandatory to assign smaller thicknesses to the portions of the device with respect to the relevant ones of the standard profiles adopted. As known, the parameter that quantifies the tendency of a cross-section to experience this phenomenon is called "class". The international codes indicate how to categorize these classes and what distinguishes them. These can vary from 1 to 4, depending on the section's post-elastic features. Class 1 sections show the best behaviour, expressed in terms of ratio between the ultimate curvature and the yielding one. As reported in the cited code "*Class 1 cross-sections can form a plastic hinge with the rotation capacity required from plastic analysis without reduction of the resistance*". On the contrary, class 4 sections are characterized by the absence of a post-elastic branch, and "*in which local buckling will occur before the attainment of yield stress in one or more parts of the cross-section*". Class 2 and Class 3 show an intermediate behaviour between the two classes above reported. Therefore, when the device is installed into an element with a specific class, the resulting class of the whole element can become higher than the initial one (thus worst). This problem is an aspect that must be accounted for during the design phase, and as further explained can be overcome.

The following sections will explain how the LRPD is constructed and how it is capable of guaranteeing the features previously discussed.

3.2 - Geometrical and mechanical model

As stated above the device must fulfill a series of requirements that make it useful to different specific structural engineering applications. This can be possible by assigning specific dimensions to it, and by adopting a suitable shape that is pre-determined. Starting from the conception of how the device is composed, it is useful to state that each beam element possesses a cross-section that can be inscribed in a rectangle of dimension $b*h$ (width and height). In MRFs, hot rolled steel profiles are generally utilized, and in the case of beams and columns they are characterized by an I-shaped cross-section. The proposed device possesses a pre-fixed length, and substitutes the relevant portion previously occupied by the original commercial steel profile. As shown in Figure 3.1 the device of this ideal volume can be contained within a parallelepiped of dimension $b*h*\ell$ (where the new parameter ℓ stands for the length of the device).

This length is divided in three different portions with different cross-sectional dimensions. Despite this, each element still has an I-shaped cross-section.

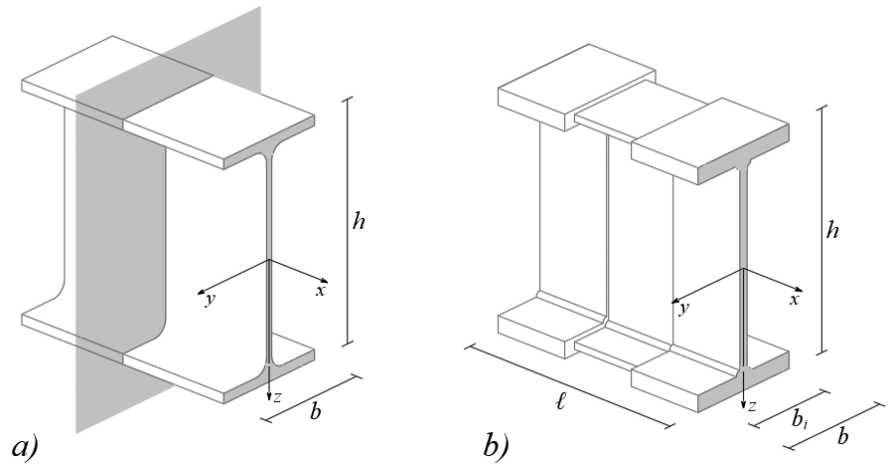

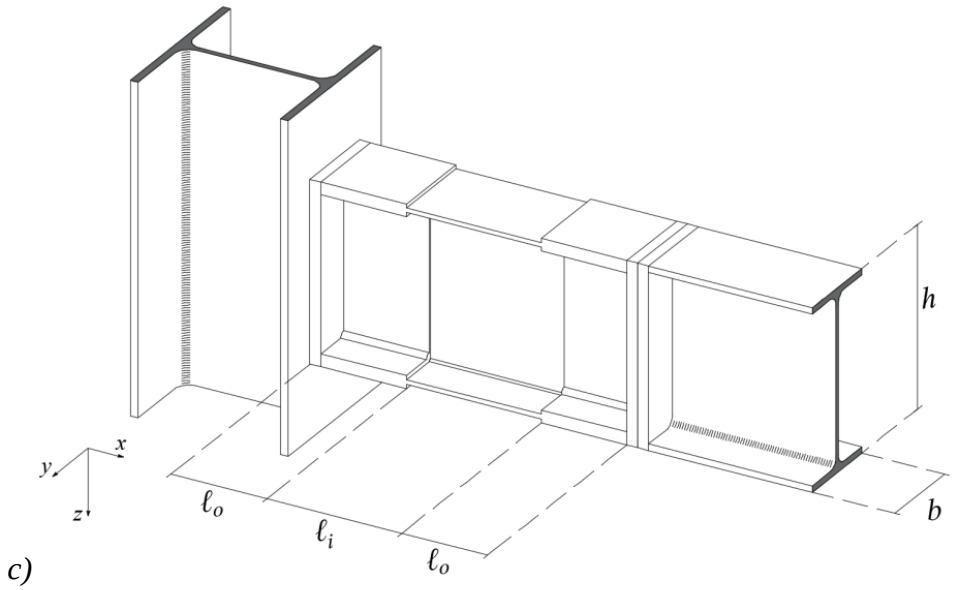

Figure 3.1 - a) Volume portion of the commercial element with the relevant dimensions; b) Sketch of the LRPD, c) assemply for a beam-column connection equipped with LRPD.

The ending sections are equal and possess the same flange and web thicknesses which are greater than the commercial steel profile of the beams and columns that they are connected to. The inner section, on the other hand, possesses smaller thicknesses and base width, and it is enclosed between the outer portions.

The particular shape described is essential to the functioning of the device. The inner portion is characterized by a smaller cross-section in order to guarantee the reduced flexural strength in terms of a lower plastic resistance modulus. The reduction is fixed on the basis of the commercial element adopted as a percentage of the original one. On the other hand, the outer ones possess greater dimensions, thus greater resistance, helping the plasticization to develop properly in the inner one. Increasing the resistance involves also increasing the moment of inertia of the cross-section, that influences the bending stiffness of the whole element, helping to balance the stiffness loss present within the inner portion.

Summarizing the salient points of the geometry of the device:

- the LRPD is symmetrical considering three orthogonal barycentric planes;
- it is characterized by three different consequent portions. The outer two with greater strength than the inner one;
- the two flanges and the web of the three portions share the same common medium plane;
- the inner portion's length is proportional to a coefficient β, variable from a minimum of 0.5 of the cross-section height and to a maximum of 1, in order to maintain a minimum portion to allow the proper plastic hinge development.

These three portions are enclosed by two flanges with a pre-assigned thickness (later known as ℓ_p), that acts, simply, as an interface between the device and the other connected elements, such as the column or another beam.

To deepen the characterization of the device and to better treat the aforementioned mechanical and kinematical properties, a series of parameters must be defined. Starting from the dimensions of a common I-shape cross-section (Figure 3.2a) its characteristics are defined through the plate thickness such as the flange thickness t_p, the web thickness t_w, the welding radius r, and the height and width already defined (b and h). Referring instead to the device, the same quantities can be named as shown in Figure 3.2b and 3.2c.

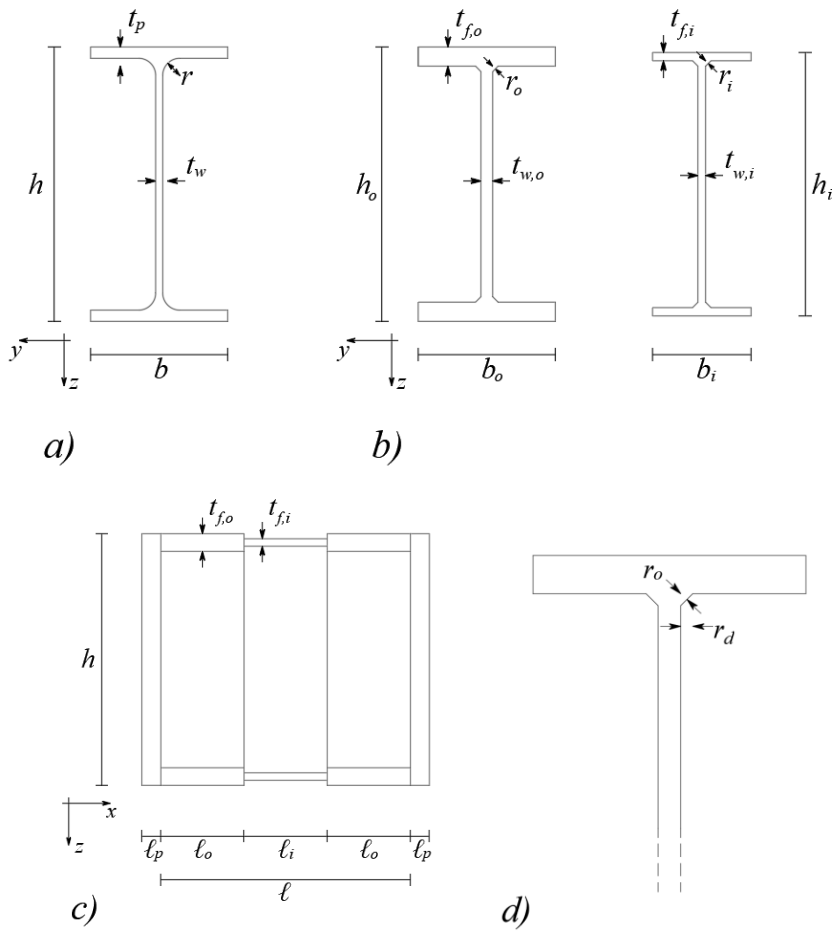

Figure 3.2 – a) Common I-Shape cross-section with reference to its geometrical parameters; b) Cross-section of the outer and inner portions of the device with the relevant thicknesses; c) lateral view of LRPD with the portions lenghts; d) particular of the welding parameters.

All the parameters reported in Figure 3.2b and 3.2c will be suitably designed through an optimization problem.

Before detailing the analytical properties of the sections, a clarification about the weldings between the flanges is required. In hot rolled beam elements these portions present a concave shape in the web-wing intersection that derives from the manufacturing process. For the proposed device this union is designed as welded using the tee joint type weld, therefore there will be a welding area in the region with a triangular shape. This area is defined

by the welding's height (the same of the triangle) and by its two legs. Reffering to the device, r_o is the welding area height, but it is of more interest to adopt r_d, i.e. the legs length of the triangle, and is $r_d = r_o\sqrt{2} \cong 0.7\ t_w$ (Figure 3.2d).

For the various portions of the device it is possible to define the cross-sectional area A, the elastic and plastic resistance modulus W_{el} and W_{pl}, and the moment of inertia J. The subscript "o" refers to the outer portions of the LRPD. By simple calculation it is possibile to obtain these quantities as follows:

$$A_o = 2b_o t_{f,o} + t_w\left(h_o - 2t_{f,o}\right) + 4\frac{{r_d}^2}{2} \tag{5}$$

$$J_o = \frac{b_o\, t_{f,o}^3}{6} + \frac{b_o\, t_{f,o}}{2}\left(h_o - t_{f,o}\right)^2 + \frac{t_w\left(h_o - 2t_{f,o}\right)^3}{12} + \frac{{r_d}^4}{9} + \frac{{r_d}^2}{2}\left(h_o - 2t_{f,o} - \frac{2r_d}{3}\right)^2 \tag{6}$$

$$W_{el,o} = 2J_o/h_o \tag{7}$$

$$W_{pl,o} = b_o\, t_{f,o}\left(h_o - t_{f,o}\right) + t_w\left(\frac{h_o}{2} - t_{f,o}\right)^2 + {r_d}^2\left(h_o - 2t_{f,o} - \frac{2}{3}r_d\right) \tag{8}$$

By substituting the subscript "o" with "i" the same parameters can be found for the inner cross section, which basically have the same shape of the outer one.

Regarding the main features required from the device, the elastic/plastic modulus and the moment of inertia play a fundamental role, making it possible to define the relevant domain of resistance and to obatin the flexural stiffness. The strength domains are useful to compare the strength of the commercial elements with the relevant one of the device installed, and their definition will be descriped in the following paragraph. As mentioned before, the contribution of the shear force is neglected in the design phase, and as a consequence its contribution to the strenght domain is also neglected. This is also true for its influence on the limit conditions of the element. Considering the high non-linearity of the problem, this, in particular, helps to simplify the model and to obtain more reliable results.

Changing the focus to the kinematical aspect, the other crucial goal of the device is to exhibit a predetermined flexural stiffness. In detail, considering the common device imagined as part of a beam to column connection, the goal can be to re-balance the stiffness loss caused by the section's reduction. Hence, the flexural stiffness must be maintained in the element when the device is installed.

To measure this stiffness with a simple equation it is possible to consider the relative rotation of the external sections of the device subjected to a unitary bending moment ($M = 1$), as visible in Figure 3.3. In formula:

$$\Delta\varphi_{LRPD} = 2\int_0^{\ell_o} \frac{1}{EJ_o} dx + \int_0^{\ell_i} \frac{1}{EJ_i} dx \qquad (9)$$

Where E is the longitudinal Young's modulus of the material, EJ represents the bending stiffness modulus of the section, and $\Delta\varphi_{LRPD}$ the relative rotation just described. Therefore, to recreate the stiffness of the substituted element the same quantity must be evaluated for the original steel profile, and can be written as:

$$\Delta\varphi_p = \int_0^{\ell} \frac{1}{EJ_p} dx \qquad (10)$$

The quantities vary for the subscripts, and here are referred to the original profile. By imposing equality between relations (9) and (10), it can be written:

$$\frac{\ell_i}{\ell_o} = 2\frac{J_i}{J_o}\left(\frac{J_o - J_p}{J_p - J_i}\right) \qquad (11)$$

This equation represents the correct balance between the involved kinematical parameteres in order to maintain the stiffness of the portion.

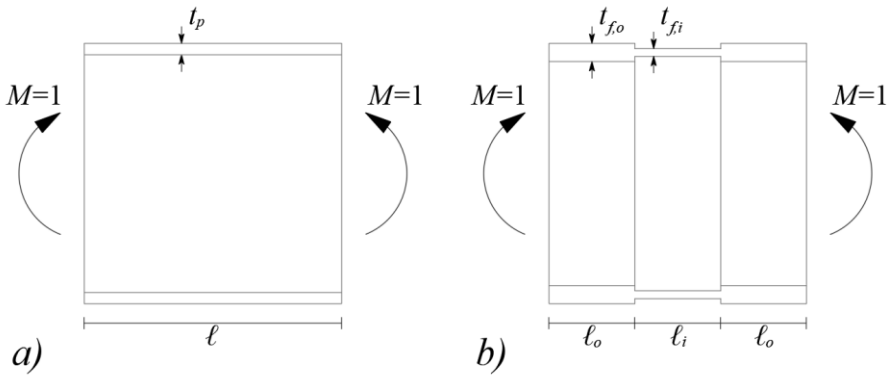

Figure 3.3 – Sketch of the model adopted for the flexural stiffness balancing. a) Commercial steel profile; b) LRPD.

All the above discussed parameters and geometrical aspects are fundamental to the functioning of the device, and represent the basis for a suitable optimal design problem, which is calibrated in order to fulfill, at the same time, the geometrical bounds and the mechanical features proposed.

3.3 - LRPD Strength domains

As stated, the resistance features of the device must be investigated considering the interaction between the different forces that act simultaneously on the element. Neglecting shear forces for now, this resistance can be represented in the graphical domain as a cartesian plane where on the *x*-axis the axial force values are reported, and on the *y*-axis the bending moment values are shown. The $N - M$ couples describing the domain's boundaries (that can have different shapes considering the type of element involved, the material and the geometry) represent the limit values that the cross-section can face.

These domains can be represented in a simplified way, usually prescribed by the codes, and in a more accurate way, as will be presented later in analytical terms. In addition, besides the differentiation made depending on the interaction of the forces and on the material, the post-elastic features of the cross-section must also be considered. For this reason, the European and the Italian codes present a way to identify the strength domains depending on the class of the cross-section of the element. Referring to the class sections cited at the beginning of this chapter, for classes 1, 2 and 3 the elastic domain can be described as follow (Figure 3.4a):

$$\left|\frac{N}{N_{el}} + \frac{M}{M_{el}}\right| = 1 \tag{12}$$

$$\left|\frac{N}{N_{el}} - \frac{M}{M_{el}}\right| = 1 \tag{13}$$

Where the subscript "el" indicates the elastic limit value of axial and bending forces, being $N_{el} = A\, f_y$ and $M_{el} = W_{el}\, f_y$. The parameter f_y is the yield stress of the material.

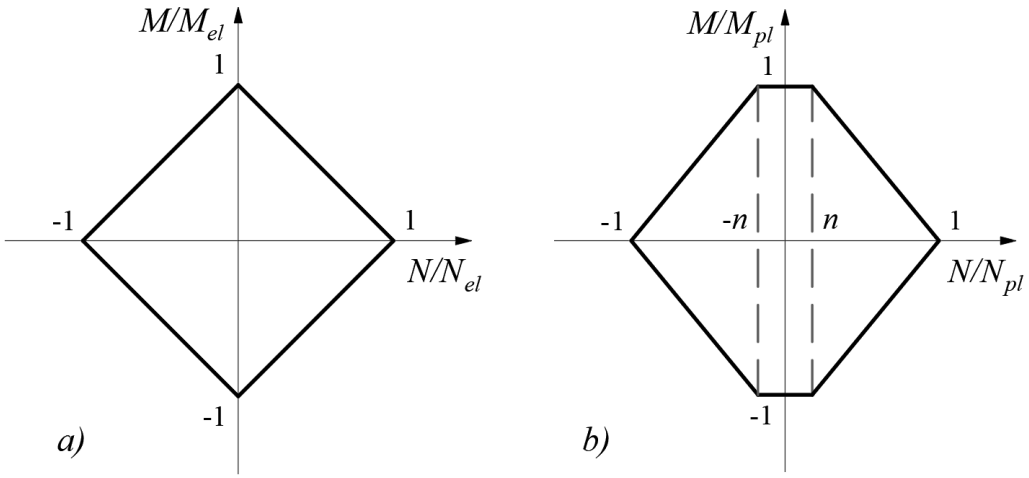

Figure 3.4 – a) Dimensionless elastic domain; b) dimensionless plastic domain.

Similarly, regarding class 4 cross-sections, the domains can be expressed by the relationships:

$$\left|\frac{N}{N_{eff}} + \frac{M+Ne_N}{M_{eff}}\right| = 1 \tag{14}$$

$$\left|\frac{N}{N_{eff}} - \frac{M+Ne_N}{M_{eff}}\right| = 1 \tag{15}$$

The difference is represented by the introduction of the "effective" parameters of the cross-sections. In particular this means that the relevant parameter is calculated by taking into account not the whole section, but only the contributing portion. The procedures to determine how to calculate these quantities are not reported here for the sake of brevity.

For the purposes of the present work it is enough to define $N_{eff} = A_{eff} f_y$ and $M_{eff} = W_{eff} f_y$ as the effective limit of axial force and limit bending moment of the effective cross-section. The parameter e_N is the eccentricity of the application point of the axial force. On the other hand, it is useful to cite how the plastic domain can be built, even though for the further discussion of the present work reference will be made to the elastic one. Regarding the plastic domain represented in Figure 3.4b, the analytical expressions are the following:

$$\left|\frac{N}{N_{pl}} + (1 - 0.5a)\frac{M}{M_{pl}}\right| = 1 \quad (16)$$

$$\left|\frac{N}{N_{pl}} - (1 - 0.5a)\frac{M}{M_{pl}}\right| = 1 \quad (17)$$

$$\left|\frac{M}{M_{pl}}\right| = 1 \quad (18)$$

The quantities $N_{pl} = A\, f_y$ and $M_{pl} = W_{pl}\, f_y$ are the plastic limit of the axial force and of the bending moment. The parameter a is a dimensionless quantity that evaluates the contribution of the web to the whole cross-sectional area and can be written as:

$$a = \left(A - 2bt_f\right)/A \quad (19)$$

The variable n is a dimensionless measure of the axial force, and represents the length of the plateau portion of the plastic domain of Figure 3.4b, and can be obtained by combining Eq. (16) and Eq. (18):

$$n = \frac{N}{N_{pl}} = 0.5a \quad (20)$$

As a consequence, considering that following the cited code the equality $a \leq 0{,}5$ must be respected, it follows that n results: $n \leq 0{,}25$. A more precise way to describe the limit domains can be obtained by considering the limit value of the axial and of the bending forces as depending on the position of the neutral axis, and not simplified as included in the cited codes.

For the generic cross-section, there are three possible positions of the neutral axis intersecting it: on the web, on the weldings or on the wings. Having z_n, as the z coordinates of the neutral axis, for the web (Fig. 3.5a) it will be:

$$0 \leq z_N \leq \frac{h_i}{2} - t_{f,i} - r \quad (21a)$$

$$N_u = 2\, t_w\, z_n\, f_y \quad (21b)$$

$$M_u = W_{pl,i}\, f_y - t_w\, z_n^2\, f_y = f_y\left[b\, t_f\left(h - t_f\right) + t_w\left(\frac{h}{2} - t_f\right)^2 + 2\, r^2\left(\frac{h}{2} - t_f - \frac{r}{3}\right) - t_w z_n^2\right] \quad (21c)$$

While for the welding area (Fig. 3.5b):

$$\frac{h}{2} - t_f - r \leq z_n \leq \frac{h}{2} - t_f \tag{22a}$$

$$N = \sigma_0 \left[2t_w z_n + 2\left(z_n - \frac{h}{2} + t_f + r \right)^2 \right] \tag{22b}$$

$$M = \sigma_0 \left\{ b\, t_f (h - t_f) + \left[t_w + 2\left(z_n - \frac{h}{2} + t_f + r \right) \right] \left(\frac{h}{2} - t_f - z_n \right) \left(z_n + \frac{h}{2} - t_f \right) + \left(\frac{h}{2} - t_f - z_n \right)^2 \left[2z_n + \frac{4}{3} \left(\frac{h}{2} - t_f - z_n \right) \right] \right\} \tag{22c}$$

And eventually for the section wings (Fig. 3.5c) the analytical formula are:

$$\frac{h}{2} - t_f \leq z_n \leq \frac{h}{2} \tag{23a}$$

$$N = \sigma_0 \left[A - 2b \left(\frac{h}{2} - z_n \right) \right] = \sigma_0 \left[t_w (h - 2t_f) + 2r^2 + 2b\, t_f - 2b \left(\frac{h}{2} - z_n \right) \right] \tag{23b}$$

$$M = b\sigma_0 \left(\frac{h^2}{4} - z_n^2 \right) \tag{23c}$$

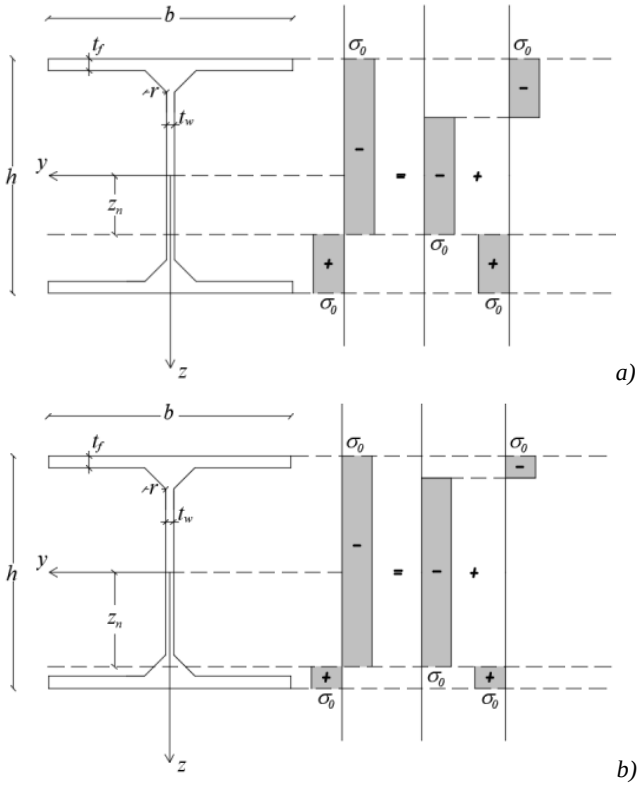

a)

b)

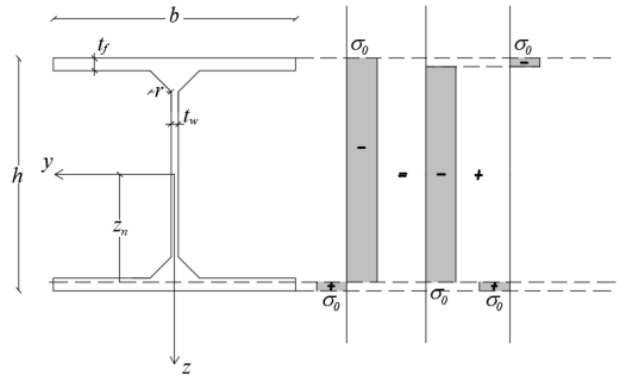

Figure 3.5 – Limit condition for the cross section; a)neutral axis on the web; b) neutral axis on the welded portion; c) neutral axis on the wing.

By using the above reported formulation to describe the limit domain of the cross section it is possible to draw the exact $N - M$ limit boundary for the positive quarter of the strength domain.

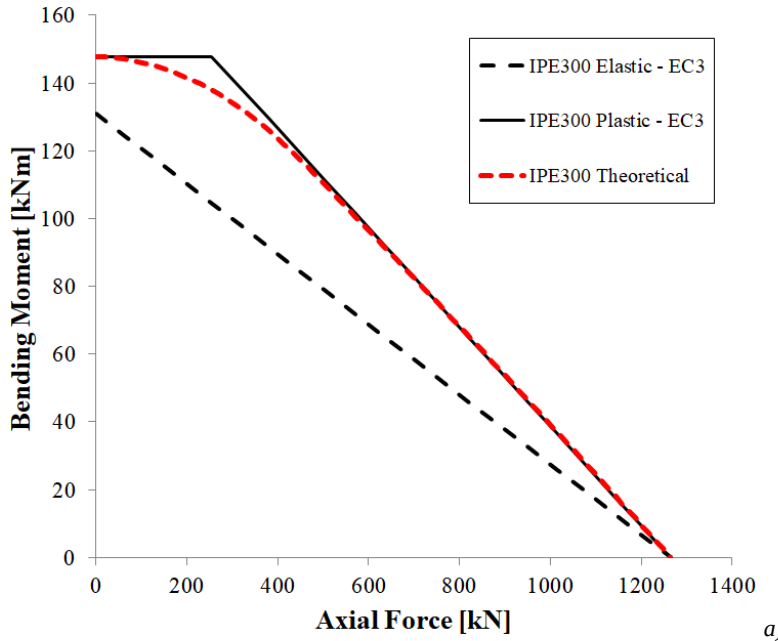

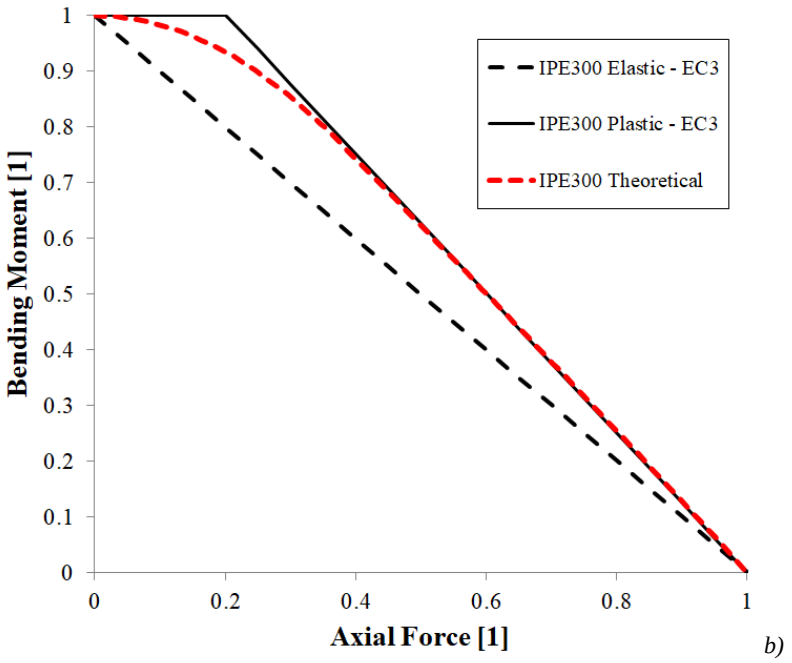

b)

Figure 3.6 – a) IPE300 limit domains comparison; b) IPE300 adimensional limit domains comparison.

Analogously it is possible to widen the domain defined by taking into account the shear forces. In this case, for sake of simplicity just the elastic domain will be defined. Taking again as a reference the typical I-shape cross-section, the limit axial force, shear force and bending moment can be defined as follows:

$$N^E = Af_y; \quad T^E = \frac{f_y J_y c}{2S'_y(G)}; \quad M^E = W_y^E f_y \tag{24}$$

where the superscript "E" stands for elastic limit, $S'_y(G)$ is the static moment of the half cross-section with respect to the y axis and c is the web thickness. To define T^E the shear limit stress on the section was assumed to be $\tau_b = f_y/2$ in compliance with the Tresca yield criterion, which has been chosen as a reference for the following formulation. The domain that involves the three forces cited can be built by considering them coupled and combining their limit analytical functions. In this way it will be, for the $N - M$ plane:

$$\frac{N}{A} + \frac{M}{W_y^E} = f_y \tag{25}$$

considering that $0 \leq N \leq N^E$ and $0 \leq M \leq M^E$ for the first quarter. The others can be derived imposing the symmetry with respect to the two axes (as visible in Figure 3.7).

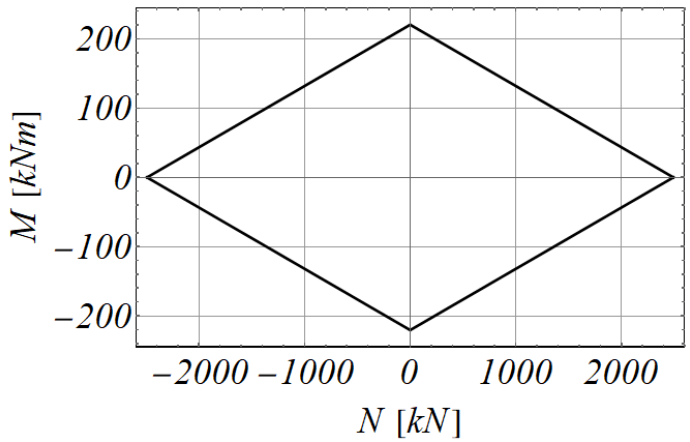

Figure 3.7 – N - M domain for an HEB240, S235 steel grade.

In the same way, for the $N - T$ interaction, the elastic limit can be drawn by following the function:

$$\left(\frac{N}{A}\right)^2 + 4\left[\frac{T\, S_y'(G)}{J_y c}\right]^2 = f_y^2 \tag{26}$$

Always stating $0 \leq N \leq N^E$ and $0 \leq T \leq T^E$ for the positive quarter, and symmetrically to the $N - T$ axes for the other three (Figure 3.8).

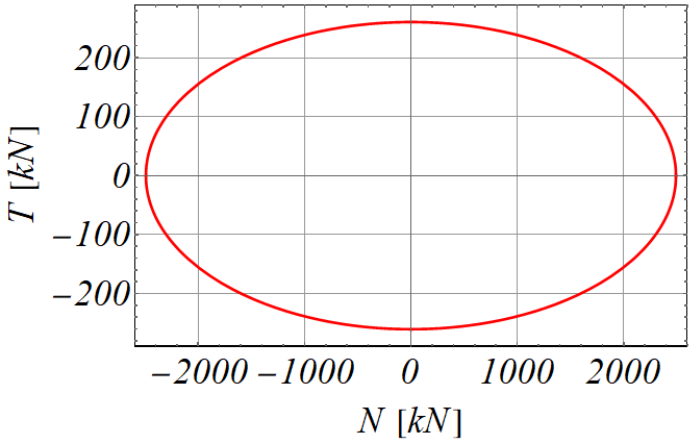

Figure 3.8 – N-T domain for an HEB240, S235 steel grade.

In the case of the $T-M$ elastic boundary, taking into account the maximum flange stress, it will be described by the function:

$$\left(\frac{M}{W_y^E}\right)^2 + 4\left[\frac{TS_y'(E)}{J_y c}\right]^2 = f_y^2 \tag{27}$$

holding for $0 \le T \le T^E$ and $0 \le M \le M^E$. In this case the set limit for the shear and bending moment values can be obtained by solving an optimization problem. This problem is based on the minimization of a suitable objective function that describes the minimum bending moment, i.e.:

$$\min_{(z)} M \tag{28a}$$

$$\left(\frac{M}{J_y} z\right)^2 + 4\left[\frac{\overline{T}S_y'(z)}{J_y c}\right]^2 \ge f_y^2 \tag{28b}$$

$$0 \le z \le \left(\frac{h}{2} - t_f\right) \tag{28c}$$

This relationship is valid for an assigned discrete list of values of shear force $\overline{T}$, and is still in compliance with the range $0 \le \overline{T} \le T^E$. As before, the remaining quarters can be obtained symmetrically with respect to the $T-M$ axes (Figure 3.9).

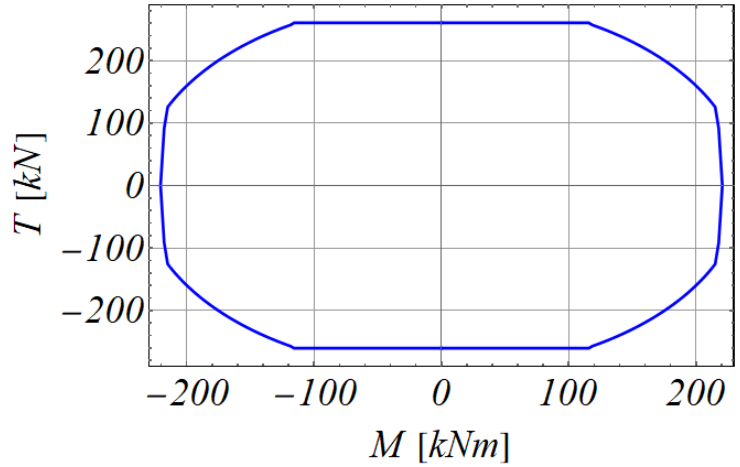

Figure 3.9 – M - T domain for an HEB240, S235 steel grade.

The bonudary surface for the first $N-T-M$ octant can be defined by combining the function:

$$\left(\frac{N}{A}+\frac{M}{W_y^E}\right)^2+4\left[\frac{\overline{T}S_y'(z)}{J_y e}\right]^2=\sigma_b^2 \tag{29}$$

which represents the maximum stress value of the flange, and provides a discrete set of functions $N-M$ related to the relevant discrete set of values for $\overline{T}$, respecting $\left(0\le\overline{T}\le T^E\right)$, and the discrete set of values of axial force, shear force and bending moment obtained by solving the minimum problem:

$$\min_{(z)} T \tag{30a}$$

$$\left(\frac{\overline{N}}{A}+\frac{\overline{M}}{J_y}z\right)^2+4\left[\frac{TS_y'(z)}{J_y a}\right]^2\ge\sigma_b^2 \tag{30b}$$

$$0\le z\le\left(\frac{h}{2}-e\right) \tag{30c}$$

for a prefixed discrete set of couples of values of $\overline{N}$ and $\overline{M}$, with $0\le\overline{N}\le N^E$ and $0\le\overline{M}\le M^E$. The remaining domain octants can be completed symmetrically with respect the coordinate system showed in Figure 3.10.

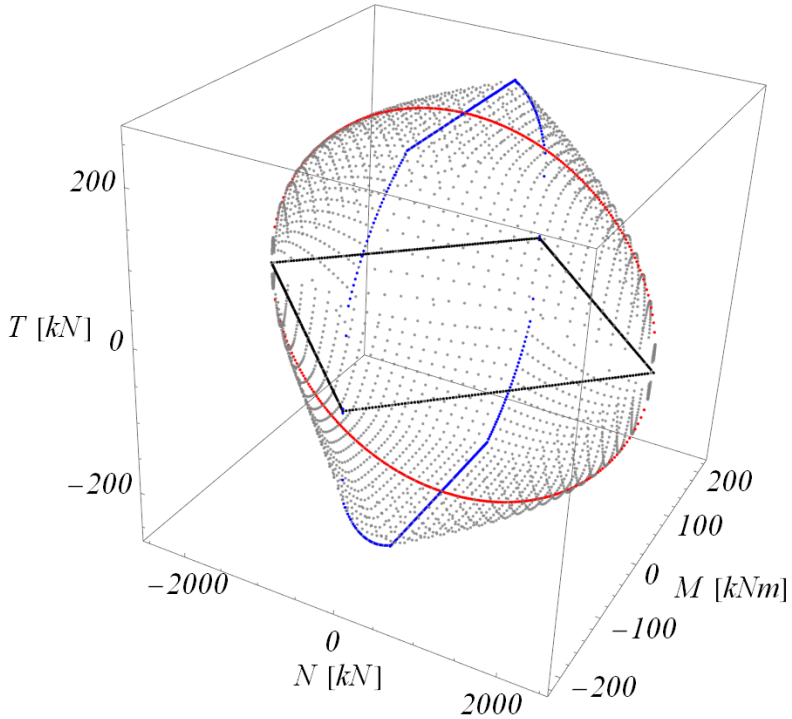

Figure 3.10 – N-T-M spatial domain for an HEB240, S235 steel grade.

After the definition of the proper strength domains for the adopted cross-section it is possible to move into the description of the design process and on the calibration of the suitable device geometry. For this purpose in the next section the optimal problem will be described, specifying the relevant constraints and assumptions made for its assessment.

3.4 - Optimal design

Different geometrical quantities have a significant influence on the functionality and on the efficacy of the device. As previously remarked, these quantities play a role in determining the mechanical and kinematical behaviour of the device.

In some cases these parameters can be defined through simple linear equations (such as the geometrical boundaries), while in some other cases they require non-linear equations for their evaluation (e.g. the elastic/plastic modulus or the moment of inertia). This makes the design of the device hard to accomplish by simply using the same tools that usually are common in civil engineering design procedures. In order to guarantee the features described at the beginning of this chapter in this device, a suitable and reliable optimal design problem must be developed.

Before delving into the description of the optimization framework it is necessary to briefly summarise the main goals that are expected from the prcedure. The designed device:

- must be as short as possibile. In order to work as a “plastic hinge” and to concentrate the plasticization in a relatively little part of the beam. Moreover, the hinge section must not be far from the connection interface with the column;
- must guarantee the possibility to independently set its limit strength and its flexural stiffness;
- must show the minimum possible volume. This with the aim of limiting the structural mass and avoiding excessive thicknesses;
- must not present significant geometrical discontinuity that can cause stress concentration and thus unpredictable ways of failure;

- must not be subjected to unpredicted local buckling phenomena, thus the class of the cross-section has to be taken into account in the design.

In general, an optimization problem is based on the definition of an objective function to be minimized or maximized depending on the purpose and on the strategies adopted in the design. In addition, the parameters previously discussed become the variables of the problem, and they must fulfill a series of requirements imposed to the problem in terms of the constraints.

The generic optimization problem can be summarized as follows:

$$\min_{(\boldsymbol{x})} f(\boldsymbol{x}) \tag{31a}$$

$$\boldsymbol{x}_{lb} \leq \boldsymbol{x} \leq \boldsymbol{x}_{ub} \tag{31b}$$

$$\boldsymbol{A_{eq}}\boldsymbol{x} \leq c_{eq} \tag{31c}$$

$$\boldsymbol{A_{in}}\boldsymbol{x} \leq c_{in} \tag{31d}$$

$$G_{in}(\boldsymbol{x}) \leq b_{in} \tag{31e}$$

$$G_{eq}(\boldsymbol{x}) = 0 \tag{31f}$$

Eq. (31 a-f) contain all the essential elements for the optimization procedure. Specifically: Eq. (31a) represents the minimization of the objective function that must be chosen; Eq. (31b) contains the boundaries of the design variables, where $\boldsymbol{x}_{lb}$ and $\boldsymbol{x}_{ub}$ are the lower bound and the upper bound vectors respectively; Eq. (31c) and (31d) are the linear equality and inequality constraints; equations (31e) and (31f) are the non-linear inequality and equality constraints.

The optimal procedure is based on an algorithm that, starting from the above mentioned problem, searches for the optimal solution in the domain as described by the boundaries and by the constraints. This algorithm is based on a non-linear programming solver, such as the “fmincon” function present in MatLab software. This function uses all the above mentioned elements in

order to return the minimum value of the objective function which satisfies, simultaneously, all the constraints.

Before moving onto the full explanation of the optimal problem, it should be specified that the actual objective of the research is that the theoretical assumptions and the numerical validation are made with reference to plane systems. As stated the influence of shear forces on the flexural limit behaviour is neglected for the sake of simplicity.

Generally, an I-shape cross-section, relies mainly on its wings for its flexural stiffness but also for its strength. It is clear, then, that the thickness of these portions, their internal level arm and their width play an important role in the overall characteristics of the device, both for the outer and for the inner portions.

In addition, in terms of stiffness, the length of the device is the quantity that mostly affects the kinematical behaviour, and must be taken into account in the optimization design procedure.

Excluding the above mentioned quantities, it can be stated that the web has a lower influence, and then, for the sake of simplicity, its thickness has been excluded from the design variables of the optimal problem, and it will be considered equal to the thickness of the steel beam connected to all of the three portions.

Another parameter which is usually neglected in traditional design of civil structures is the welding radius of the I-shape cross-sections. This part of the section can possess different shapes and its calculation can make the evaluation of the relevant properties of the section more difficult. For this reason it is easier to exclude it from the design variables vector and also from the analytical formulation for the optimal geometry research.

In the following parts of this section the various components of the optimization procedure are discussed.

First, it is important to define which one of the variables presented should be considered in this problem. Generally it is recommended to use only variables which are the strictly necessary, avoiding an excessive amount of them in the problem. By doing this it is possible to simplify the research of the optimal solution. The chosen design vector for the LRPD otpimal problem is:

$$\boldsymbol{x}^T = |t_{f,o} \quad t_{f,i} \quad \ell_o \quad b_i| \tag{32}$$

According to what is stated above, it looks clear what role is played by the parameters. The thicknesses create a bond to the line of reasoning about the resistance and the stiffness, and in particular the outer portion thickness $t_{f,o}$ acts with the goal of balancing the loss of flexural stiffness developed in the weaker inner portion, while the inner portion thikness $t_{f,i}$ is aimed at contributing to the limit bending moment reduction of the device. Analogously, the base width b_i acts in the same direction of the inner flange thickness reducing the capacity of the cross section, and on the other hand ℓ_o helps to balance the stiffness along with the outer flange thickness.

These variables are useful to calculate the objective function of the problem, that must be minimized in order to find the optimal solution. The chosen function is the volume of the overall device:

$$f(\boldsymbol{x}) = 2V_o + V_i \tag{33}$$

This decision derives from what was discovered while investigating[19] the influence of the different parameters that mostly represent a technological requirement, and that can lead to a reasonable geometry in terms also of spatial coherence and functionality. In this way it is possible to accomplish at the same time a small overall volume for the device and a low structural mass. This is also in compliance with the common measures for the dogbone techniques discussed in the relevant chapter, which, as stated, in the different

[19] On the post-elastic behaviour of LRPH connections. Benfratello et al. (2019).

international codes, usually develops in a length embedded between the height of the connected beam and its midpoint.

Once selected the variables and the objective function to be minimized, it is mandatory to define also a validity domain for the problem in order to limit the potentially infinite range of acceptable values for the solution. This can be made in terms of upper and lower bounds as expressed in the following equations:

$$\boldsymbol{x}_{lb}{}^{T} = |t_p \quad 0 \quad 0 \quad 3\,t_w| \tag{34a}$$

$$\boldsymbol{x}_{ub}{}^{T} = |h/2 \quad t_p \quad +\infty \quad b| \tag{34b}$$

These bounds are related to reasonable and desired geometrical features and behaviour expected from the device. In the first column of the two vectors, for example, in order to balance the stiffness loss caused by the reduction of the inner portion with respect to the beam, the thickness $t_{f,o}$ must not be lower than the commercial beam flange's thickness (t_p), and must not be greater than the half of its height (for obvious geometrical reasons). For analogous reasons, the inner flange thickness $t_{f,i}$ can not exceed t_p, and the internal base width must be greater than welding length added by the web thickness, and lower than the connected cross-section's base width. In the third column, the outer portion length does not present any particular boundary, but it is a crucial variable in order to balance the loss of stiffness present in the inner portion. On the other hand, the inner length is fixed, and is related to the height of the connected beam element through a scalar parameter β, that is commonly in the range $0.5 \leq \beta \leq 1$. This is to ensure that the inner part will fully plasticize, and it has been proved[20] that as range of values it is suitable for the purpose.

After the definition of the proper variable vector, of the objective function, and of the boundaries of the problem, it is mandatory to discuss the

[20] On the post-elastic behaviour of LRPH connections. Benfratello et al. (2019).

constraints to apply to the optimization problem. The reference for their assessment and writing is made to the requirements listed at the beginning of this section and those cited when defining what the LRPD represents. Therefore, the logical pattern followed was to define the technological or mechanical features desired from the device, and describe it in analytical terms. The choice of assigning a specific constraint as linear or non-linear, as equality or disequality, depends also on the techonological requirements that form the basis of its purpose.

Starting from the linear constraint it is possible to write:

$$A_{eq} = |1 \quad 0 \quad 0 \quad 0| \tag{35a}$$

$$c_{eq} = |H - h^*| \tag{35b}$$

It is useful to ensure the presence of a single common plane for the outer and inner portion wings. Another core goal of the focused optimization procedure was to obtain, at the end of the process, a device with a specific class-section to prevent local buckling phenomena. This is possibile by choosing:

$$\boldsymbol{A}_{in}{}^{T} = |0 \quad -18\,\varepsilon \quad 0 \quad 1| \tag{36a}$$

$$c_{in} = 3\,t_w \tag{36b}$$

Where:

$$\varepsilon = \sqrt{\frac{235}{f_y}} \tag{37}$$

In Eq. (37) ε represents a suitable coefficient that depends on the yielding strength of material, f_y. This last constraint derives from the Italian code about the I-shape flange for Class 1, which states:

$$\frac{c}{t} \leq 9\varepsilon \tag{38}$$

Considering $c = b/2 - 3t_w/2$, and assuming $t = t_{f,i}$. The minimization of this ratio helps in preventing the local buckling of the whole element because of the resulting lower slenderness of the section flanges.

The balance of the flexural stiffness is accomplished in compliance with what was discussed in Section 3.2, and particularly in Eq. (9), Eq. (10), and Eq. (11). Therefore:

$$\boldsymbol{G}_{in} = \frac{\ell_i}{\ell_o} - 2\frac{J_i}{J_o}\left(\frac{J_o - J_p}{J_p - J_i}\right) \tag{39a}$$

$$q_{in} = 0 \tag{39b}$$

The last constraint to be imposed is related to the limit strength assigned to the inner portion of the device, and corresponds to the crucial parameter to make the LRPD behave like a common RBS device. Considering again what was discussed in terms of the mechanical model, the simultaneous presence of the axial force and of the bending moment must be taken into account for a correct evaluation of the limit resistance of the device, and their values represent an input data.

The starting value for choosing the limit resistance of the devices are the axial and bending forces. All of the $N - M$ couples that can be chosen correspond to a position of the neutral axis, which as stated in Section 3.2 can intersect the web, the welding radius and the wings. To simplify the model and the calculation, and considering that the welding radius can be neglected due to its relatively low contribution, it will also be neglected in the discretization of the region where the neutral axis can be placed. There will be, then, just two possibilites: neutral axis intersecting the web and neutral axis intersecting the wings.

For the first case its position can be identified by writing:

$$z_n = \frac{N_a}{2\, t_w\, f_y} \tag{40a}$$

And the limit reported in Eq. (31f) can be written as:

$$G_{eq} = f_y\, W_{pl,i} - \frac{N_a^2}{4\, t_w\, f_y} - M_a \tag{40b}$$

On the other hand, when the neutral axis intersects the wings, the same relations become:

$$\boldsymbol{z_n} = \frac{N_a}{2\, b_i\, f_y} - \frac{A_i}{2\, b_i} + \frac{h^* + t_{f,i}}{2} \tag{41a}$$

$$\boldsymbol{c_{eq}} = b_i\, f_y \left[\frac{\left(h^* + t_{f,i}\right)^2}{4} - \frac{N_a}{2\, b_i\, f_y} - \frac{A_i}{2\, b_i} + \frac{\left(h^* + t_{f,i}\right)^2}{2} \right] - M_a \tag{41b}$$

The reference in terms of original strength has been made to the plastic resistance modulus instead of the elastic one, considering that it represents the limit condition reachable by the device. In some cases, the elastic resistance modulus can be beneficial to be adopted instead of the plastic one, and this can happen for example to take into account higher tolerances for the development of the plastic hinge or when more devices are used at once. For design purposes it is more helpful to control the hinge behaviour in the beginning instead of the limit behaviour.

In practical cases, analogously to the dogbone and to the other RBS strategies previously mentioned, the strength reduction obtained through the constraints of Eq. (38) and Eq. (39) can involve a strength reduction between 10% and 50% with respect to the original strength of the structure. It has been studied that percentages under the lower value reported (as is the case of input forces values too close to the limit thresholds) can lead to negating the contribution of the device in the element where it is placed. On the other hand a higher strength reduction (with low input forces) can lead the procedure to find solutions physically unconvenient or inconsistent, e.g. the thicknesses is too high or too low, or unrealistic lengths. This error can be the equivalent of a wrong profile choice made in the design phase.

Concluding, by choosing reasonable inputs for the problem, such as the connected commercial beam element, forces and the material, and by utilizing the previous reported methodology, it is possible to obtain, as an output, the design variable values that minimize the objective function. Before moving onto the validation of this procedure something must be said about some technological aspects of the device's utilization.

3.5 - Technological aspects

One of the most crucial aspects in the characterization of the device is represented by the connection between it and the other structural elements. This, currently, is only an issue which will briefly mentioned, and it will be properly addressed in further studies and in further experimental applications. In Figure 3.11 the first LRPD samples are shown. To connect the device to the column, and to the other beam elements, suitable screws are welded directly on its end plates. The column-side features a pierced welded end flange to host the bolt screws, or the device can be connected directly to the wings of the column if they are suitably pierced.

Figure 3.11 – Sample of LRPD devices with welded screws.

In Figure 3.12 is possible to note how the typical beam-to-column connection with the device is imagined. As discussed, the column wing shows the holes to host the device screws. The other side, on the contrary,

can presents a simple welded flange used to host the beam section size (as cited, characterized by the same overall dimension as the device itself). These features are therefore obtained during the manufacturing process.

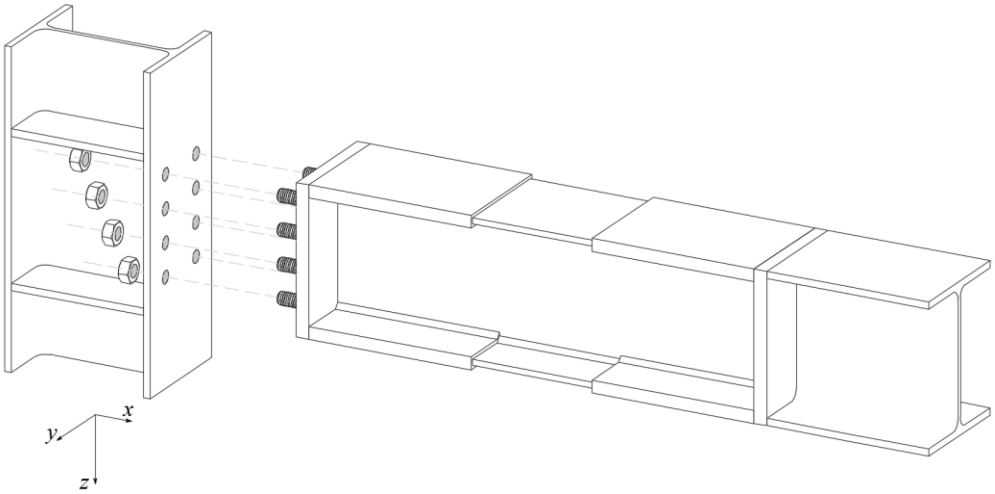

Figure 3.12 – Typical beam to column connection of the LRPD device.

The idea of considering this type of union with this geometry derives from the desire to maintain a limited volume, and to not exceed the overall cross-sectional sizes of the connected element. By ensuring this, in terms of a practical application, the positioning of the device would cause no geometrical inconvenience. In particular, the welded side can be assumed to be a proper moment resisting connection which guarantees the consequent kinematical behaviour. The bolted side, considering the positioning directly on the column, permits to the bolted flange to be assigned greater dimensions if required, permitting also the same suitable behaviour on this other side. In addition, to weld the device-beam couple directly during the manufacturing process is helpful in order to reach higher levels of precision and reliability in the samples produced.

In the ideal scenario, the LRPD should be built using a high precision process, such as 3D printing for steel or a numerically controlled welding procedure. The cited procedures, however, are commonly used in industrial

or higly standardized processes, therefore, in the experimental activities conducted during this research, the samples were realized by means of traditional steel manufacturing techniques.

This involves the device being constructed by simply cutting plates and welding them togheter in order to realize the desired geometries. The first attempts showed that this method causes the resulting samples to exhibit a lot of uncertainties and variability. These can be attributed to the thermal deformations that the welding procedure causes in the elements, especially considering their limited thicknesses, or in the intrinsic level of uncertainties of a substantially “handmade” process, and so on. To fix these issues, little can be done, even though for the inner portion the uncertainties can be reduced by obtaining the reduced thickness by means of a lathe manufacturing process instead of the common plates cutting and consequent welding processes. By doing this it is possibile to accomplish a reduction of the the possible misalignments of the medium planes between the outer/inner portions.

CHAPTER 4 – APPLICATIONS

The previous chapters discussed, in detail, different aspects which were useful to deepen our knowledge of and to better understand how the LRPD works. Furthermore, the previous sections also describe the motivation and the reasoning behind the LRPD's conception. A detailed initial discussion of the scenario where the proposed device can be applied, before moving onto the explanation of the different competiting devices which are present in literature. A full description of the device was also reported in order to better grasp the reasoning behind its design process while allowing the reader to better understand the context surrounding the discussion of the LRPD's conception. By means of an optimization procedure which was presented and examined in detail, in this chapter the evaluation of the efficacy of the proposed device is discussed. Thanks to different applications it will be possible to evaluate if the LRPD resulting from the previous discussions works as predicted and the possible side-effects that its use can cause in the structures where it is present.

In summary, in the following chapter the two following points will be discussed:

- LRPD in steel frames, in the case of normal bidimensional beam structures (making the device acts like a special RBS device);
- LRPD in masonry buildings, inserting it into masonry openings reinforcing frames (usually designed to meet only the stiffness requirements).

But before delving into these specific tasks, it is useful, and in a certain way mandatory, to test the device starting from its design model and its simplest load configurations. In the following sections how the device works

will be thoroughly evaluated by means of a dimensioning procedure and numerical analyses.

4.1 - Model validation

For a device which relies mainly on its flexural features to fulfill the purposes it was designed for, the most simple scenario to consider in order to analyze its behaviour, and to validate it, is the constant bending moment load condition (pure bending). In this case the flexural stress is constant along all the longitudinal axes of the beam that hosts the device. Therefore, by reducing the resistance of the element this quantity can be found, and used as an input for the previously discussed optimal problem.

In research, as well as in practical situations, being able to have a simplified version of the problem is always a good approach. This permits some qualitative and quantitative information about the designed system to be known, and also allows to validate the theory behind that system. The simplified model can be used to dimension the device, but also to conduct experimental proofs and to better understand the behaviour and what to expect from it.

In order to accomplish this validation, and in lieu of more realistic and accurate analyses, it is useful to conduct numerical simulations about the device adopting a simplified version of the optimal problem proposed and, consequently, a simplified loading condition. These analyses are developed with FEM software, specifically, Simulia Abaqus, which after the modelling and processing phases permits the manipulation and visualization of the output of the simulation.

The steel sections utilized are the same as those used in practical situations, and in particular HEA and IPE profiles will be considered. The

choice of taking into account two types of I-shaped beam elements are due to their differences: in HEA beams, its height and its base width are equal, while IPE presents a higher height compared to the base width. The different shape ratio causes small differences in their behaviour. For instance, for typical bending elements, such as a beam or a cantilever, an IPE can be profitably used, while for a column a HEA or a HEB are more preferable.

In the following section HEA200, HEA300, IPE200 and IPE270 will be subjected to an increasing constant bending force in order to obtain the related moment-curvature diagram. This is useful to make the device reach its limit condition, and to monitor if the plasticity spreads properly through the height of the cross-section by observing the distribution of its internal stresses.

The material is a S235 steel (which means 23,5 kN/cm^2 of yielding stress), with an elastic modulus of $E = 210.000$ MPa and a elasto-plastic $\sigma - \varepsilon$ relationship. The device is designed as completely fixed on one side, and subjected to a pure bending moment on the oppposite one. The samples chosen can be distinguished by their strength reduction (described through the scalar coefficient $\alpha = W_{pl,i}/W_{pl,}$), and by the ratio between the inner portion length and the height of the cross section, β. Utilizing the above reported parameters as the input to the optimal problem, and the relevant quantities of each cross-section adopted, the sample studied for this first proof can be summarized in Table I.

Table I – Optimal design of the samples considered. Dimensions in cm.

	HEA200			
β	0.75		1	
α	0.5	0.8	0.5	0.8
h^*	16.9286	17.1233	16.9286	17.1233
$t_{f,o}$	2.0714	1.8767	2.0714	1.8767
$t_{f,i}$	0.4892	0.8628	0.4892	0.8628
ℓ_o	22.2089	6.6138	29.6119	8.8184
ℓ_i	15.0000	15.0000	20.0000	20.0000
ℓ_{tot}	59.4179	28.2276	79.2238	37.6368

	HEA300			
β	0.75		1	
α	0.5	0.8	0.5	0.8
h^*	26.0722	26.3381	26.0722	26.3381
$t_{f,o}$	2.9278	2.6619	2.9278	2.6619
$t_{f,i}$	0.6914	1.2132	0.6914	1.2132
ℓ_o	32.2653	9.5248	43.0204	12.6998
ℓ_i	22.5000	22.5000	30.0000	30.0000
ℓ_{tot}	87.0306	41.5497	116.0408	55.3995

	IPE200			
β	0.75		1	
α	0.5	0.8	0.5	0.8
h^*	18.0285	18.2283	18.0285	18.2283
$t_{f,o}$	1.9715	1.7717	1.9715	1.7717
$t_{f,i}$	0.3458	0.7097	0.3458	0.7097
ℓ_o	21.8718	6.2328	29.1624	8.3104
ℓ_i	15.0000	15.0000	20.0000	20.0000
ℓ_{tot}	58.7436	27.4656	78.3247	36.6208

	IPE270			
β	0.75		1	
α	0.5	0.8	0.5	0.8
h^*	24.6166	24.8451	24.6166	24.8451
$t_{f,o}$	2.3834	2.1549	2.3834	2.1549
$t_{f,i}$	0.4133	0.8475	0.4133	0.8475
ℓ_o	28.4867	8.0062	37.9822	10.6750
ℓ_i	20.2500	20.2500	27.0000	27.0000
ℓ_{tot}	77.2234	36.2625	102.9645	48.3500

As is visible, two different levels of resistance reduction (0.5 and 0.8) and two different height/inner length ratios (0.75 and 1) were chosen, reaching sixteen samples. For all the samples a suitable optimal problem has been solved and consequently its functionality has been proved by means of a FEM analysis by using Abaqus, with the goal of constructing a moment-curvature diagram. The modelling in Abaqus is quite simple and multiple ways of doing it can be chosen. In the case reported a 3D model of the sample was developed using 3D CAD software (such as Autocad), and then the resulting model was exported in .SAT file format. In Abaqus it is possible to import this format of file, and it can be renamed and identified as a single "part" of the model, to which specific material and other desired features can be assigned. In the case of the commercial profile samples just two "parts" were defined (the beam element, created by solid extrusion of the starting

commercial cross-section, and the ending plate). Differently, in the case of LRPD samples, there were at least 4 parts: the two outer portions, the inner portion and the plate. The resulting parts, after their modelling, are tied together in the Abaqus environment with different boundary conditions. In this case, for instance, the connection between the plate and the rest of the sample is fully tied. As external boundary one of the two ends of the device is fully fixed in terms of degree of freedoms, i.e. each one of the possible displacements/rotations is forbidden.

The strategy of modelling different parts, and the way of joining them, can lead to different mesh discretizations, which do not always represent the best option in terms of reliability, cleanliness and efficacy of the analysis process. In terms of mesh dimension a reasonable choice must be made in order to balance the need of obtaining reliable analysis results with an affordable analysis time (and then computational cost). In the case of modelling thin plate steel elements, the choice of this size can not ignore the thickness of the discretized elements, and the strategy followed was to use this as minimum reference for the mesh dimension. For the model above, mesh dimensions between $3-10$ mm were utilized, resulting in 50.000/150.000 nodes (depending on the profile). Another parameter to define when using FEM simulations is the mesh shape. For simple geometry, such as cubes or parallelepipeds, the most regular and the best fit is reachable with a cubic mesh. In the case where the shape is characterized by irregularities or curved edges/corners, other geometries must be chosen for the mesh, such as the tetrahedrical one (utilized for the sample modelled). In Figure 4.1 an example of meshed model is reported. As visible, for different parts, different meshing techniques can be used in order to optimize the convergence and the mesh sizes, even though attention must be paid in the interface region, where an

accurate modelling must be done in order to ensure congruence of the mesh nodes for the different parts which are joined.

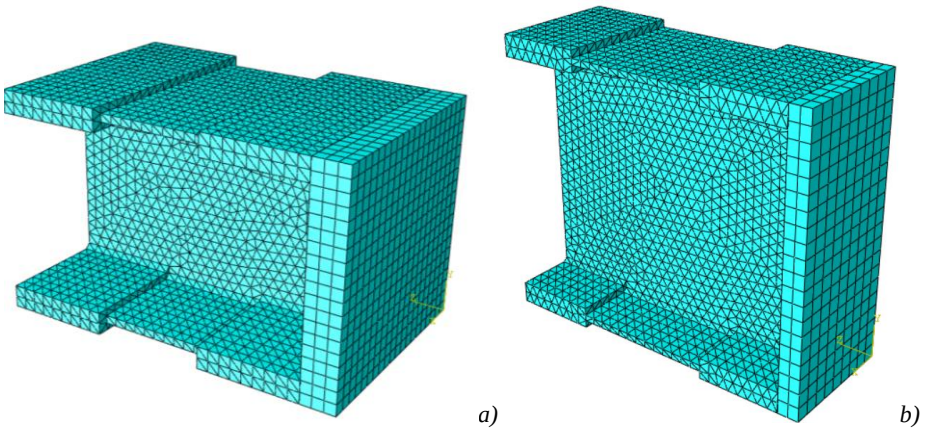

a) *b)*

Figure 4.1 – Mesh model of the LRPD; a) HEA mesh model; b) IPE mesh model.

In Figure 4.2 the digital model analyzed is reported and the applied load is specified. This model is composed of different elements, from the fixed side to the free end:

- first there is the part to be analyzed (characterized by commercial profiles or by the device itself). Its initial section is totally fixed, hence none of the degrees of freedom is allowed;
- subsequently there is a plate, with a suitable thickness, useful to redistribute the loads through the sample, reducing the presence of stress concentrations. Considering that what happens inside this part is not relevant for the purpose of the simulation, and to avoid its deformability having an influence on the analysis' results, the cited plate is composed by a material with a Young's modulus one thousand times greater than the common steel adopted. Furthermore, this plate is totally tied with the sample (full compatibility is guaranted);
- lastly, the load is applied as a linearly distributed pressure through the external face of the plate. The stress values' distribution derives from the

elastic Navier law for the rectangular section subjected to the plastic bending moment.

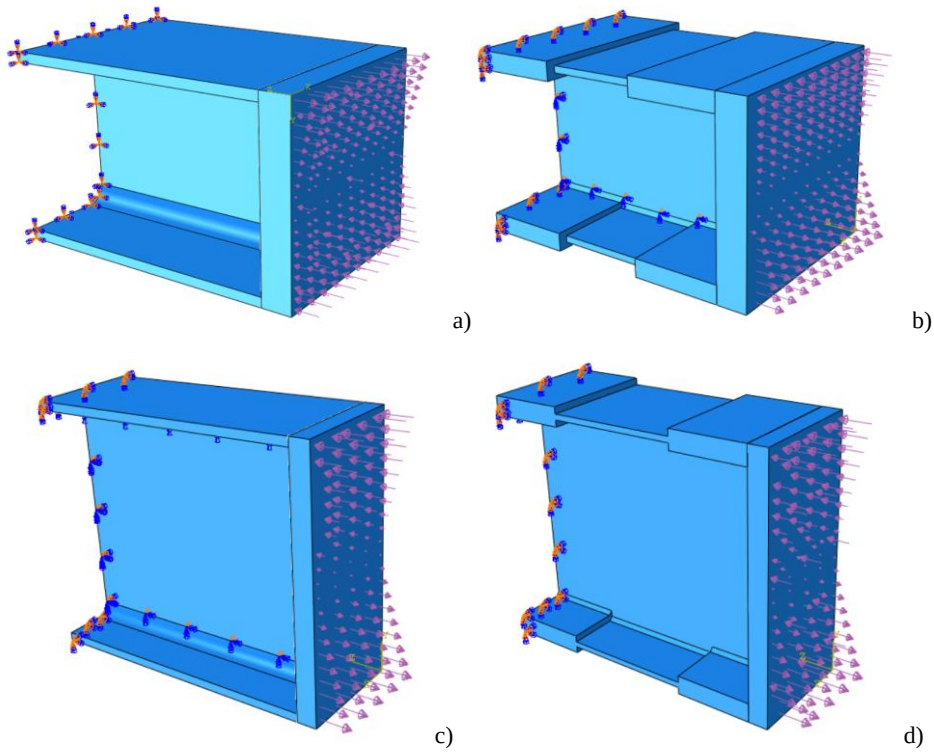

Figure 4.2 – Sample model configuration, load and boundary. a) HEA200; b) LRPD for HEA200; c) IPE200; d) LRPD for IPE270.

In particular the load follows a monotonic increasing law, which starts with a null value and ends with the assigned limit value (in this case it was fixed to be the plastic bending moment).

The first step consists of making a benchmark of the commercial profiles to compare the results from the samples equipped with the devices. Using these as a reference, and dimensioning the device with the properties listed in Table I, several models were created in order to be processed with Abaqus. Below the adimensional bending moment-curvature curves are reported, where by writing “theoretical” refererence is made to the unaltered commercial steel beam curve.

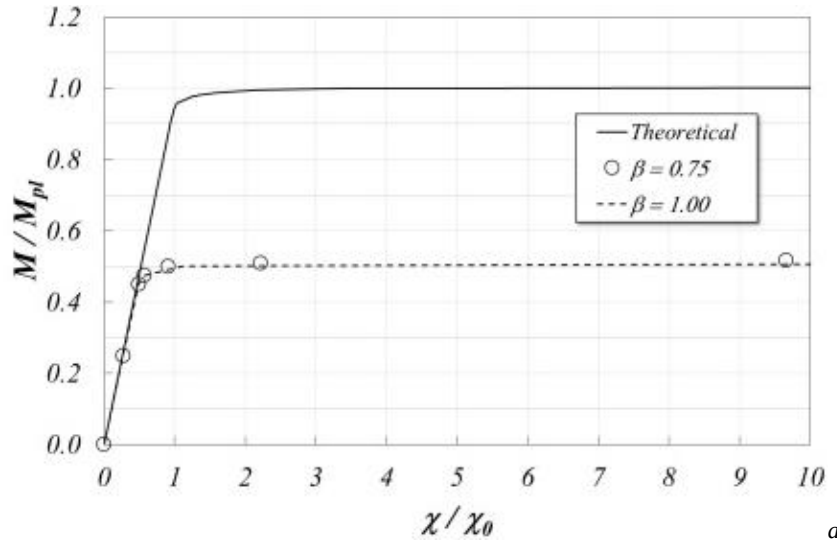

a)

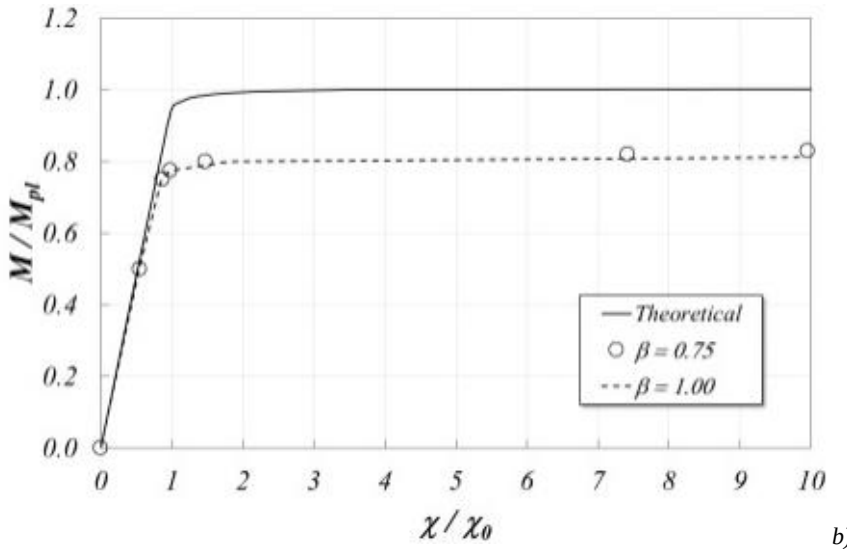

b)

Figure 4.3 – Adimensional bending moment – curvature diagrams for different values of α and β. a) HEA200 $\alpha = 0.5$; b) HEA200 $\alpha = 0.8$.

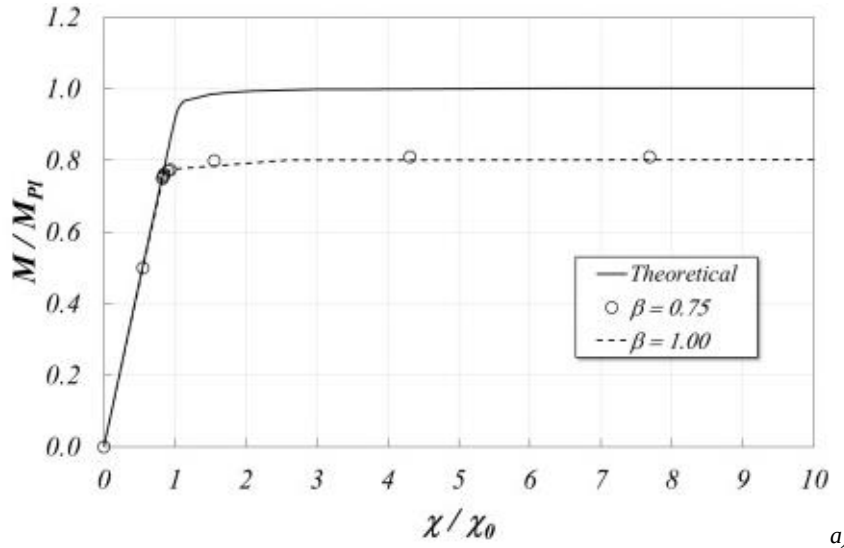

a)

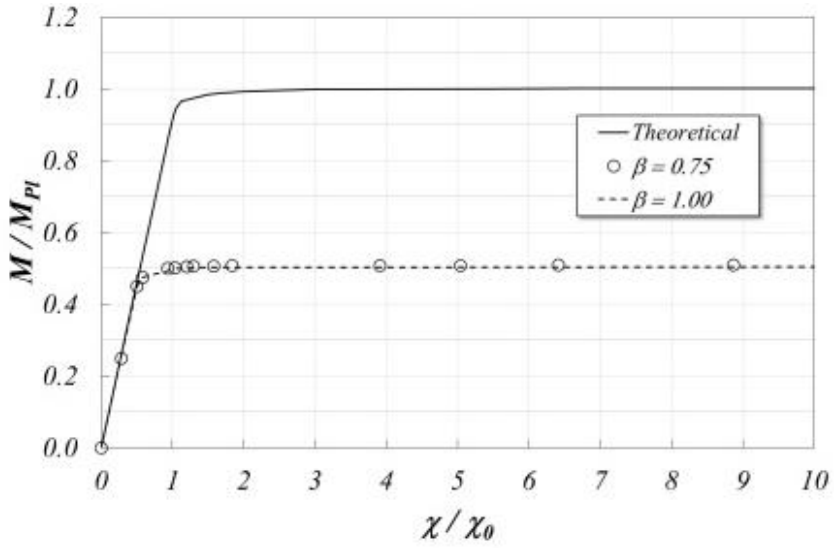

b)

Figure 4.4 – Adimensional bending moment – curvature diagrams for different values of α and β. a) HEA300 $\alpha = 0.5$; b) HEA300 $\alpha = 0.8$.

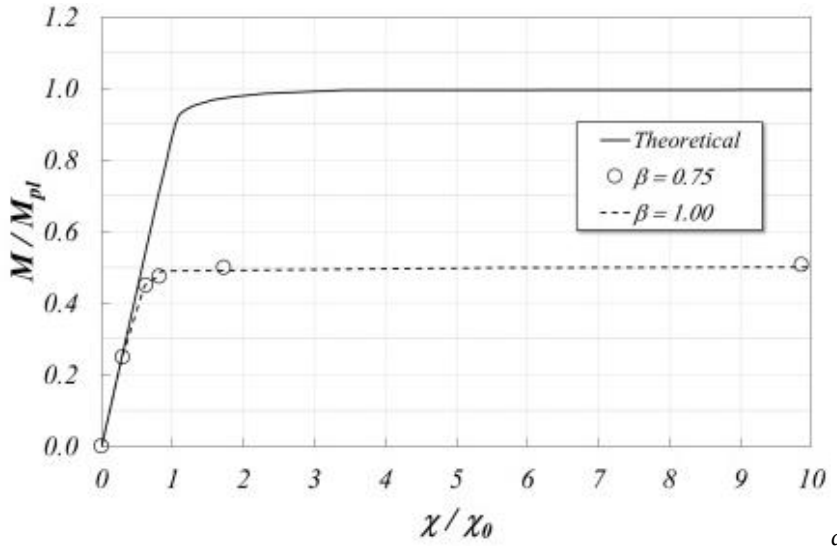

a)

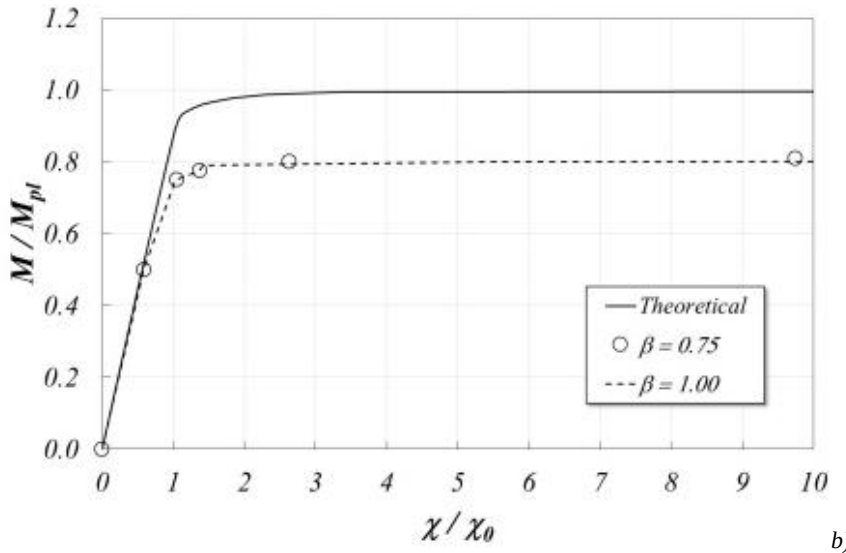

b)

Figure 4.5 – Adimensional bending moment – curvature diagrams for different values of α and β. a) IPE200 $\alpha = 0.5$; b) IPE200 $\alpha = 0.8$.

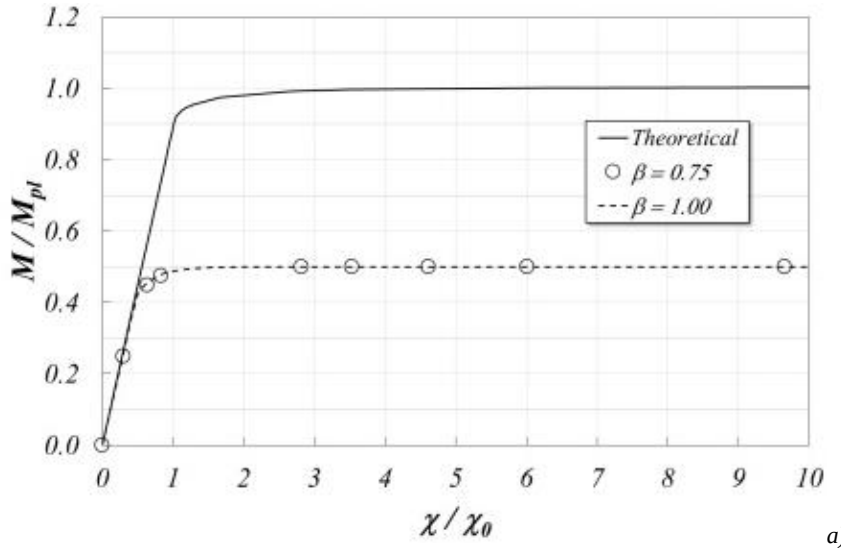

a)

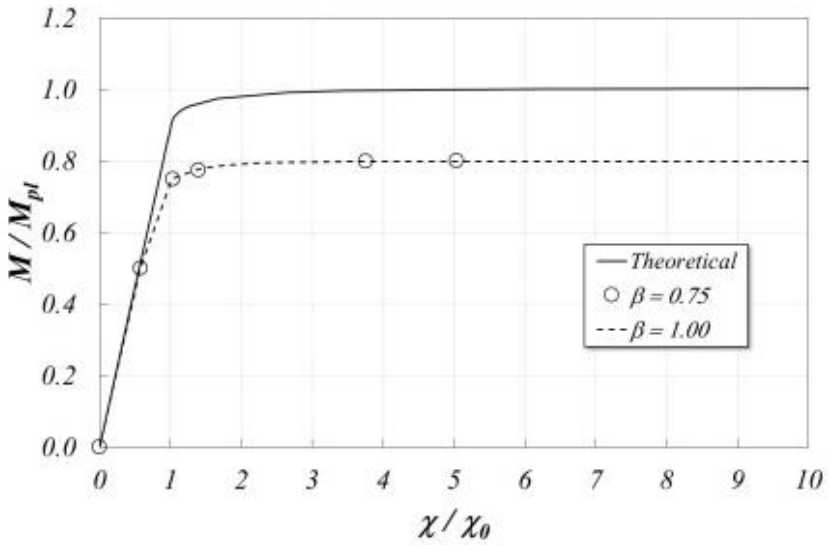

b)

Figure 4.6 – Adimensional bending moment – curvature diagrams for different values of α and β. a) IPE270 $\alpha = 0.5$; b) IPE270 $\alpha = 0.8$.

As shown by the results above the samples under investigation possess the exact behaviour desired in the design phase. This is demonstrated by two indicators that confirm the reliability of the model and of the procedure. The inclination of the linear portion, in the graphs, suggests that, in terms of elastic flexural stiffness, the behaviour of the samples fitted with an LPRD

are the same as the commercial samples (demonstrating the invariance of the stiffness properties of the connection as discussed in the previous sections); in addition, about its duties of reduced beam section, the features exhibited are satisfying, and is proved by the limit value assumed in the graphs, which tends to balance the scalar value assigned as input (when $\alpha = 0.5$ it will be that the limit adimensional bending moment will converge to 0.5 in the curve). The colour map of the Von Mises stress of the device at the load step that represents its strength limit value is presented to prove, graphically, that the inner portion undergoes plasticization.

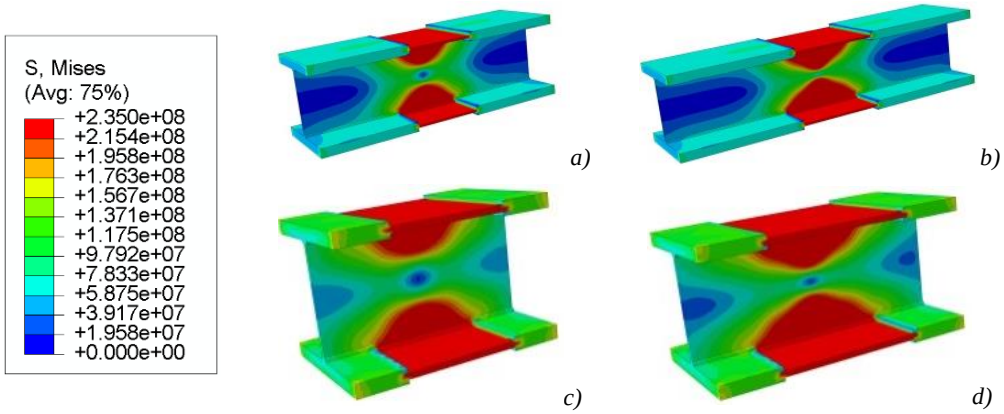

Figure 4.7 – Stress map (Von Mises) of the HEA200 equipped with LRPD [MPa].
a) $\alpha = 0.5$ *and* $\beta = 0.75$*; b)* $\alpha = 0.5$ *and* $\beta = 1$*;*
c) $\alpha = 0.8$ *and* $\beta = 0.75$*; d)* $\alpha = 0.8$ *and* $\beta = 1$.

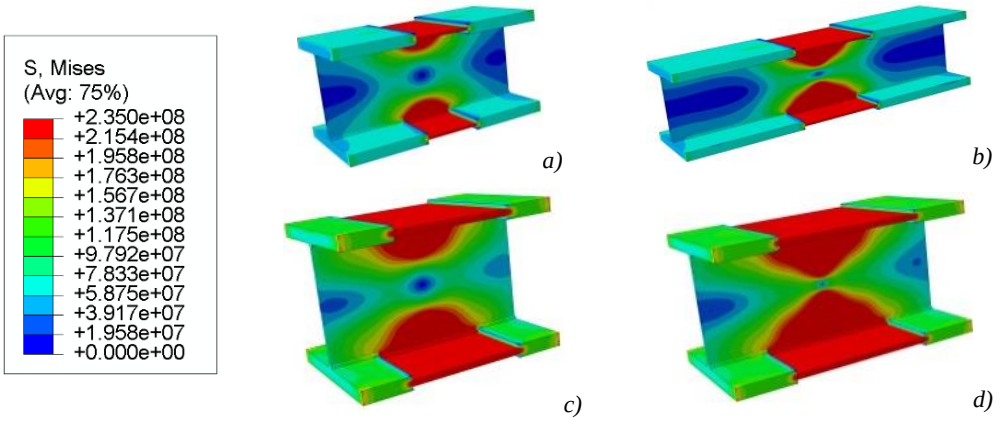

Figure 4.8 – Stress map (Von Mises) of the HEA300 equipped with LRPD [MPa].

a) $\alpha = 0.5$ *and* $\beta = 0.75$*; b)* $\alpha = 0.5$ *and* $\beta = 1$*;*

c) $\alpha = 0.8$ *and* $\beta = 0.75$*; d)* $\alpha = 0.8$ *and* $\beta = 1$.

Figure 4.8, above, shows that for HEA200 and HEA300 steel profiles the medium cross-section presents a null stress point on the baricentrical axis (the neutral axis) and full plasticization occurs in the wings. The plastic hinge is, therefore, fully formed even if it must be noted that for $\beta = 0.75$ plastic deformations are less developed than in the case of $\beta = 1$. This happens due to the greater length of the beam section. This hypothesis comes from the classical beam theory assumption that a reasonable value for the ratio between the length/cross-sectional height must be respected (considering the flexural nature of the theory itself). This slight difference can also be observed in Figures 4.3 and 4.4, where the $\beta = 0.75$ curves (the dotted ones) converge at a higher limit value.

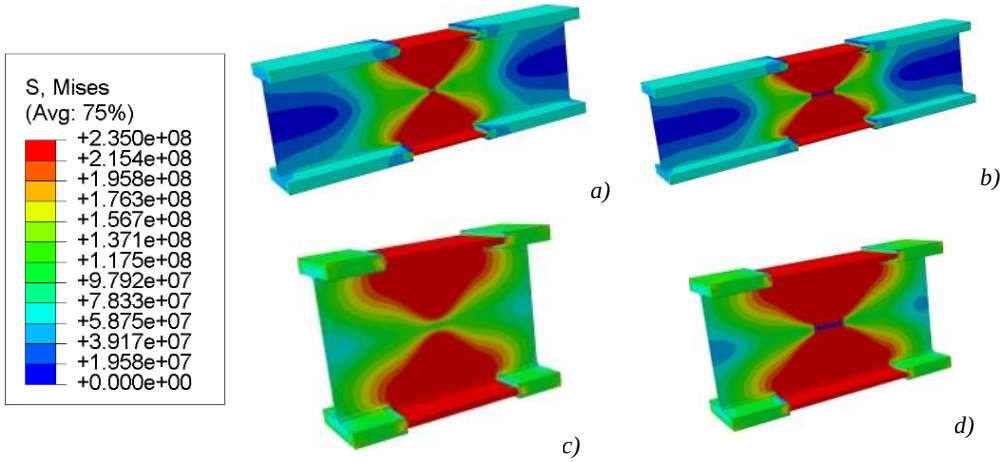

Figure 4.9 – Stress map (Von Mises) of the IPE200 equipped with LRPD [MPa].

a) $\alpha = 0.5$ *and* $\beta = 0.75$*; b)* $\alpha = 0.5$ *and* $\beta = 1$*;*

c) $\alpha = 0.8$ *and* $\beta = 0.75$*; d)* $\alpha = 0.8$ *and* $\beta = 1$.

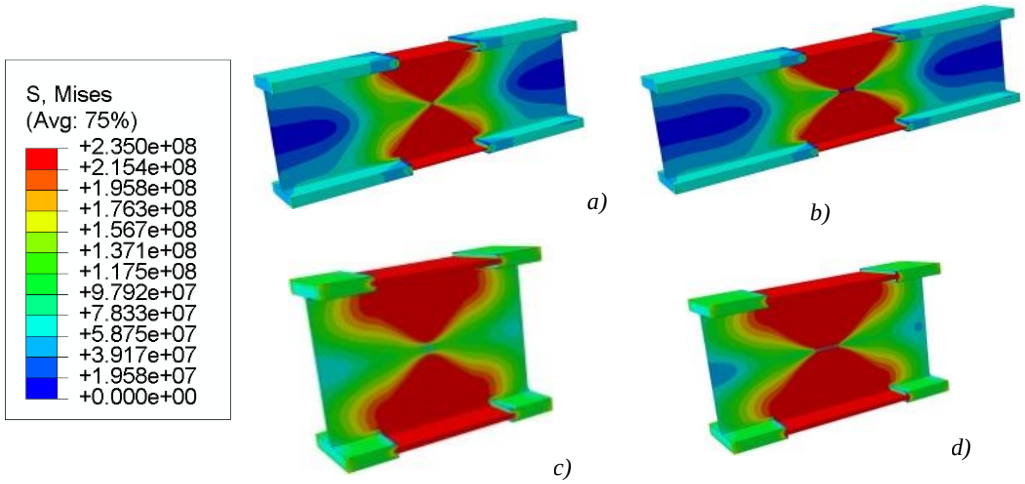

Figure 4.10 – Stress map (Von Mises) of the IPE270 equipped with LRPD [MPa].

a) $\alpha = 0.5$ *and* $\beta = 0.75$*; b)* $\alpha = 0.5$ *and* $\beta = 1$*;*

c) $\alpha = 0.8$ *and* $\beta = 0.75$*; d)* $\alpha = 0.8$ *and* $\beta = 1$.

For IPE200 and IPE270 the results are similar to the HEA sections, even if in this case, the differences are less perceptible. The behaviour of the IPE is superior compared to the HEA cross-sections, and this can be ascribed to

their better shape, and in particular the lower contribution of their flange on the limit strength and on their greater influence of the web on the flexural behaviour.

4.2 - LRPD in frames

The validation of the device must take into account not only the simplified loading conditions but also its behaviour inside a full structural system, such as a building, with all the forces and specific situations that are expected to occur during its lifetime.

Before moving on to the explanation of this chapter focus, the simplified hypotheses made in the optimal problem section regarding the actions must be considered. It has been explained that for the device's design, the optimal problem, until now, has neglected a set of forces that are deeply connected to tridiminensional buildings and to the practical situation of the use of this device (such as bending moment on the vertical axis, torsion, etc.). But as remarked, at this stage of the present research, a simpler hypothesis and simpler theoretical models were adopted. For this reason, to fit with these assumptions, the practical application studied in this section will regard only bidimentional steel structures equipped with the LRPD, such as plane frames.

Another useful tool to the reader to understand the validity of the LRPD can be a comparison between the LRPD and the other RBS techniques within a frame (Figure 4.11). By doing this, the aim was to compare the efficacy of the LRPD with the dogbone, investigating their peculiar behaviours and their differences in a common multistorey and multispan steel frame, which can usually be found in civil buildings.

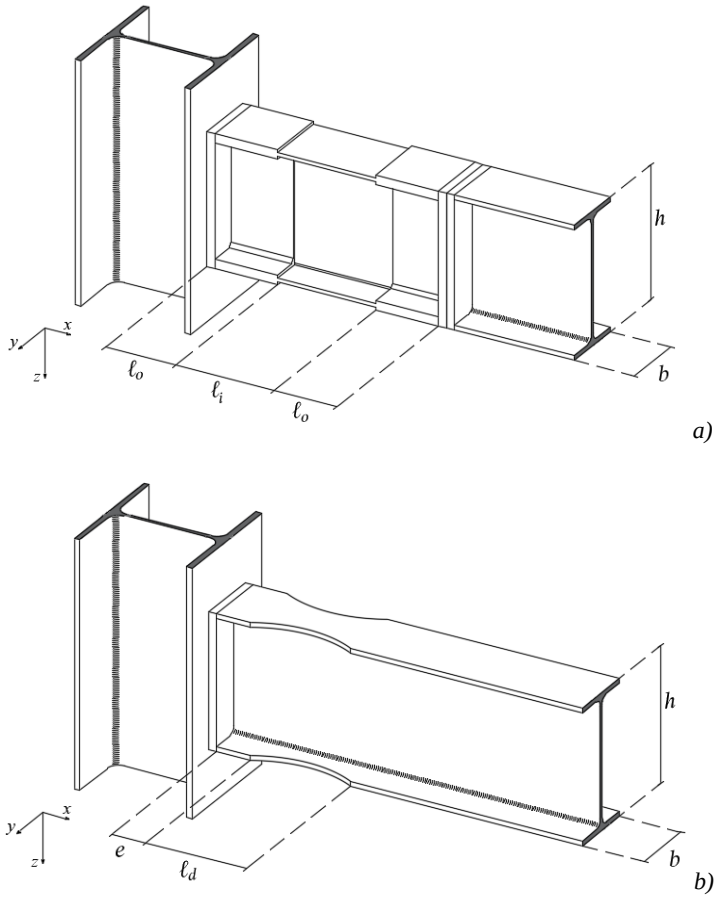

Figure 4.11 – a) Scheme of LRPD device in a beam-column joint;b) scheme of a dogbone in a beam-column joint.

Considering the practical nature of the goal, a feasible strategy can be to consider a practical example. For this purpose a common frame (Figure 4.12) is considered as a sample for the following analyses. The frame reported is composed of two spans and three floors with the cross-sections and using a S275 grade steel, with assigned geometry, typical of residential frame buildings with their permanent and variable loads $(q = G_1 + G_2 + G_k)$ listed in Table II. The software adopted for the following analyses is Sap2000, which is based on a concentrated plasticity model, and therefore for the description of the non-linear behaviour of the frame, it is necessary to define the location and the relationships of the hinges.

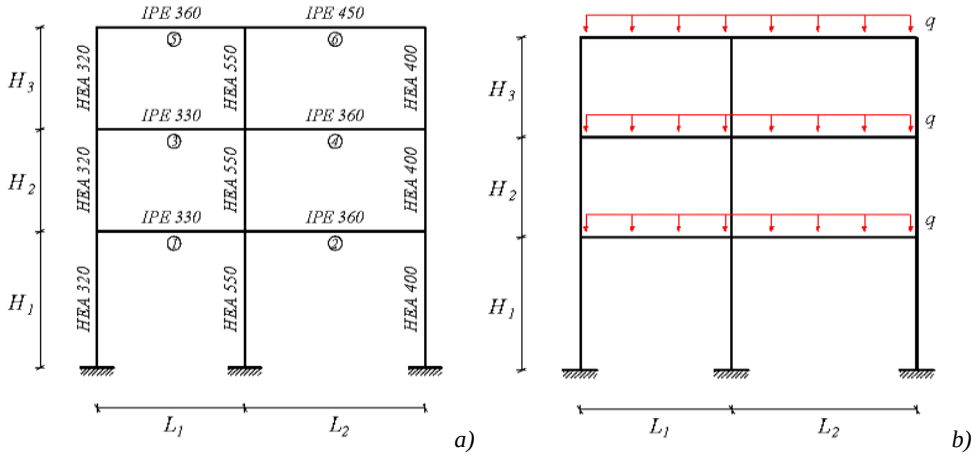

Figure 4.12 – Sample frame considered. a) Geometry and cross-sections; b) Loads.

Table II – Geometry and loads of the proposed frame.

Frame geometry [m]				*Loads [kN/m]*			
H_1	4.0	L_1	4.5	$q\,(G_1)$	25.0	$q\,(G_k)$	20.0
$H_2 = H_3$	3.0	L_2	5.5	$q\,(G_2)$	15.0		

The devices of the application were dimensioned as follow:

1. the percentage of the reduction of the base of the beam elements must be chosen (in order to model the sample dogbones);
2. the distance from the column, the length of cut and its shape must be defined;
3. starting from the dogbone as previously dimensioned, the relevant LRPD device must be designed through the relevant optimal problem;
4. finally the two frames, one with the dogbone and one with the LRPD device, can be modelled and analyzed.

The passages listed above summarize the steps to perform the comparison of this section. The cross-sections of the two compard devices are sketched in Figure 4.13.

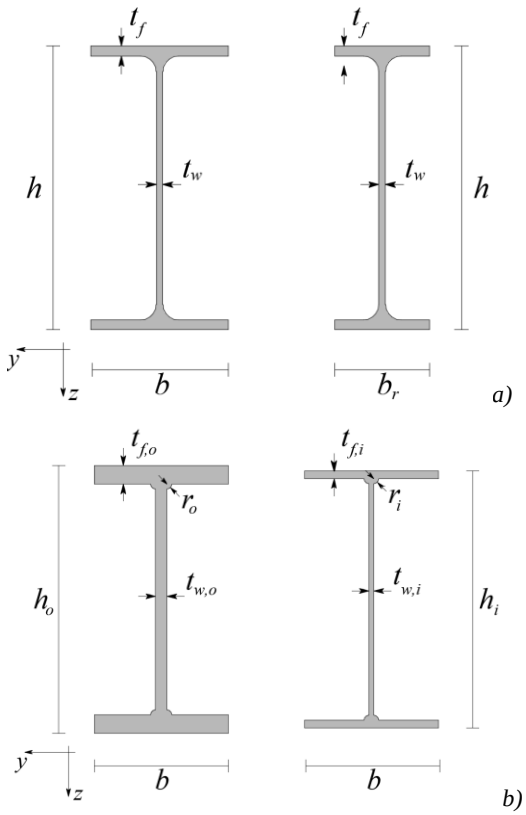

Figure 4.13 – a) Dogbone cross-sections (not reduced, and reduced); b) LRPD cross-sections (outer and inner).

The reduction percentage cited was set to be 40% of the initial base width, and following this choice, the distance from the column, e, and the length of the cut, ℓ_d, were defined to be $h/4$ and 3 $h/4$ respectively. To move from step 2 to step 3 it is necessary to define the elastic resistance modulus W_{el}^d for the dogbone, with the aim of creating a bond to balance the resistance of the first and the second one. Neglecting the welding radius, as in the previous chapters, this quantity can be expressed as follow:

$$W_{el}^d = \left\{\frac{t_w h^3}{6} + t_f(b_r - t_w)\left[\left(h - t_f\right)^2 + \frac{t_f^2}{3}\right]\right\} \qquad (42)$$

Stating the knowledge of the defined material it is possible to define the bending moment corresponding to the yield limit:

$$M_{el}^d = W_{el}^d f_y \qquad (43)$$

where, for S275 steel $f_y = 27.5\,\mathrm{kN/cm^2}$. These quantities, compared to the commercial beam element, lead to the determination of the scalar factor α to understand on what level to set the limit yield resistance of the LRPDs:

$$\alpha = W_{el}^{d} / W_{el,p} \tag{44}$$

where $W_{el,p}$ is the elastic resistance modulus of the different connected beam elements. By collecting these values for each cross-section composing the beams of the frame, it is possible to dimension the relevant LRPD devices by using these parameters as the input value to fix the resistance reduction threshold ($W_{el,i}^{LRPH} = \alpha\, W_{el,p}$). The cross-section to be reduced in the LRPD, as discussed before, is the inner one, and its elastic resistance modulus can be defined as:

$$W_{el,i}^{LRPD} = \left[\frac{b\, t_{f,i}^{3}}{3} + b\, t_{f,i}\left(h_i - t_{f,i}\right)^2 + \frac{t_{w,i}\left(h_i - 2t_{f,i}\right)^3}{6}\right] \tag{45}$$

And the associated limit bending moment:

$$M_{el,i}^{LRPD} = W_{el,i}^{LRPD}\, f_y \tag{46}$$

Then, imposing Eq. (43) to be equal to Eq. (46), and guaranteeing that the LRPD fulfills the constraints imposed by the respective optimization problem, it is possible to obtain the same limit strength for both the device and the dogbone.

The modelling developed with a software using the concentrated plasticity theory at the base, puts some limitations on the full development of the plastic hinge through the frame, simply because every potential hinge must be defined, a-priori, in a pre-defined location (such as the beam ends, or the inner part of a weakened portion, as necessary in this case). The dogbone has been modelled as a variable beam section (Figure 4.14), i.e. the reduced part is characterized by a variable base width which starts from the commercial beam width to finish into the desired reduced base width. In particular the quantity that varies is the base width, and it varies linearly from the initial

cross-section, i.e. the commercial beam, to the suitably reduced cross-section typical of the dogbone.

In addition, in order to make the frame experience its post-elastic behaviour, the hinge position must be defined. This position must corresponds to the main representative cross-sections, such as the midspan of the reduced strength devices. The moment-curvature model of the cited plastic hinge is elasto-plastic, defined in the relevant hinge property window of the software by simply imposing that once reaching the yield bending moment in the defined cross-section the hinge activates.

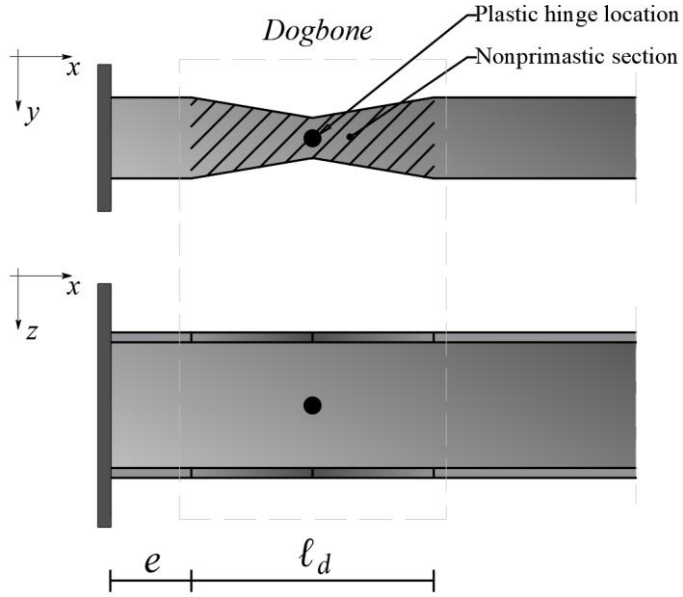

Figure 4.14 – Sap2000 modelling of dogbone.

The LRPD has been modelled in the same way as the dogbone, but the three consecutive portions are just three I-shaped profiles with different thicknesses and the same common medium planes, so no variable cross-section elements were necessary to model the devices. The location along the beam elements of the plastic hinge in the sample frames corresponds to the middle cross-section of the inner portion of the device for the LRPD, and to the middle cross-section of the reduced base for the dogbone.

The analyses evaluating the response of the sample frames, modelled as explained, consist of a static non-linear analaysis (pushover) and a dynamic linear analysis. The pushover is useful to relate the base shear vs the head displacement reaching a capacity curve of the system. The profile of the forces applied for this analysis is linear and, after the suitable definition of the plastic hinge location and characteristics, the load is increased in order to test the post-elastic features of the frame.

The dynamic linear analaysis is useful to subject the frames to the seismic force. This is possibile by means of a spectral modal analysis. For the evaluation of the interstorey drift the serviceability state limit is considered (with the spectrum reported in Figure 4.15a), and on the other hand, for the limit behaviour the relevant ultimate conditions are adopted (with the spectrum shown in Figure 4.15b).

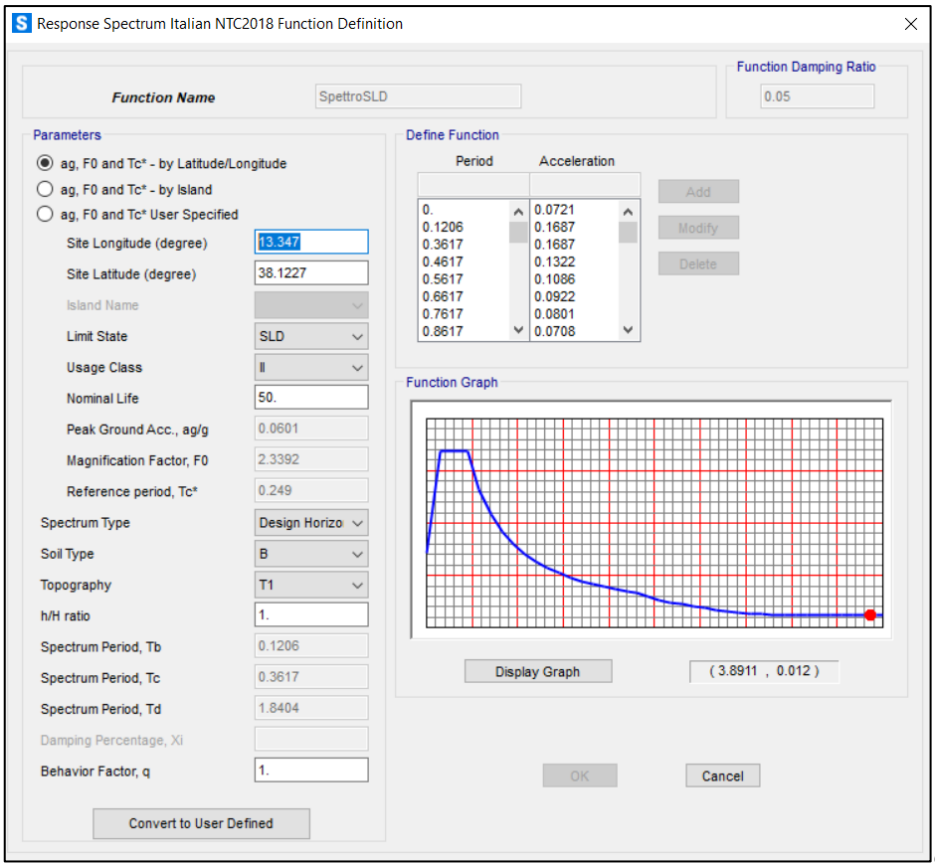
Response Spectrum Italian NTC2018 Function Definition
Function Name
SpettroSLD
Function Damping Ratio
0.05
Parameters
ag, F0 and Tc* - by Latitude/Longitude
ag, F0 and Tc* - by Island
ag, F0 and Tc* User Specified
Site Longitude (degree)
13.347
Site Latitude (degree)
38.1227
Island Name
Limit State
SLD
Usage Class
II
Nominal Life
50.
Peak Ground Acc., ag/g
0.0601
Magnification Factor, F0
2.3392
Reference period, Tc*
0.249
Spectrum Type
Design Horizo
Soil Type
B
Topography
T1
h/H ratio
1.
Spectrum Period, Tb
0.1206
Spectrum Period, Tc
0.3617
Spectrum Period, Td
1.8404
Damping Percentage, Xi
Behavior Factor, q
1.
Convert to User Defined
Define Function
Period
Acceleration
0. 0.0721
0.1206 0.1687
0.3617 0.1687
0.4617 0.1322
0.5617 0.1086
0.6617 0.0922
0.7617 0.0801
0.8617 0.0708
Add
Modify
Delete
Function Graph
Display Graph
(3.8911 , 0.012)
OK
Cancel

a)

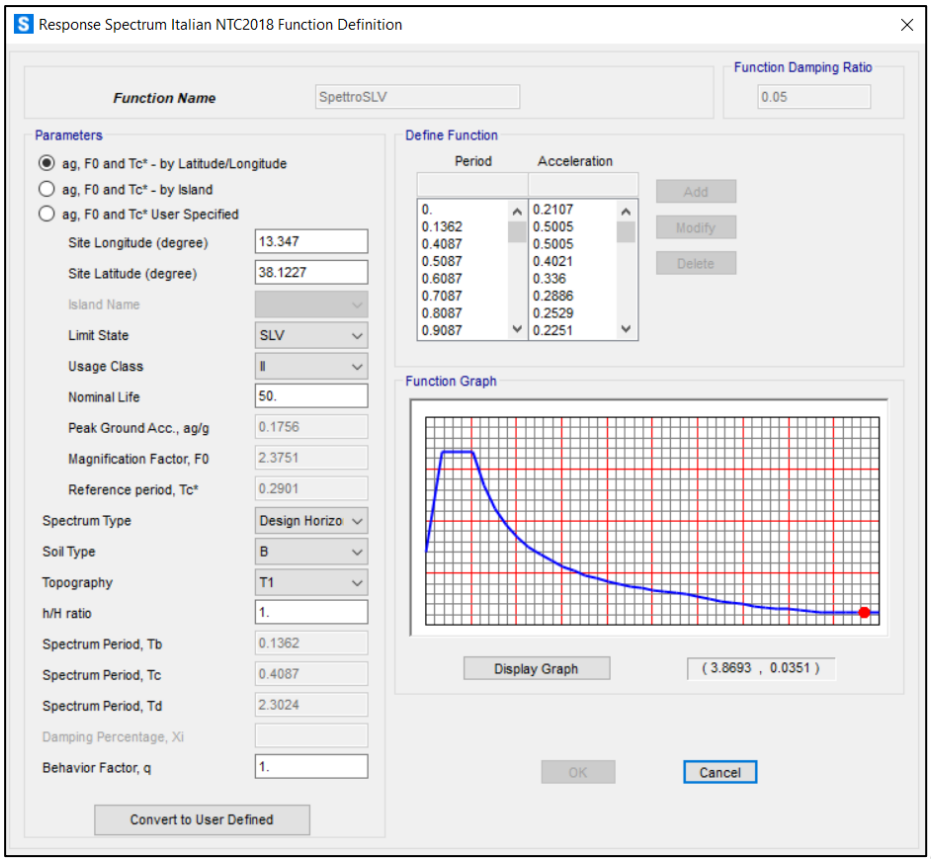

b)

Figure 4.15 – Response spectrum considered; a) Serviceability condition; b) ultimate conditions.

By using the pushover and the dynamic analysis the capacity curve (Figure 4.16a) and the interstorey drifts (Figure 4.16b) of the sample frame without RBS devices are collected.

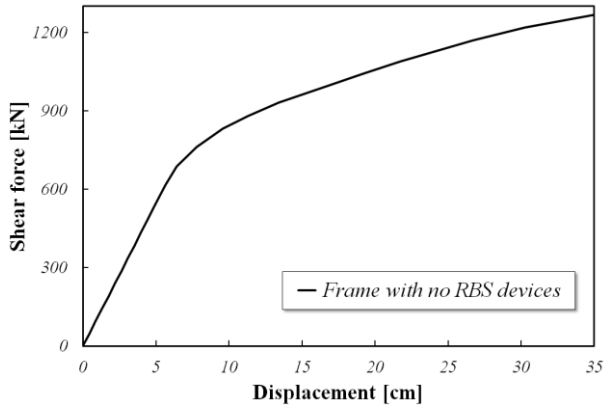

a)

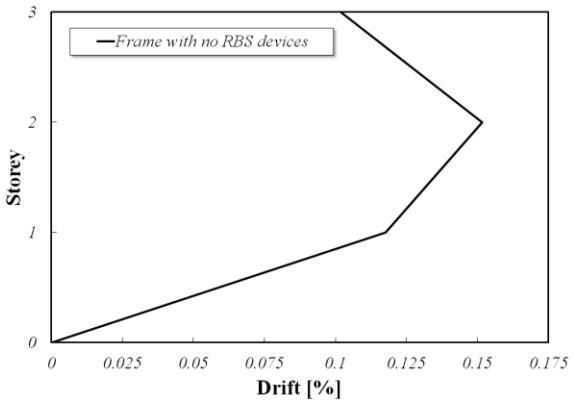

b)

Figure 4.16 – a) Capacity curve of the simple frame (no devices); b) Interstorey drift of the same frame.

These have been used as a benchmark in the evaluation of the different efficacies of the dogbone and the LRPD. In order to have an idea of the effect of the device on the deformability of the beams the midspan deflections have also been collected.

The frames equipped with dogbone and LRPD were then analyzed, and the same results as before were collected and reported in Figure 4.17.

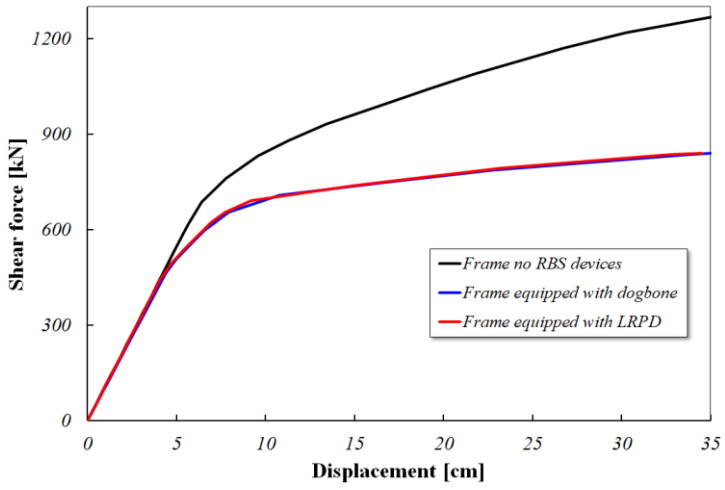

a)

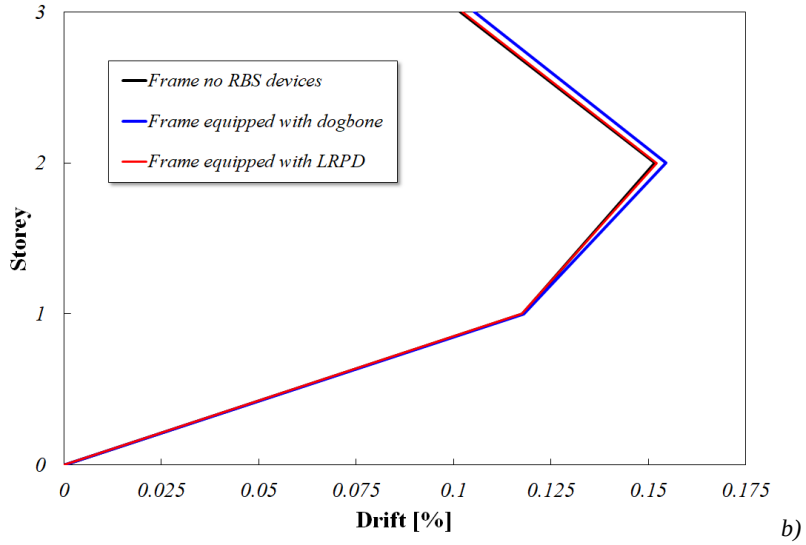

Figure 4.17 – a) Comparison of the capacity curves of the samples; b) Comparison of the interstorey of the samples.

In terms of capacity curves the behaviour of LRPD and dogbone can appear exactly the same. But quantifying the elastic stiffness of the two samples, and by comparing them numerically it has been shown that the dogbone causes a variation of 3.24% in the frame, while a variation of only 0.49% is seen in the frame equipped with the LRPD. This is coherent with the assumption of unalteration of flexural stiffness that can be accomplished thanks to the LRPD. The limit behaviour is legitimately similar, because of the fact that the two internal reduced portions of the two devices present the same limit strength, and a similar distance from the beam-column interface (therefore experiencing a similar amount of bending moment).

The interstorey drifts were collected from the dynamic analysis. Also in this case the differences are limited and the two frames show similar behaviours. In Table III the deflections at the midspan of each beam are collected.

Table III – Midspan deflections for each beam element.

Beam deflections [cm]						
	1	*2*	*3*	*4*	*5*	*6*
Normal	0.4117	0.5788	0.4317	0.5959	0.4048	0.4131
Dogbone	0.4274	0.6042	0.4478	0.6219	0.4164	0.4514
LRPD	0.4192	0.5897	0.4394	0.6070	0.4107	0.4457

Comparing the deflections of the different configurations it is possible to note the improvement caused by the adoption of the LRPD within the sample frames.

The results of the provided example show the efficacy of the LRPD in acting as a reduced beam section, with its additional benefits in terms of flexural stiffness.

4.3 - Restoring masonry panel strength and stiffness

In this section the LRPD will be tested in the field of masonry structure reinforcement, and specifically when a panel, or a portion of it, is removed and a steel frame is required in order to guarantee the prescribed overall structural behaviour.

As stated in section 1.2, for masonry panels the creation of a breach and, the inclusion of a frame to allow this opening, is a matter causing mechanical and kinematical modifications. As is well known in this case, the usual strategy adopted by structural designers is to fit a steel frame of suitable mechanical characteristics in the opening. Actually, the great difference between the mechanical characteristics of the frame and those of the masonry panel leads to the problem that usually can cause problems to the masonry panel. This is true even if the stiffness frame and the surrounding masonry panel is analogous to that of the original panel, due to the higher strength of the frame.

The characteristics of the LRPD, described in the previous sections, suggest that it can be adopted in the reinforced steel frame to limit strength modifications, while maintaining the benefit of restoring the original stiffness. This goal will be demonstrated in the following section by reporting some examples which take into account the peculiarity of the structural problem under examination.

The device will be tested using two different samples. For each, the characteristics of the panel will be investigated in the following four configurations: a panel without opening, a panel with an opening without reinforcement, a panel with an opening reinforced by a steel frame, and a panel with an opening reinforced by a steel frame equipped with LRPDs.

By suitably sizing the frame and the devices it is possible to compare the obtained results, and to prove the efficacy of the LRPD in the panel's overall behaviour.

In order to reduce the computational effort the analyses have been conducted by means of a distributed plasticity approach, based on a fiber modelling of the cross-section, as will be explained below.

To confirm the reliability of the obtained results, they will be compared with those achieved by means of 3D FEM models developed in Abaqus environment.

Before to move into the specific focus of this section it is useful to introduce breifly the FSDB model adopted in the numerical examples reported in the following. In detail, the cited approach[21] is based on the Fiber Smart Displacement Based (FSDB) model, characterized by a peculiar beam element with an uniform cross-section with specific adaptive displacement shape functions, which are continuously updated during the post-elastic phase of the analysis. The evolution of the displacement shape functions depend strictly to the plastic deformation evolution within the beam element considered. The adaptive generalized displacement shape is created by choosing an equivalent tangent beam at each step to represent the beam's current inelastic state. These equivalent tangent beams are characterized by abrupt changes in the flexural stiffness.

The method is based on the formulation of a Smart Displacement Based (SDB) beam element, easier to implement with respect to other common beam element, but distinguished by comparable results. The word "smart" serves the meaning of emphasize the element's capacity to upgrade the displacement field in accordance with the effective inelastic state. As deeper

[21] A smart displacement based (SDB) beam element with distributed plasticity. B. Pantò et al. (2017). And from the same authors: A Fibre Smart Displacement Based (FSDB) beam element for the nonlinear analysis of reinforced concrete members (2019).

explained in the cited reference, the adoption of the FSDB model brings the great advantage of avoiding both the mesh discretization and the Gauss point adjustement during the analysis.

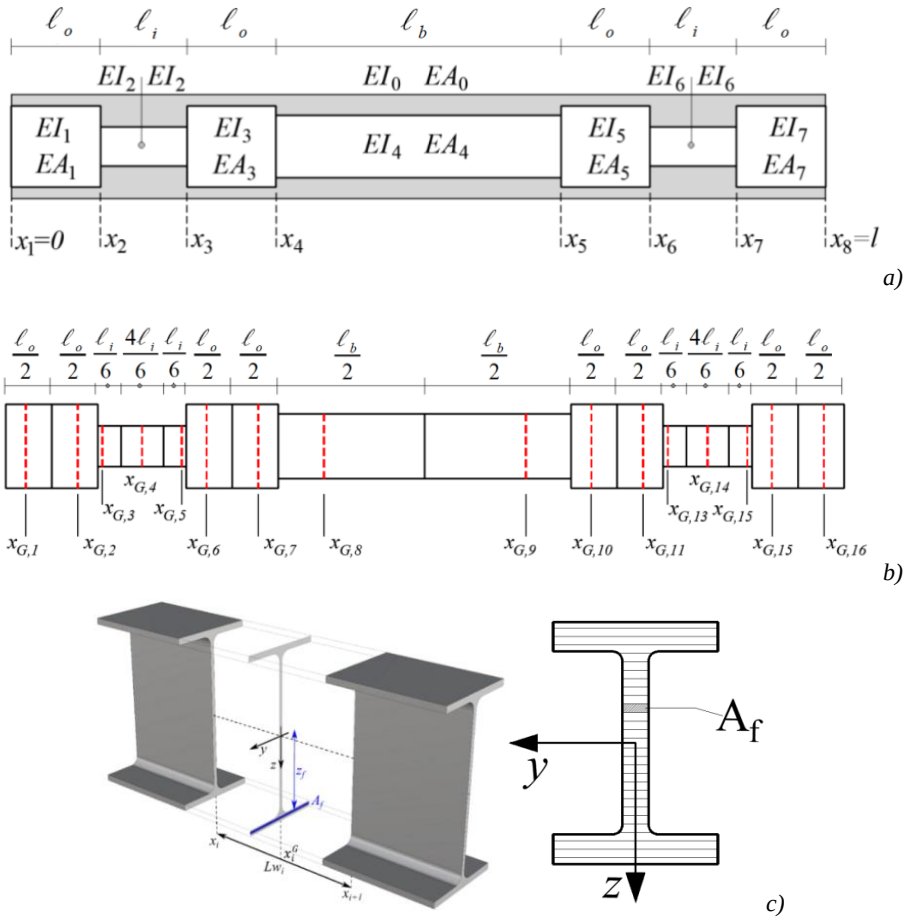

Figure 4.18 – a) Discretized beam portions with relevant axial and flexural modulus; b) Position of Gauss integration cross-sections; c) Cross-section fiber discretization.

The LRPD was implemented in FSDB by modelling it as sketched in Figure 4.18. The different portion of the device were defined with their specific geometry, and for a beam three main cross-sections can be identified: outer, inner and commercial profile connected. The stiffness properties of the LRPD implemented beam are defined as reported in Figure 4.18a. For each one of these cross-section a suitable number of Gauss points, and their

position, must be defined. The choice of the Gauss points depends on the local results accuracy required. For example, the inner portion, which represents the first region to undergo plastic deformations, possesses the greater number of Gauss points (i.e. three, as reported in the cited Figure 4.18.b). Thanks to the adoption of FSDB model, thererfore, it is possible to consider both the variability of the cross-section and that of the material along the beam's length. Even though, in the case proposed in the following section, only the geometrical variability has been taken into account.

The masonry panel has been modelled using a discrete macro-element approach implemented by 3D Macro software. Briefly, the macro elements in this software can have different shapes and sizes, and are joined together by a distribution of a finite number of nonlinear links to simulate the axial and flexural behaviour of the masonry. The shear behaviour is represented by a Mohr-Coulomb yield criterion with a suitable elasto-plastic constitutive law.

The first example is represented by a simple panel (named Panel 1) to be substituted by a steel frame. The assigned masonry panel is sketched in Figure 4.19 while the geometrical and mechanical characteristics are reported in Table IV.

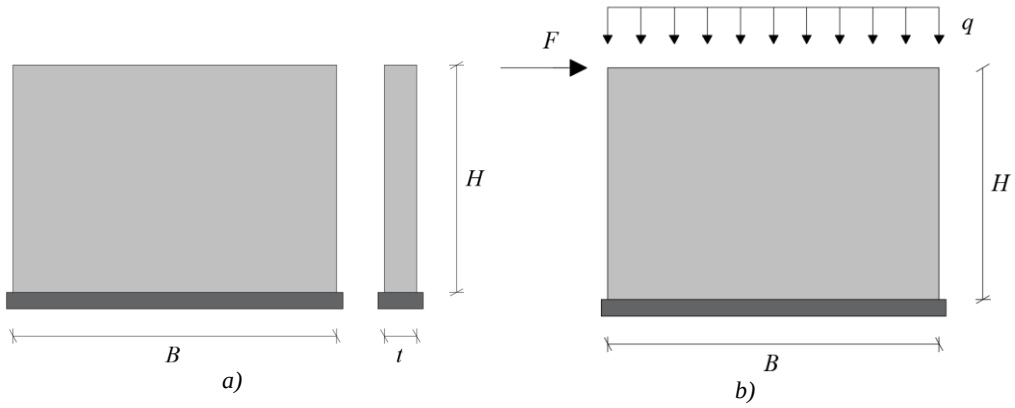

Figure 4.19 – a) Sample Panel 1; b) Loads.

Table IV – Panel 1 characteristics.

B	5.00 m	G	400 MPa
H	3.50 m	f_m	2.00 MPa
T	0.50 m	f_{tm}	0.10 MPa
E	1000 MPa	f_{v0}	0.25 MPa

The behaviour of the panel is evaluated through the application of a lateral load, monotonically increased until its collapse, obtaining the base shear / displacement relationships and the corresponding panel capacity curve (Figure 4.20a). The adopted software also provides the collapse mechanism which is sketched in Figure 4.20b.

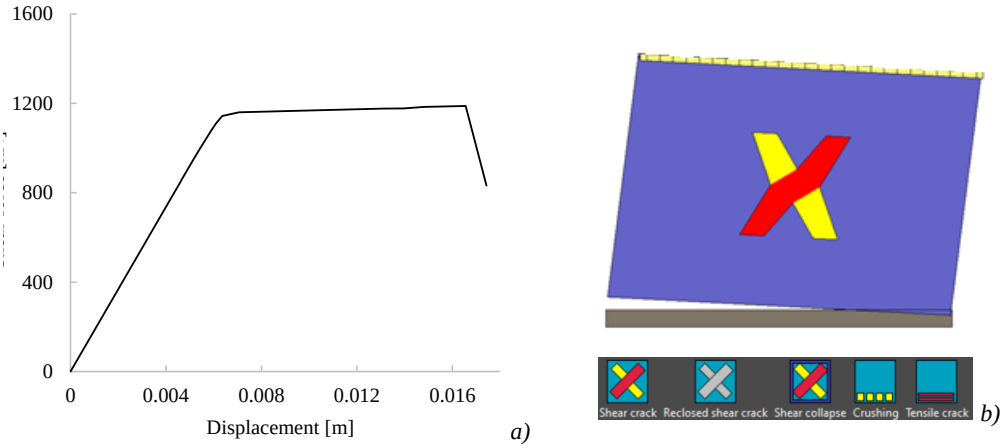

Figure 4.20 – a) Panel 1 capacity curve; b) Mechanism of collapse: in this case shear.

The frame has been designed to take into account that the overall dimensions of the frame are the same as the masonry panel. Starting from these dimensions the stiffness of the panel is evaluated by means of its capacity curve; consequently the cross-sections of beam and columns are crucial in order to obtain a frame stiffness as close as possible to that of the masonry panel. The obtained results are reported in Figure 4.21.

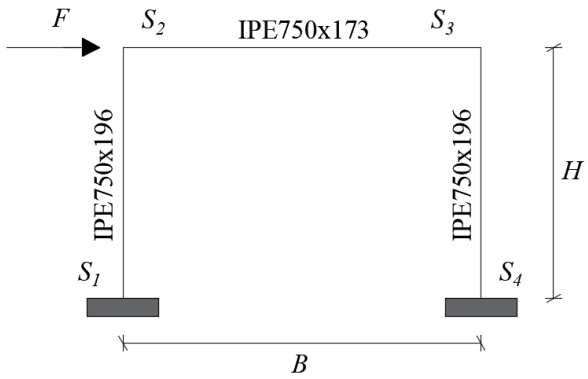

Figure 4.21 – Frame 1 profiles and sections.

The results obtained for the frame in terms of capacity curves adopting the FSDB beam model are reported in Figure 4.22.

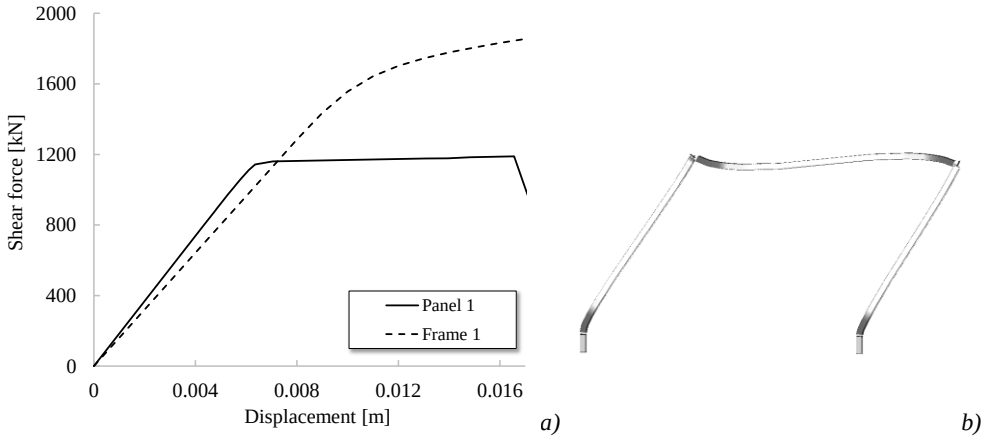

Figure 4.22 – a) Frame 1 capacity curve; b) Deformed shape.

From Figure 4.22a it is possible to note that the stiffness of the frame does not fully recreate that of the original panel and the reason for such behaviour is strongly related to the choice of utilizing standard commercial profiles. However, the stiffness change can be considered small and neglegible. Another very important remark is that the strength of the frame is significantly higher than that of the panel.

This example shows that thanks to the design and position of the LRPDs it is possible to arrange the strength of the frame to be as close as possible to

that of the masonry panel. In particular, it has been decided to arrange the LRPDs at the base of the columns and at the endings of the beam, as sketched in Figure 4.23. This means that the maximum level of flexural force can be found in these positions, and therefore the strength reduction goal can be accurately fulfilled.

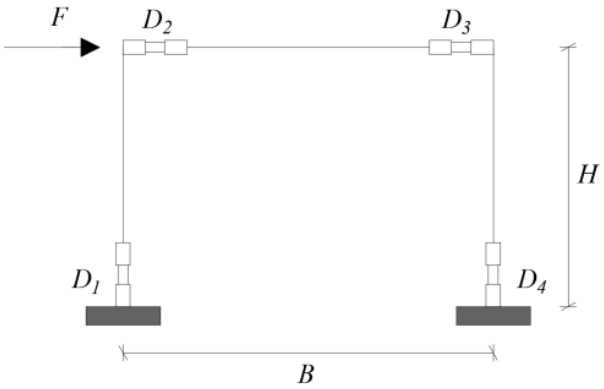

Figure 4.23 – Frame 1 equipped with LRPD.

The LRPDs design is defined using the optimal procedure reported in section 3.4, and different approaches for the plastic hinge activation have been developed.

In the first approach the plasticization of the four LRPDs is set to occur once reaching a defined amount of lateral load, hence , simultaneously, causing the activation of the four plastic hinge, ideally this results in a perfectly bilinear shape of the relevant capacity curve characterized by a plateau value equal to $F_{lim} = 1{,}150$ kN. The lateral force F_{lim} has been applied at the beam level of the frame, and the consequent axial force and bending moment diagrams have been collected. The magnitude of these forces acting on the selected locations have been used as input design parameters for the devices' optimization procedure.

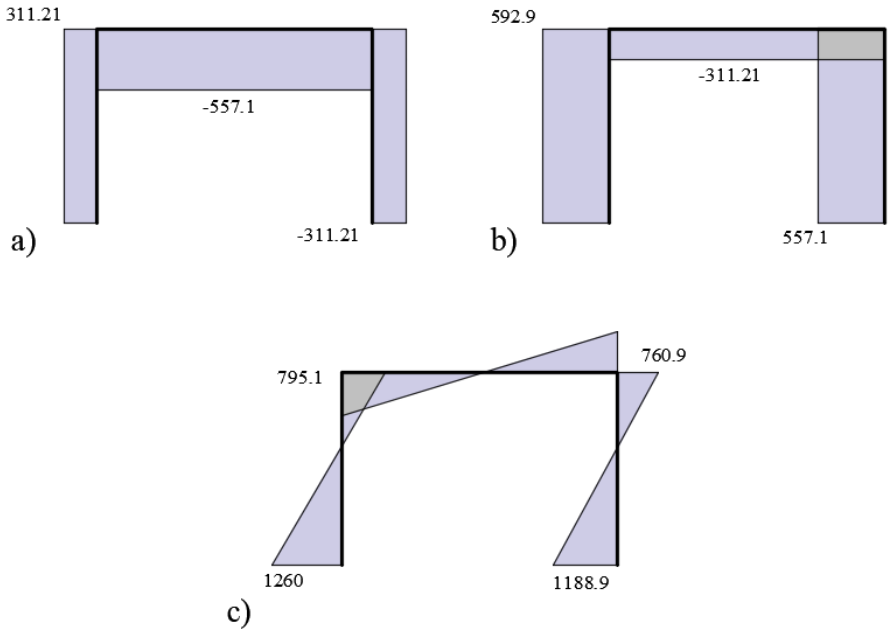

Figure 4.24 – Internal forces within the Frame 1 subjected to F_{lim} as horizontal force; a) axial force [kN]; b) shear force [kN]; c) bending moment [kNm].

An important result discovered during the development of this example is that, to obtain better results, it is required to take into account, properly, the variation of the bending moment along the beam's axis. This has been accomplished by imposing a balance between the internal work generated by the constant bending moment in the inner cross-section, and those generated by the variable bending moment within the same portion of the device, as sketched in Figure 4.25.

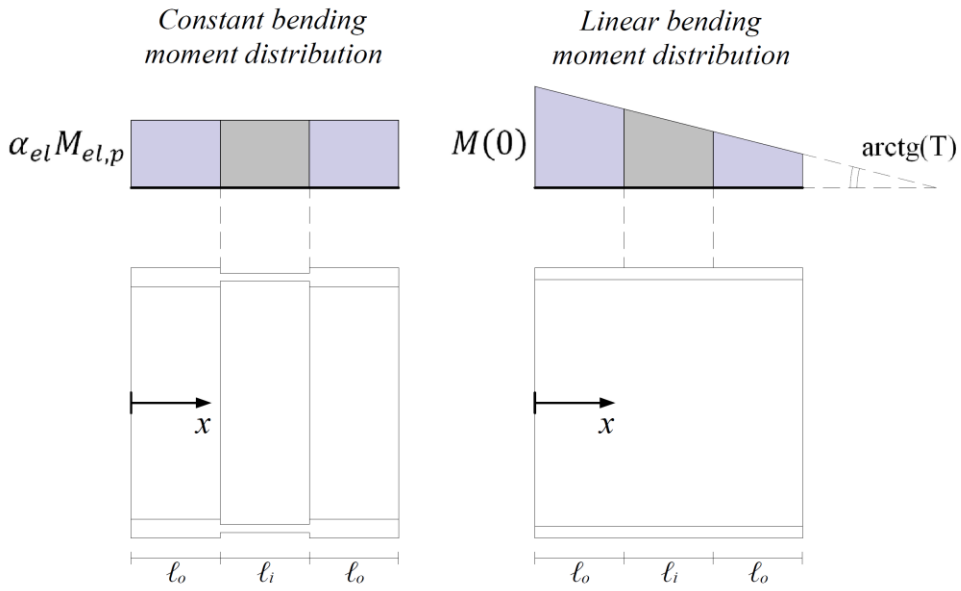

Figure 4.25 – Energetic balance between the device inner portion and the relevant portion of the commercial beam element selected.

Given the equivalnce that can be observed in Figure 4.25, the two works can be balanced and written as follow:

$$\frac{(\alpha_{el}M_{el,p})^2\ell_i}{J_i} = \int_{\ell_o}^{\ell_o+\ell_i}\frac{[M(0)-Tx]^2}{J_p}dx \qquad (47)$$

The term on the left represents the flexural work developed in the inner portion of LRPD in the scenario of simply scaling the initial yield bending moment. The term on the right represents the analogous work developed within the selected commercial profile with the linearly variable bending moment law ($M(x) = M(0) - Tx$).

Another important result observed during the development of this example is that, to improve the behaviour of the frame equipped with LRPDs, the design of the device has to be performed by adopting the elastic limit bending moment in the optimal design procedure instead of the plastic one. This result has been obtained by considering that the onset of the full plastic hinge does

not occur suddenly but after the proper development in the plasticization process of the inner portion of the device.

As reported in literature[22] it has been observed that choosing the plastic limit as a design value can lead to cause an over-resistance in the substituting frame. The reason for such behaviour is due to the device's short length, that theoretically, would require higher β values to express its full flexural properties.

Taking this variation into account, Eq. (12) can be modified as follows:

$$\left|\frac{N_a}{A_i f_y} + \frac{\alpha_{el} M_{el,p}}{W_{el,i} f_y}\right| = 1 \tag{48}$$

Where α_{el} is visible in Figure 4.25. Consequently, Eq. (47) can be written in terms of α_{el}:

$$\alpha_{el} = \frac{1}{M_{el,p}}\left(\frac{I_i}{\ell_i J_p}\int_{\ell_o}^{\ell_o+\ell_i}[M(0) - Tx]^2\, dx\right)^{\frac{1}{2}} \tag{49}$$

By substituting Eq. (49) in Eq. (48) it is possibile to obtain the modified version of the constraint shown in Eq. (31f):

$$G_{eq}(x) = \frac{N_a}{A_i(x) f_y} + \frac{\left(\frac{I_i}{\ell_i I_p}\int_{\ell_o}^{\ell_o+\ell_i}[M(0)-Tx]^2 dx\right)^{\frac{1}{2}}}{W_{el,i}(x) f_y} - 1 \tag{50}$$

A third very important result obtained during the development of this example is that to avoid torsional problems the web thickness of the inner part is considered as a design variable.

By utilizing the input data reported in Table V the LRPDs have been designed and the corresponding results are reported in Table VI.

[22] Smart Beam Element Approach For LRPH Device. Benfratello S. et al. (2020).

Table V – Input for Frame 1 LRPD design

LRPD	D_1	D_2	D_3	D_4
β	0.5	0.5	0.5	0.5
ℓ_i	38.5	38.1	38.1	38.5
$H = h$ [mm]	770	762	762	770
b [mm]	268	267	267	268
$t_{f,p}$ [mm]	25.4	21.6	21.6	25.4
$t_{w,p}$ [mm]	15.6	14.4	14.4	15.6
N_a [kN]	311.21	-557.1	-557.1	311.21
$M_{el,p}$ [kNm]	1,466.63	1,269.47	1,269.47	1,466.63
f_y [MPa]	235	235	235	235
I_p [cm^4]	240,300	205,800	205,800	240,300

Table VI – Frame 1 devices

	D_1	D_2	D_3	D_4
h^*	70.9971	70.096	69.214	70.5488
$t_{f,o}$	6.0029	6.104	6.986	6.4512
$t_{f,i}$	1.538	0.8422	0.7585	1.3598
ℓ_o	31.5238	62.9476	72.2173	39.8098
$t_{w,o}$	3.3805	3.6614	4.0829	3.5869
$t_{w,i}$	0.8745	0.5098	0.4489	0.7648

The frame equipped with the devices has been analyzed by means of the FSDB beam element approach, adopting 40 fibers for each cross-section. The obtained capacity curves and collapse shape are sketched in Figure 4.26.

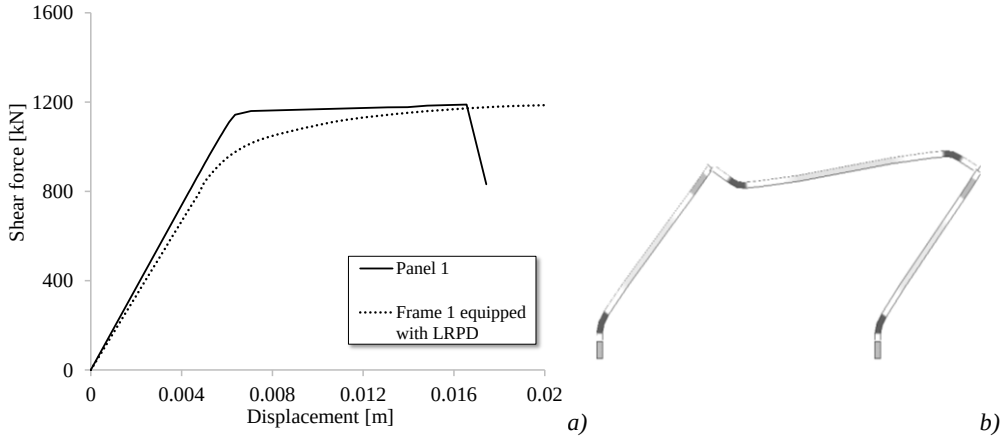

Figure 4.26 – Frame 1 equipped with devices capacity curve; b) Deformed shape.

An examination of these figures shows that the optimal problem, suitably modified as reported above, leads to a very satisfactory result.

A second example is presented, in which the substitution of the masonry panel, named Panel 2, whose geometrical and mechanical characteristics are reported in Table VII, and is sketched in Figure 4.27. The main differences between Panel 1 and 2 lie in the different capacity curves and in the different collapse mechanisms.

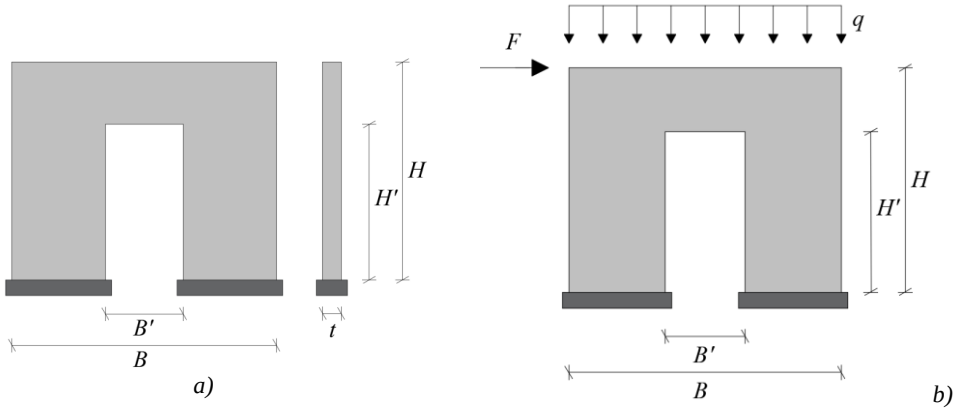

Figure 31 – a) Sample Panel 2; b) Loads configuration.

Table VII – Panel 2 characteristics.

B/B'	4.25/1.25 m	*G*	550 MPa
H/H'	3.5/2.5 m	f_m	2.60 MPa
T	0.30 m	f_{tm}	0.10 MPa
E	1250 MPa	f_{v0}	0.25 MPa

The steps performed in this case are identical to those described for Panel 1. The capacity curve of the panel and its collapse mechanism are sketched in Figure 4.28a and 4.28b, respectively. In Figure 4.29a the frame with the closest stiffness to that of the panel is sketched, where the selected commercial cross-sections are also indicated, while in Figure 4.29b the capacity curves of the panel and of the frame are reported and compared.

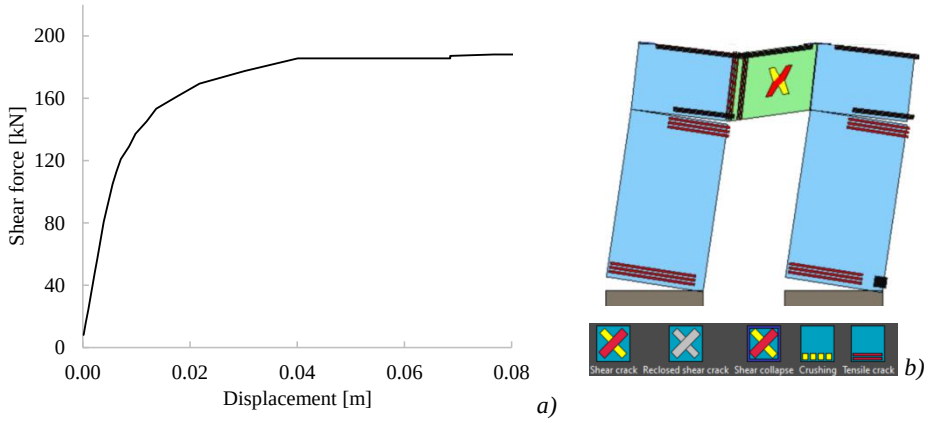

Figure 4.28 – a) Panel 2 capacity curve; b) Mechanism of collapse.

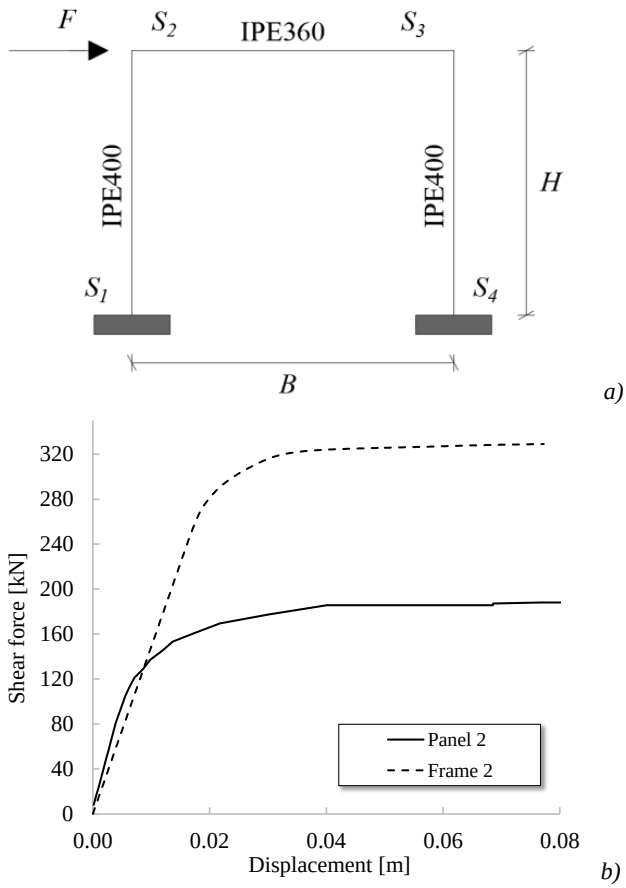

Figure 4.29 – a) Frame 2 profiles and sections; b) Capacity curves comparison.

The limit plateau can be identified as equal to $F_{lim} = 180$ kN, and at this level the consequent distribution of the internal forces is represented in Figure 4.30.

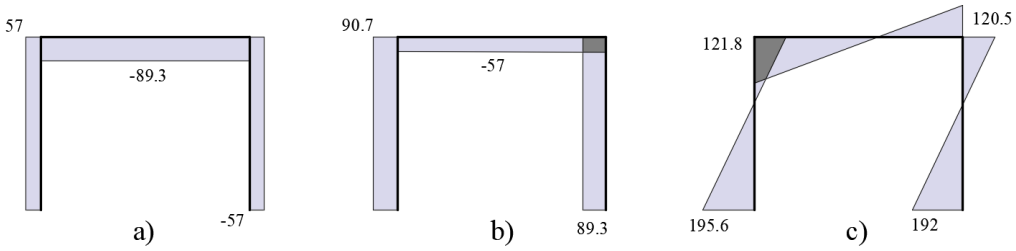

Figure 4.30 – Internal forces within the Frame 2 subjected to F_{lim} as horizontal force; a) axial force [kN]; b) shear force [kN]; c) bending moment [kNm].

As in the earlier example, it has been decided to locate the LRPDs at the base of the columns as well as at the beam's ends, and that the plasticization of the four is set to occur at the same level of lateral force. The results of the optimal design are reported in Table VIII.

Table VII – Input for Frame 2 LRPD design

	D_1	D_2	D_3	D_4
β	0.5	0.5	0.5	0.5
ℓ_i	200	180	180	200
$H = h$ [mm]	400	360	360	400
b [mm]	180	170	170	180
$t_{f,p}$ [mm]	13.5	12.7	12.7	13.5
$t_{w,p}$ [mm]	8.6	7.5	7.5	8.6
N_a [kN]	57	-89.3	-89.3	-57
$M_{el,p}$ [kNm]	195.60	121.80	120.50	192.00
f_y [MPa]	235	235	235	235
I_p [cm^4]	23,130	16,270	16,270	23,130

Table VIII – Frame 2 devices

	D_1	D_2	D_3	D_4
h^*	35.6884	33.4034	33.4004	35.5361
$t_{f,o}$	4.3116	2.5966	2.5996	4.4639
$t_{f,i}$	0.3355	0.9845	0.9812	0.3245
ℓ_o	69.0266	9.666	9.7619	71.7029
$t_{w,o}$	2.268	1.4706	1.4721	2.3306
$t_{w,i}$	0.1792	0.5607	0.5587	0.1722

The capacity curve of the frame (sketched in Figure 4.31) has been obtained, in this case, by the FSDB beam model with 40 fibers to discretize the cross-sections.

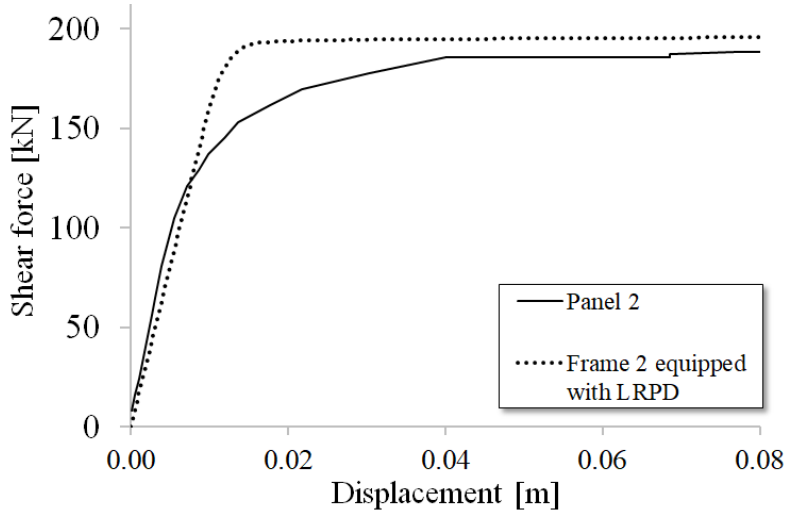

Figure 4.31 – Frame 2 equipped with devices capacity curve.

An examination of this figure leads to remarks which are analogous to those reported for Panel 1, confirming the capability of LRPDs to create a capacity curve of the frame which is similar to that of the masonry panel also in the case of panels with lower strength and different collapse mechanisms.

As reported above, the results have been obtained assuming that the plasticization of the LRPDs occurs simultaneously. Starting from this assumption, the next step has been the evaluation of the LRPDs plasticization order of activation into the results. Assuming the same locations for the LRPDs as presented above it follows that it is possible to activate the plasticization of the LRPDs, at most, four different force levels (quadrilinear frame). In order to obtain the best approximation between the capacity curve of the frame and that of Panel 2, the force levels reported in Table IX have been considered where the load levels D_1 and D_4 are the same since it has been decided to simultaneously activate the LRPDs at the column's base.

Table IX – Force level for the devices activation.

Load level [kN]	
D_1	$F_1 = 95$
D_2	$F_2 = 150$
D_3	$F_3 = 180$
D_4	$F_4 = 95$

The corresponding forces at the three force levels are collected in the following figures.

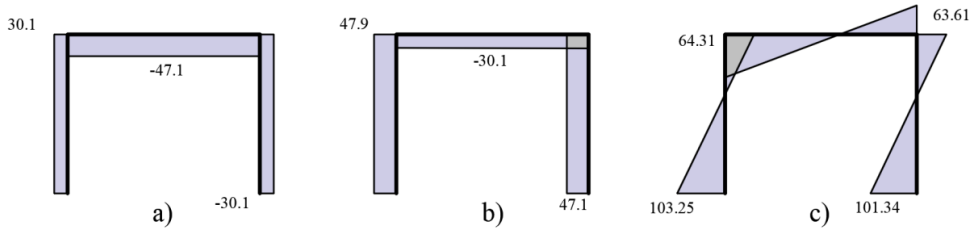

Figure 4.32 - Frame 2 elastic response for load level $F = F_1$: a) axial force (kN); b) shear force (kN); c) bending moment (kNm).

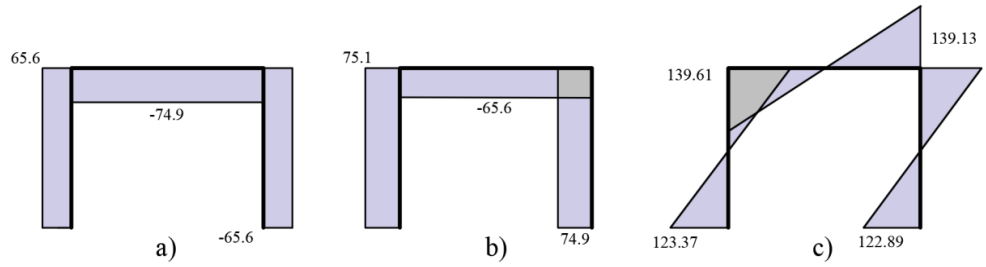

Figure 4.33 - Frame 2 response with devices active for load level $F = F_2$: a) axial force (kN); b) shear force (kN); c) bending moment (kNm).

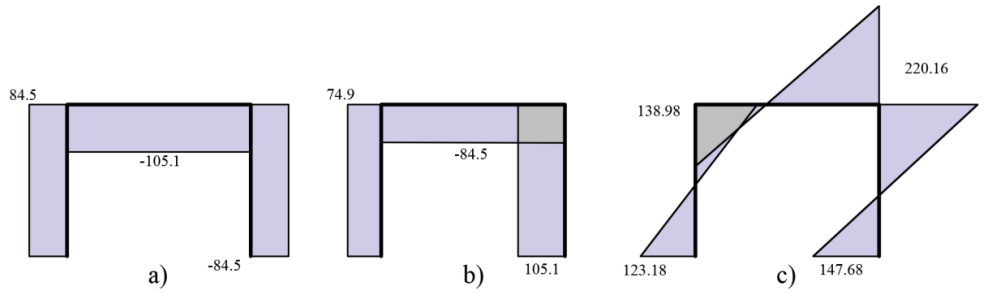

Figure 4.34 - Frame 2 response with device active for load level $F = F_3$: a) axial force (kN); b) shear force (kN); c) bending moment (kNm).

The elastic response shown in Figure 4.32 has been adopted to design the two devices to be placed at the column's base; Figure 4.33 to design the LRPD at left end of the beam; the Figure 4.34 to design the LRPD at right end of the beam. The input values for this new optimization problem are reported in Table X, while the results of the optimal designs are reported in Table XI.

Table X – Input for Frame 2 LRPD design

	D_1	D_2	D_3	D_4
β	0.5	0.5	0.5	0.5
ℓ_i	200	180	180	200
$H = h$ [mm]	400	360	360	400
b [mm]	180	170	170	180
$t_{f,p}$ [mm]	13.5	12.7	12.7	13.5
$t_{w,p}$ [mm]	8.6	7.5	7.5	8.6
N_a [kN]	30.1	-65.6	-105.1	-30.1
$M_{el,p}$ [kNm]	103.25	139.61	220.16	101.34
f_y [MPa]	235	235	235	235
I_p [cm^4]	23,130	16,270	16,270	23,130

Table XI – Frame 2 devices

	D_1	D_2	D_3	D_4
h^*	35.6884	33.1692	33.7556	35.5361
$t_{f,o}$	4.3116	2.8308	2.2444	4.4639
$t_{f,i}$	0.3355	0.6735	1.2519	0.3245
ℓ_o	69.0266	22.4221	3.1521	71.7029
ℓ_i	20	18	18	20
$t_{w,o}$	2.268	1.5838	1.2946	2.3306
$t_{w,i}$	0.1792	0.3796	0.7244	0.1722

Thanks to these dimensions the devices were modelled and analyzed following the strategy and the methods previously utilized. The response of Frame 2 with the desired quadrilinear shape of the curve is reported in Figure 4.36a, while in Figure 4.36b the relevant deformed shape is shown.

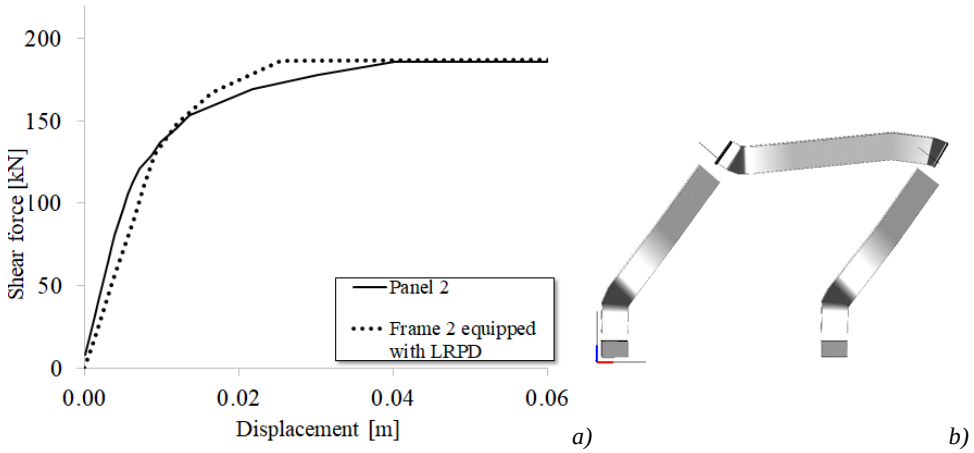

a) *b)*

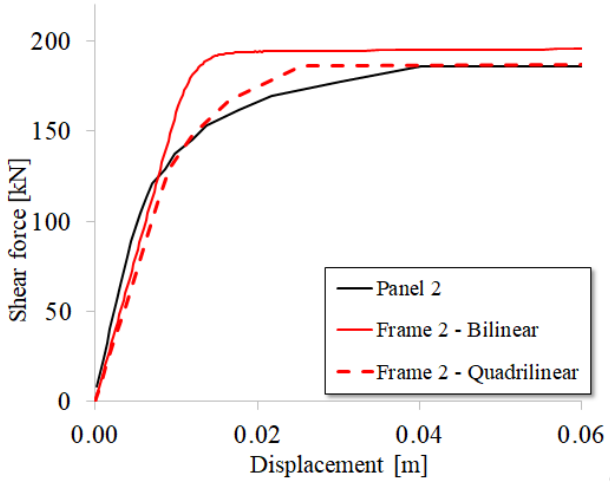

c)

Figure 4.35 – a) Frame 2 quadrilinear vs originale panel; b) deformed shape; c) comparison between quadrilinear and bilinear capacity curves.

From an examination of Figure 4.35 the improvement of the results obtained by activating the LRPDs at different force levels is evident, confirming the efficacy of the proposed approach and of the adoption the LRPDs.

As stated at the beginning of this section, the results obtained by the proposed approach have been compared with those acquired from a 3D FEM analysis in ABAQUS environment. An example of the frame analysed by FEM is sketched in Figure 4.36.

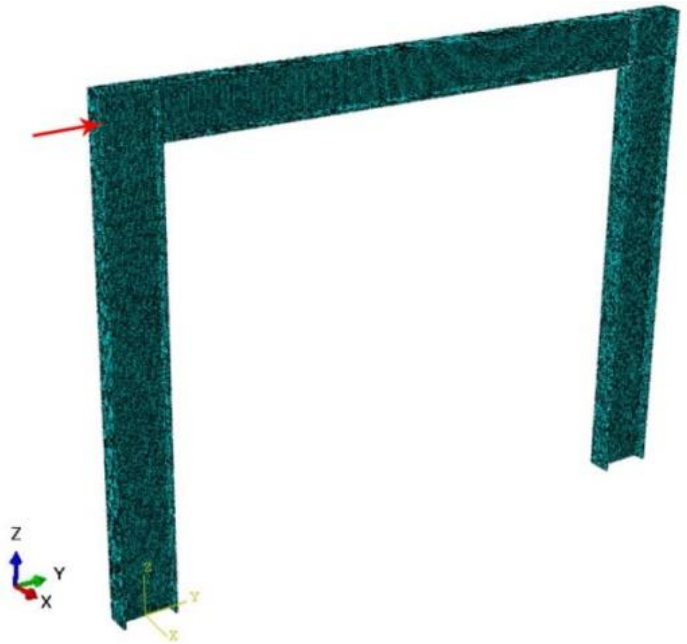

Figure 4.36 – Sample of frame modelled in Abaqus environment with mesh discretization.

The 3D FEM analysis has been performed in the case of frames equipped with the LRPDs and the results for Frame 1 are reported in Figure 4.37a and in Figure 4.37b for Frame 2. An examination of these figures confirms the results obtained by the proposed approach.

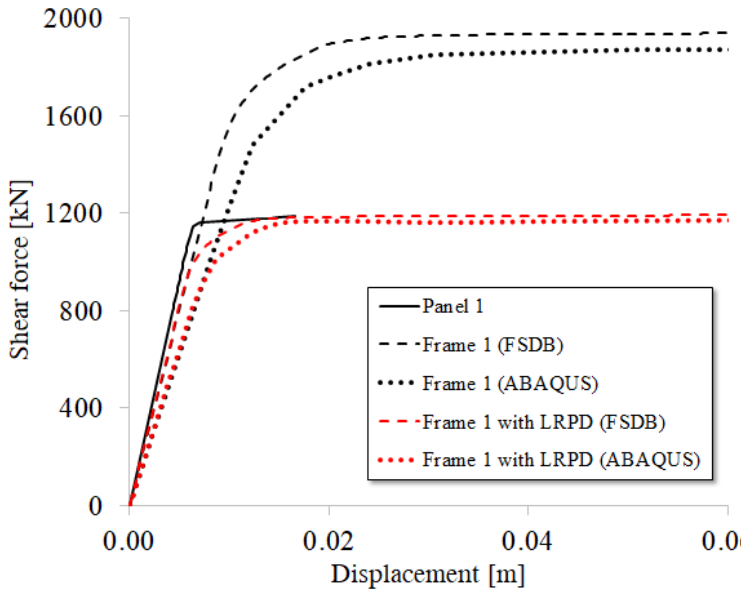

a)

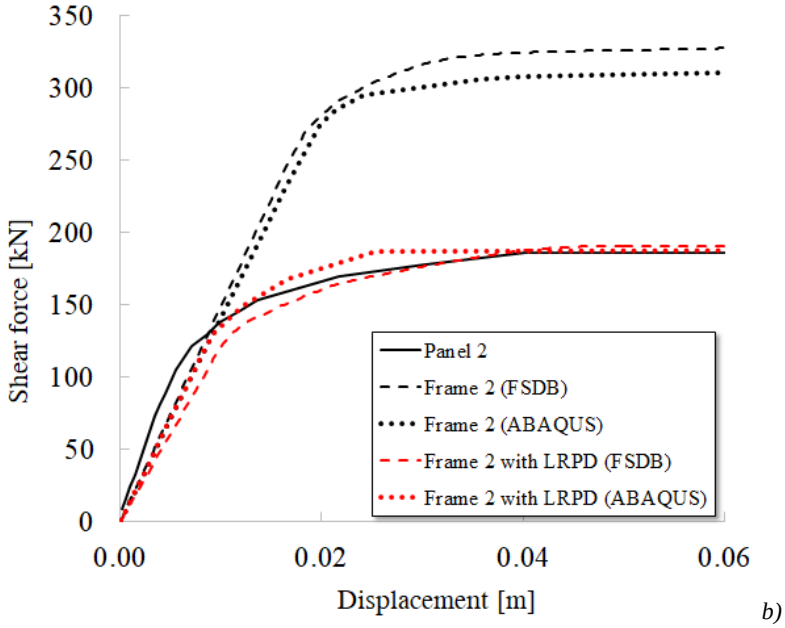

b)

Figure 4.37 – a) Panel 1 - Frame 1 benchmark; Panel 2 – Frame 2 benchmark.

4.4 - Aleatory domains

The manufacturing and assembling process of both the LRPD and the dogbone are intrinsically characterized by uncertainties. Considering the nature of the LRPD, the different uncertainties are related to the length of the portions, their thickness, their angle of assembly, among other factors. The dogbone is also subjected to analogous uncertainties, but the number of uncertain parameters is significantly lower due to the simpler manufacturing process. One source of uncertainty, for example, is the reduced base width, considering that even if it is realized by means of a cut of the wings performed through numerically controlled machine, still maintains an uncertainty due to the tolerance of the machine itself.

Moreover, the commercial steel profiles are influenced by production issues, and as mentioned their suppliers indicate tolerances and ranges of variation. Therefore the LRPD and the dogbone devices remain subjected to these uncertainties, along whit some others which may be caused by the manufacturing process.

Usually the technical codes prescribe the use of safety coefficients to account the uncertainties of the involved quantities. Of course this strategy leads to safer structures, but the cost is a slight overdimensioning of the structural elements. The proposed coefficients depend on the material adopted and on the manufacturing processes (sometimes performed directly on the construction site). In the perspective of utilizing the LRPD in practical applications in the following section the role of the uncertainties is presented.

In this section the discussion about the safety coefficient will differ from the common meaning of it. In detail, this coefficent can be imagined as an indicator of the difference between the strength of the end section of the beam compared to the reduced section of the RBS device, therefore the higher this coefficient the higher this difference.

In order to realize this comparison it is useful to present a numerical example, that can be taken as a qualitative indicator of the performance of the proposed device. This numerical example is based on the determination of the random variables, on the estimation of their stochastics characteristics and on the comparison of the relevant $N - M$ domains. These domains can be analytically determined through the model developed in Section 3.2, where the analytical equations and the theoretical analytical model are reported. The profiles chosen are a HEA300 and an IPE300, with the limiting plastic domains visible in Figure 4.42. The material is class S275 steel characterized by an elastic modulus $E = 210$ GPa.

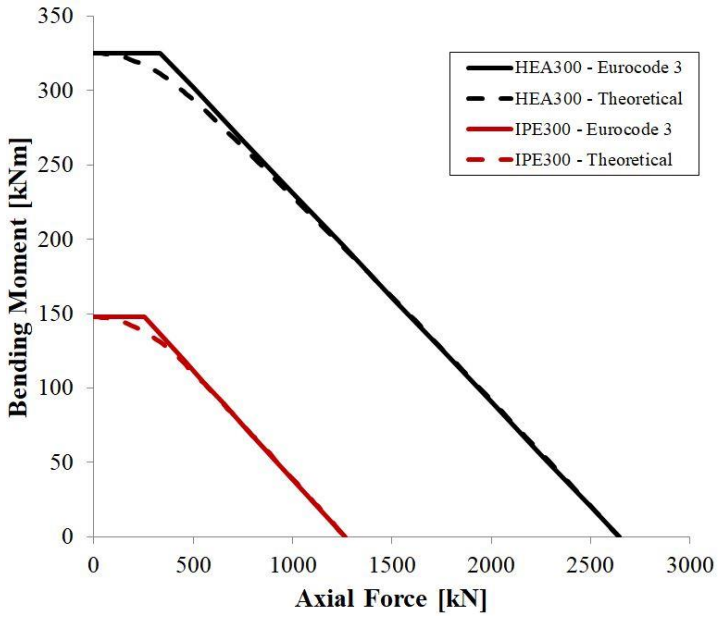

Figure 4.42 – Limit domains for HEA300 and IPE300:
code version (Eurocode 3) and theoretical (obatined by mean of the beam theory).

The mechanical behaviour of the I-shaped cross-sections is usually characterized by their $N - M$ domain. From a stochastic point of view the parameters involved are related to the material (the yield stress f_y) and to the

geometry (height h, width b, web thickness t_w, flange thickness t_f, welding radius r). These parameters can be listed in a vector as follows:

$$v^T = |h \quad b \quad t_f \quad t_w \quad r \quad f_y| \tag{51}$$

Eq. (51) can be applied to each case under examination (commercial, dogbone, LRPD). Considering the nature of the analysis presented in this section, these variables have to be looked at through their non-deterministic nature. To organize the different variables involved for the different configurations the variable vectors can be listed as follows:

$$\tilde{v}^{db} = |h \quad b_i \quad t_f \quad t_w \quad r \quad f_y| \tag{52a}$$

$$\tilde{v}^{0} = |h_0 \quad b \quad t_{f,0} \quad t_w \quad r_0 \quad f_y| \tag{52b}$$

$$\tilde{v}^{i} = |h_i \quad b \quad t_{f,i} \quad t_w \quad r_i \quad f_y| \tag{52c}$$

$$\tilde{v}^{p} = |h \quad b \quad t_{f,p} \quad t_{w,p} \quad r \quad f_y| \tag{52d}$$

The vector $\tilde{v}^{db}$ regards the dogbone variables. In detail Eq. (52b) and (52c), respectively, are related to the outer and to the inner cross-section of the LRPD. The last vector is (almost) equal to the one reported in Eq. (51) and is referred to the commercial steel profile which is used as a benchmark. The dogbone cited here is dimensioned similarly to the dogbone presented in section 4.2, where by setting an initial base reduction for the dogbone (in this case 0.6 of the initial width) the relevant LRPD with the same value of limit resistance was derived, thus $W_{pl,dogbone} = W_{pl,LRPD}$.

The quantification of the safety factor of the different strategies chosen, can not avoid the determination and characterization of the aleatory variables involved. To avoid overcomplicating the theory and the calculations, supporting this analysis, a normal probability distribution is used. This distribution can be fully described by defining only the standard deviation and the mean value of the aleatory variable. In addition, the different random variables will be considered to be statistically indipendent. Even if these two assumptions lead to a slight approximation of the complexity of the problem

this can be accepted considering what was stated at the beginning of this section, i.e. that the aim is to understand if the reliability grows or drops depending on the LRPD/dogbone equipped, not to investigate the non-deterministic aspects of the reduced beam section.

For each device the mean value considered is the deterministic tabular data for the commercial profiles. The variances are derived from international standards[23], and are reported in the following vector:

$$\tilde{\sigma}^2 = |0.09 \quad 0.09 \quad 0.04 \quad 0.01 \quad 0.64 \quad 0.01| \qquad (53)$$

A Monte Carlo simulation (10^6 samples) has been performed for each case under examination (for the LRPD the case of inner and outer portions have been treated separately), considering either IPE300 or HEA300 commercial profiles. The dogbone's base reduction was set to be 40%, and the LRPDs were consequently sized as presented in section 4.2 in order to recreate the same limit resistance.

The results of the simulations are sketched in Figures 4.43 and 4.44.

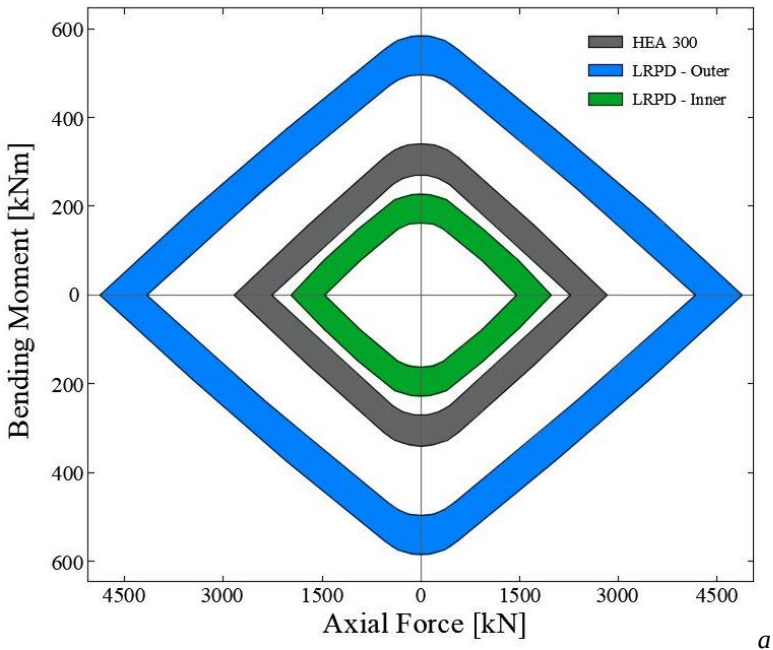

a)

[23] UNI EN 10365:2017, Hot rolled steel channels, I and H sections - Dimensions and masses.

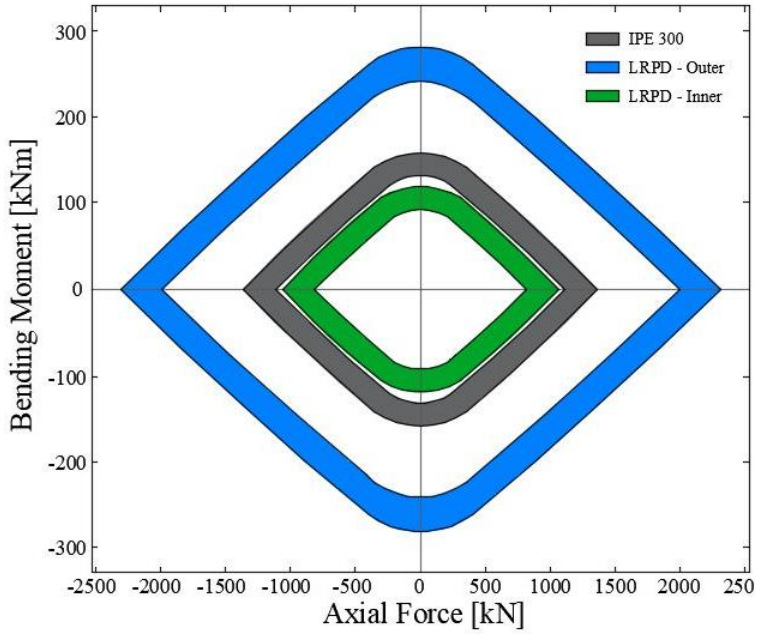

b)

Figure 4.43 – M-N domains comparison; a) HEA300 vs LRPD; b) IPE300 vs LRPD.

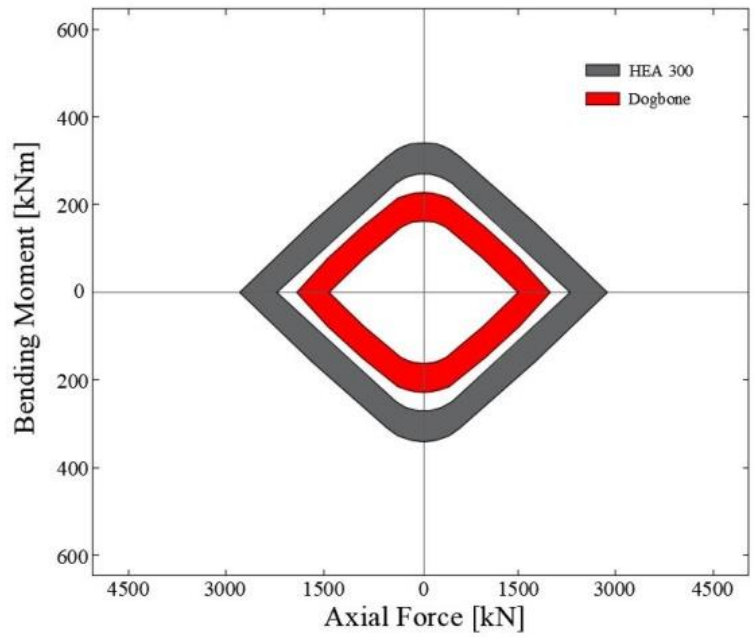

a)

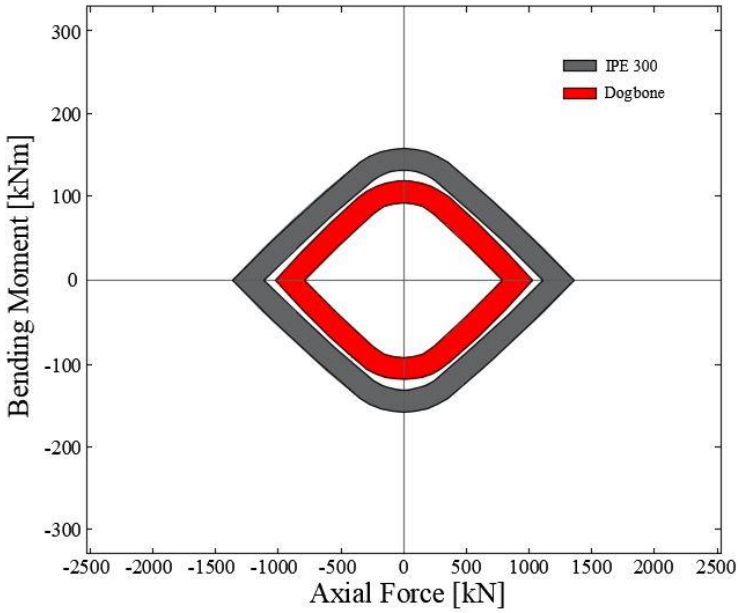

b)

Figure 4.44 – M-N domains comparison; a) HEA300 vs dogbone; b) IPE300 vs dogbone.

For simplicity's sake, in Figures 4.43 and 4.44 the region occupied by all the possible outcomes (normally represented by a cloud of points) is represented here by a homogeneous colour. The coloured regions represent the portion of the domain occupied by the possible values of the random variables.

An examination of Figure 4.43 immediately confirms that, as expected, the outer portion of the LRPD shows a mechanical behaviour which is greater than that of the inner portion which is also lower than that of the commercial profile. To define a safety coefficent χ it is possible to simplify by considering the lower distance between the fixed section and the reduced strength region. Hence, as visible in Figure 4.45a, for the LRPD this distance will be between the inner edge of the outer portion and the outer edge of the inner portion domains. In Figure 4.45b the analogous coefficient is defined in the case of a dogbone, assuming the distance as that between the commercial

profile and the reduced portion. In Figure 4.45a the green curve is almost perfectly overlapped with that of the dogbone.

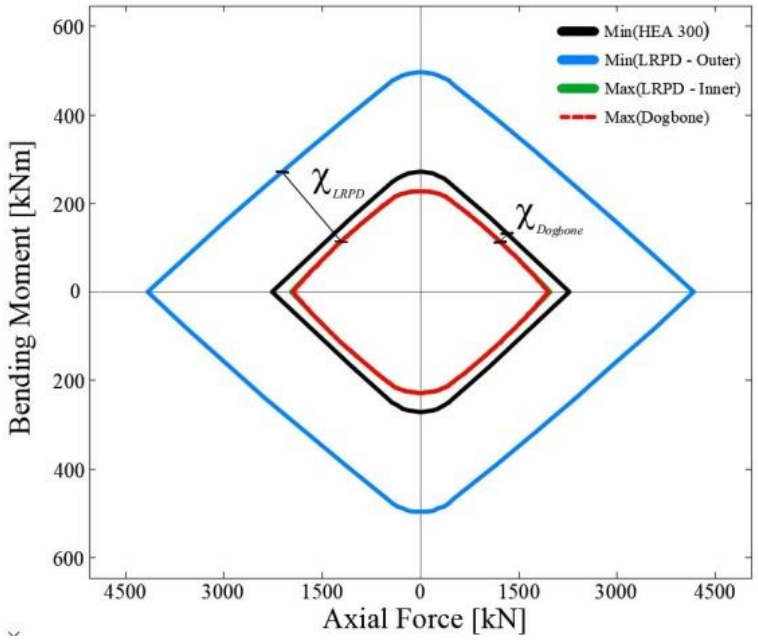

a)

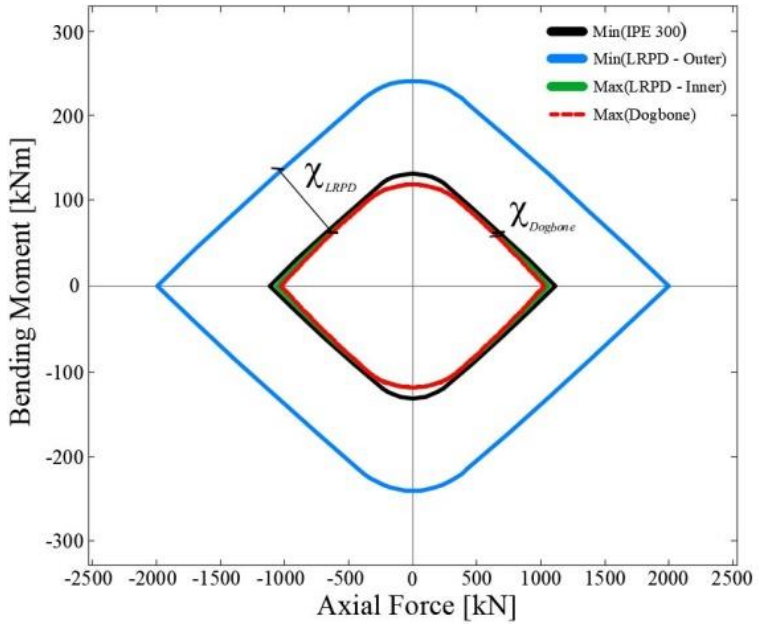

b)

Figure 4.45 – Safety coefficients comparison; a) HEA300-LRPD-Dogbone; b) IPE300-LRPD-Dogbone.

Finally, the purpose of this approach was to define a simple and clear safety coefficient that also takes into account the variability of some of the uncertain parameters of the manufactured hot rolled beam elements. Thanks to this parameter, it was also possible to compare the influence of this aspect for both the LRPD and the dogbone, determining that, at least in this aspect, the proposed device allows a greater margin of safety.

4.5 - Simplified optimization procedure

In section 3.4 the optimal design problem to find the best geometry configuration to assign the desired performances to the LRPD was discussed. However, the computational effort and the preliminary work required to define the problem can pose serious limitations to the utilization and the adoption of the device. One of these limitations regard the basic design usually accomplished in common practical engineering, that usually does not involve any optimization procedure unlike that described in Chapter 3. In addition, another limitation involves the huge variability of the input that is collected before approaching the proposed design procedure.

Therefore, the possibility to simplify the whole design process can be advantageous, even at the cost of an acceptable approximation of the results. To accomplish this goal, a series of simplificative assumptions will be proposed, using the optimization procedure as a starting point, leading to a simplified set of optimal solutions.

The starting design variables are reported in Eq. (32). The objective function to minimize (i.e. the volume of the device) can be written as follows:

$$V(d) = A_i \ell_i + 2A_o \ell_o =$$
$$= \left[2b_i t_{f,i} + t_w\left(h^* - t_{f,i}\right)\right]\ell_i + 2\left[2b_p t_{f,o} + t_w\left(h^* - t_{f,o}\right)\right]\ell_o =$$
$$= \left[2b_i t_{f,i} + t_w\left(h^* - t_{f,i}\right)\right]\beta h_p + \left[4b_p t_{f,o} + 2t_w\left(h^* - t_{f,o}\right)\right]\ell_o \qquad (54)$$

In Eq. (54) the relation $\ell_i = \beta h_p$ has been adopted and the welding's contribution has been neglected. It is useful to remember that the parameter β relates the cross-sectional height and the inner portion length, ensuring the minimum length useful to allow the correct onset of the plastic strains.

Considering that the flanges of the three portions possess a unique common medium plane, the relation $h^* + t_{f,o} = h_p$ can be written. Consequently, Eq. (54) becomes:

$$V(d) = \left[2b_i t_{f,i} + t_w\left(h_p - t_{f,o} - t_{f,i}\right)\right]\beta h_p + \\ +\left[4b_p t_{f,o} + 2t_w\left(h_p - 2t_{f,o}\right)\right]\ell_o \quad (55)$$

The function reported must be minimized respecting the constraints of the problem. As reported in section 3.4, the strength constraint used changes depending on the position of the neutral axis. If it cuts the flange, Eq. (31c) becomes an equality, permitting b_i to be written as a function of only $t_{f,i}$ by using the terms presented in Eq. 36, i.e.:

$$b_i = 18\, t_{f,i}\sqrt{\frac{235}{f_y}} + 3t_w \quad (56)$$

In this way, b_i can be removed from the design variables vector:

$$x^{\mathrm{T}} = |t_{f,o} \quad t_{f,i} \quad \ell_o| \quad (57)$$

In the other case, $t_{f,i}$ tends to t_p (becoming a fixed parameter) and b_i can remain an independent design variable. In this case, the design variable vector is:

$$x^{\mathrm{T}} = |b_i \quad t_{f,o} \quad \ell_o| \quad (58)$$

The two cases are differentiated by the value of the acting axial force N_a, that reflects on the positition of the neutral axis. For the first case N_a is given by:

$$N_a \geq t_w\left(h_p - 2t_{f,p}\right)f_y = \overline{N} \quad (59)$$

while for the second:

$$N_a < t_w\left(h_p - 2t_{f,p}\right)f_y = \overline{N} \quad (60)$$

By fulfilling the condition reported in Eq. (59) it is possible to write the limit condition of the cross-section related to the couple N_a and M_{a} as follows:

$$\frac{N_a}{2}\left[2t_{f,i} + \frac{t_w}{f(t_{f,i})}\left(h_p - t_{f,o} - t_{f,i}\right) - \frac{N_a}{2f(t_{f,i})f_y} - \left(h_p - t_{f,o} + t_{f,i}\right)\right] + \\ +f_y\left[f\left(t_{f,i}\right)t_{f,i} + \frac{t_w}{2}\left(h_p - t_{f,o} - t_{f,i}\right)\right] * \\ *\left[\left(h_p - t_{f,o} + t_{f,i}\right) - t_{f,i} - \frac{t_w\left(h_p - t_{f,o} - t_{f,i}\right)}{2f\left(t_{f,i}\right)}\right] = M_a \quad (61)$$

Eq. (59) represents the constraint reported in Eq. (40b) without considering b_i as a free design variable. Solving this equation, where $0 \leq t_{f,i} \leq t_f$ and $t_f \leq t_{f,o} \leq \frac{h_p}{2}$, it is possible to obtain the set of admissible values of $t_{f,i}$ and $t_{f,o}$.

On the contrary, when the level of axial force is in compliance with Eq. (60), Eq. (61) can be written as follows:

$$b_i t_f \left(h_p - t_{f,o}\right) + t_w \left(\frac{h_p - t_{f,o} - t_f}{2}\right)^2 = \frac{N_a^2}{4 t_w {f_y}^2} + \frac{M_a}{f_y} \tag{62}$$

As can be observed, the independent variables of the above equation are only b_i and $t_{f,o}$. If $t_f \leq t_{f,o} \leq \left(h_p - t_f - \frac{N_a}{t_w f_y}\right)$ and $3t_w \leq b_i \leq b_p$, Eq. (62) gives the admissible design values for b_i and $t_{f,o}$.

Moreover, depending on the equation adopted, whether the choice fell on Eq. (59) or Eq. (60), the remaining independent variable ℓ_o can be found from the volume function by writing:

$$\ell_o = \frac{\beta h_p \left[2 b_p t_{f,o}^3 + 6 b_p t_{f,o} \left(h_p - t_{f,o}\right)^2 + t_w \left(h_p - 2 t_{f,o}\right)^3\right]}{4 f\left(t_{f,i}\right) t_{f,i}^3 + 12 f\left(t_{f,i}\right) t_{f,i} \left(h_p - t_{f,o}\right)^2 + 2 t_w \left(h_p - t_{f,o} - t_{f,i}\right)^3}$$
$$\frac{12 I_p - 2 f\left(t_{f,i}\right) t_{f,i}^3 - 6 f\left(t_{f,i}\right) t_{f,i} \left(h_p - t_{f,o}\right)^2 - t_w \left(h_p - t_{f,o} - t_{f,i}\right)^3}{2 b_p\, t_{f,o}^3 + 6 b_p t_{f,o} \left(h_p - t_{f,o}\right)^2 + t_w \left(h_p - 2 t_{f,o}\right)^3 - 12 J_p} \tag{63}$$

$$\ell_o = \frac{\beta h_p \left[2 b_p t_{f,o}^3 + 6 b_p t_{f,o} \left(h_p - t_{f,o}\right)^2 + t_{w,p} \left(h_p - 2 t_{f,o}\right)^3\right]}{4 b_i t_{f,p}^3 + 12 b_i t_{f,p} \left(h_p - t_{f,o}\right)^2 + 2 t_{w,p} \left(h_p - t_{f,o} - t_{f,p}\right)^3}$$
$$\frac{12 I_p - 2 b_i t_{f,p}^3 - 6 b_i t_{f,p} \left(h_p - t_{f,o}\right)^2 - t_{w,p} \left(h_p - t_{f,o} - t_{f,p}\right)^3}{2 b_p t_{f,o}^3 + 6 b_p t_{f,o} \left(h_p - t_{f,o}\right)^2 + t_{w,p} \left(h_p - 2 t_{f,o}\right)^3 - 12 J_p} \tag{64}$$

The simplified procedure reported above allows a discrete set of sub-optimal solutions to be obtained, where the grade of precision can be chosen depending on the discretization level.

In order to provide a proof of the reliability of the simplified procedure a practical test is reported.

A common European profile HEB240 S235 steel grade has been chosen for this example. As discussed in section 3.4, the input data for the strength reduction depends upon the effective axial force N_a and bending moment M_a. Potentially, within the yield domain of the selected cross-section there are infinite couples of allowable values that can act as the input for the optimal problem. From a practical point of view it is reasonable to reduce the range of the strength reduction coefficient limiting its range between 0.5 and 0.9 with a resistance reduction from 10% to 50%. In Figure 4.46 the domain for the selected profile and the quadrant hereinafter under examination are reported.

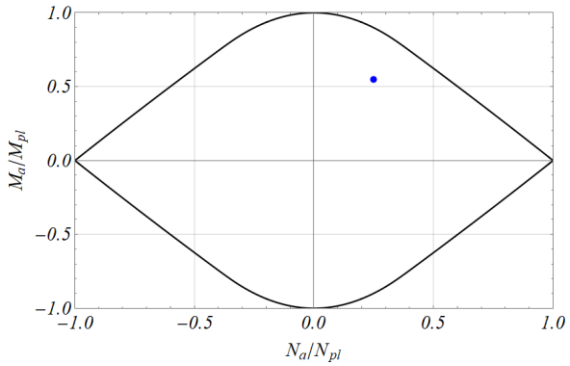

a)

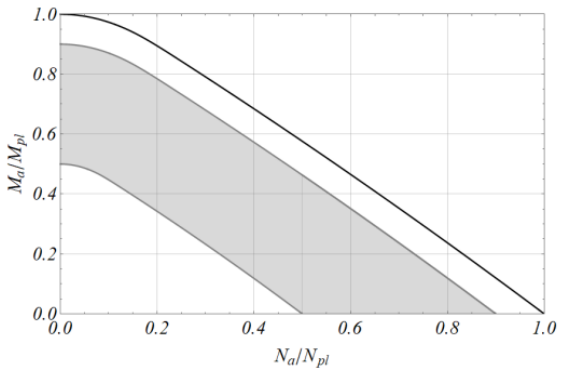

b)

Figure 4.46 - a) Example of possible N-M couple of values;
b) HEB240 focused portion of the dimensionless N-M domain (gray area).

Different levels of acting bending moment have been considered for the simplified procedure, but for the sake of brevity only two are reported: $M_a/M_{pl} = 0.2$ (with $0.35 \leq N_a/N_{pl} \leq 0.73$), and $M_a/M_{pl} = 0.8$ (with $0.00 \leq N_a/N_{pl} \leq 0.18$). For the HEB240 section the discriminating value for $\overline{N} = t_{w,p}(h_p - 2t_{f,p})f_y = = 10 \times (240 - 2 \times 17) \times 0.235 = 484.1$ kN, and the relevant ratio with the limit axial force $\overline{N}/N_{pl} = 484.1/2{,}491 = 0.194$. Therefore, in the case of $N_a/N_{pl} > 0.194$ it is possible to write Eq. (60) in terms of $t_{f,o}$:

$$t_{f,o} = \frac{A}{f_y\, t_{w,p}\left(t_{w,p} - 2f(t_{f,i})\right)} \tag{65}$$

Where A is:

$$A = t_{w,p}\left[-N_a + f_y t_{w,p}(h_p - t_{f,i})\right] + N_a f(t_{f,i}) + \tag{66}$$
$$-2f_y f(t_{f,i})\left[t_{w,p}(h_p - t_{f,i}) + t_{f,i} f(t_{f,i})\right] + \left[f(t_{f,i})\right]^{\frac{1}{2}}$$
$$\left\{-4f_y M_a t_{w,p}^2 + f(t_{f,i})\left[8f_y M_a t_{w,p} + \left(N_a + 2f_y t_{f,i} t_{w,p}\right)^2\right.\right.$$
$$\left.\left. + 4f_y t_{f,i} f(t_{f,i})\left(-N_a - 2f_y t_{f,i} t_{w,p} + f_y t_{f,i} f(t_{f,i})\right)\right]\right\}^{\frac{1}{2}}$$

Differently, for $N_a/N_{pl} < 0.194$ Eq. (61) can be written in terms of b_i:

$$b_i = \left[\frac{N_a^2}{4t_{w,p}{f_y}^2} + \frac{M_a}{f_y} - t_{w,p}\left(\frac{h_p - t_{f,o} - t_{f,p}}{2}\right)^2\right] / \left[t_{f,p}(h_p - t_{f,o})\right] \tag{67}$$

For each value assigned to b_i, $t_{f,o}$ and $t_{f,i}$ by using Eq. (54), Eq. (63) and Eq. (65), the relevant set of volume and ℓ_o values can be obtained. The precision and accuracy of the procedure depends on this discretization: the larger set of values is considered the most accurate and the most optimal the solution. In Figures 4.47 and 4.48 a comparison between the design variables obtained by means of the simplified sub-optimal procedure (black lines) and corresponding values obtained by the optimal procedure developed with MatLab's optimization tools (red dots) for the two values of the dimensionless bending moment are reported. The sub-optimal results

were obtained by discretizing the possible design variables in a set of 50 values.

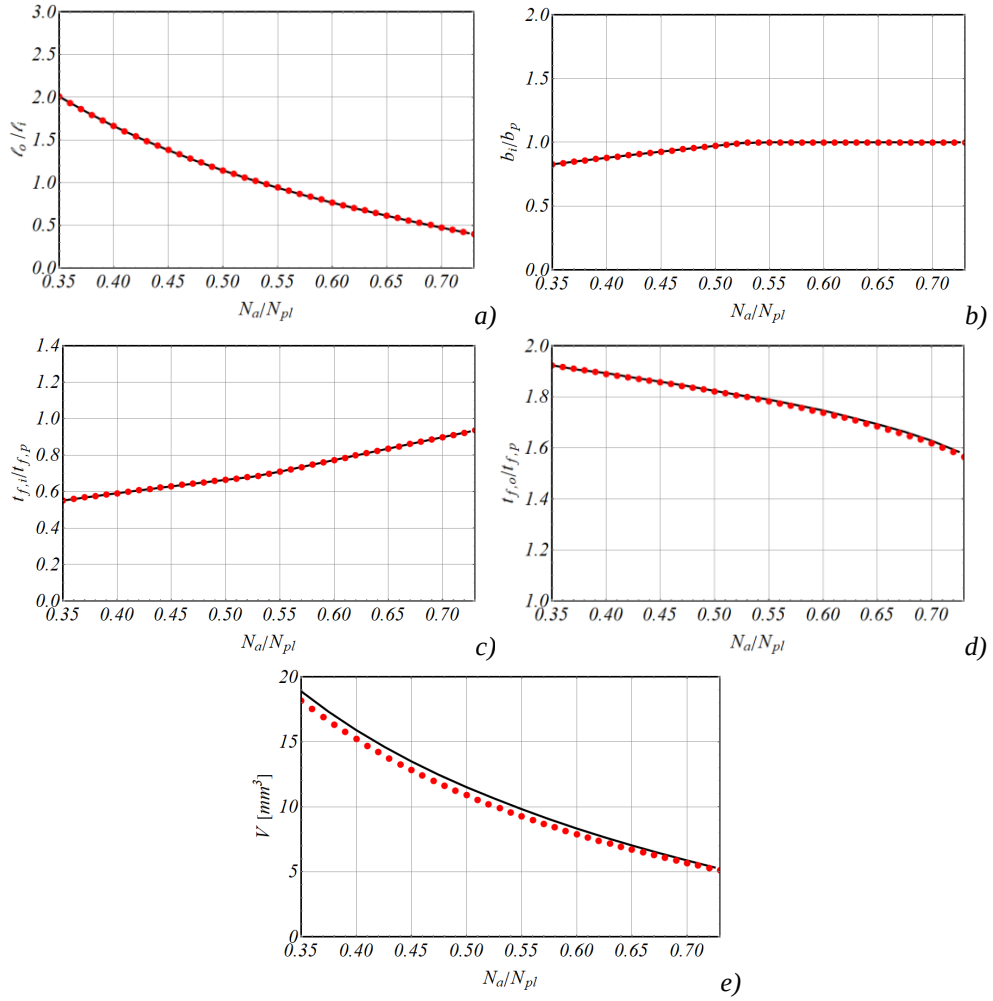

Figure 4.47 – Design variables obtained by the sub-optimal procedure (black) and the MatLab tool (red) for HEB240 and $M_a/M_{pl} = 0.2$. a) ℓ_o/ℓ_i ; b) b_i/b_p ; c) $t_{f,i}/t_{f,p}$; d) $t_{f,o}/t_{f,p}$; e) volume ($\times 10^6$).

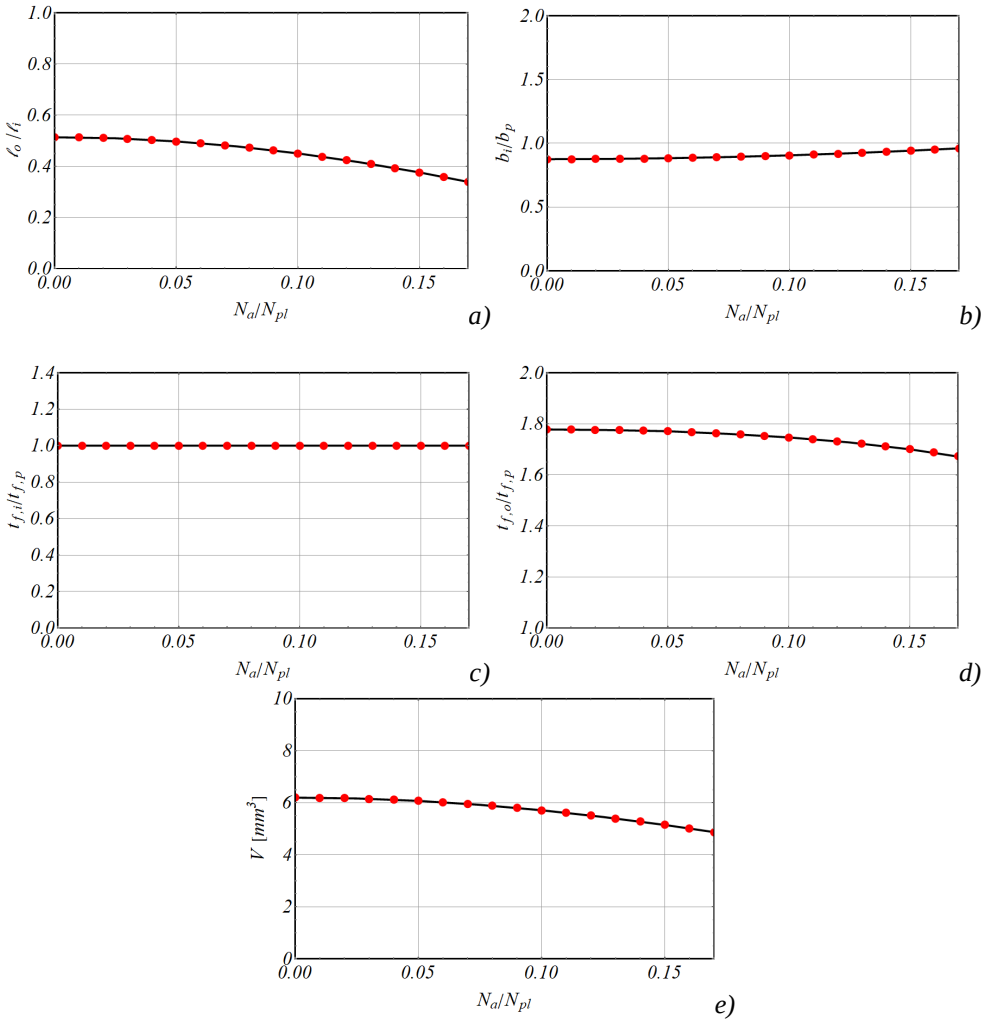

Figure 4.48 – Design variables obtained by the sub-optimal procedure (black) and the MatLab tool (red) for HEB240 and $M_a/M_{pl} = 0.8$. a) ℓ_o/ℓ_i ; b) b_i/b_p ; c) $t_{f,i}/t_{f,p}$; d) $t_{f,o}/t_{f,p}$; e) volume ($\times 10^6$).

An examination of these figures shows that the results of the sub-optimal procedure are almost coincident to those obtained in MatLab. While it is true that for the values of dimensionless bending moment, the volume obtained by the sub-optimal procedure is slightly greater than in the exact solution, however always leading to satisfactory results.

CHAPTER 5 – EXPERIMENTAL ACTIVITY

In the previous sections the LRPD has been described and the analytical formulation has been developed and discussed in detail. This allowed the device's efficacy and usability to be proven in different applications from a numerical point of view. To complete the validation procedure, however, a series of experimental investigations were performed to model the real behaviour of the device. This step is seen as mandatory as analytical results should be thoroughly validated by experimental means.

Therefore, thanks to the partnership with Tecnozinco s.r.l., which provided the samples to the structural engineering laboratory of the Department of Engineering of the University of Palermo, it was possible to design and to carry out the experimental activity that will be explained in this chapter.

As has been explained in the preceding sections, the LRPD is a device which aims to develop a flexural plastic hinge at a preselected bending moment. The experimental campaign, therefore, was focused on the bending behaviour of LRPD and, thus, a four-point bending test was performed. The first step involved the selection of a HEB240 cross-section in which $\alpha = M_u^{LRPD}/M_u^{HEB240} = 0.67$ has been fixed. The results of the optimal design are reported in Table XII.

Table XII – Sample geometry.

$t_{f,o}$	20 mm
$t_{f,i}$	16 mm
b_i	170 mm
ℓ_i	120 mm
ℓ_o	380 mm

To simplify the manufacturing process it has been decided to assemble the beam to be tested following the scheme sketched in Figure 5.1. As can be observed the sample is constituted of three different plates, two for the

flanges and one for the web, of constant thicknesses which were suitably welded together.

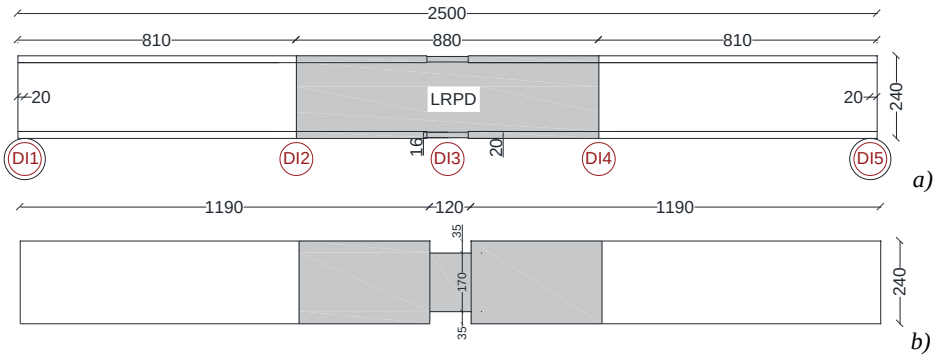

Figure 5.1 – Specimen under investigation with specification of the monitored cross-sections: a) lateral view; b) upper view.

In the same figure the selected cross-sections, where the displacement has been monitored are reported and indicated in red.

Initially, the mechanical properties of the material constituting the three flanges were identified by performing a standard tensile test (ISO 6892-1:2019) of the specimens extracted from the original plates. The results are reported in Table XIII and they show that the material has properties consistent with that of a S275 grade steel.

Table XIII – Material mechanical characterization.

Part	E [MPa]	f_y [MPa]	f_u [MPa]	A_g [%]	A_{gt} [MPa]
Web	208426	384.85	466.19	17.86	18.08
Flanges	231822	339.71	477.56	15.63	15.83

Once the mechanical and geometrical characteristics of the beam's material have been determined, the limit bending moment of the LRPD is derived, i.e. 241.8 kNm, corresponding to a total load equal to 612 kN. The setup is sketched in Figure 5.2.

Figure 5.2 – Experimental setup photograph.

The setup is composed of (starting from the top to the bottom):

- a CLF-1 class 1 AEP load cell (payload 1000 kN);
- a hydraulic jack (payload 1000 kN) driven by a ENERPAC pump;
- an AEP MP-10 digital indicator of the force level;
- a rigid beam (in blue) able to apply the acting force on the selected sections of the beam;
- two cylinders for distributing the force across the specimen's width;
- the specimen which is suitably instrumented to detect the forces and displacements;
- two rigid supports (painted green).

The displacements of the beam were monitored and collected using a Mitutoyo DIGIMATIC Digital indicator (with a 25 mm stroke), positioned at the location indicated in Figure 5.1a. The response of the sample was also characterized in terms of strain acting at the midspan of the cross-section, i.e. the inner portion of LRPD. The strain was registered by means of seven

different HBM K-CLY-41/120 strain gauges (6 mm length) distributed as sketched in Figure 5.3 and acquired by a HBM MGCPlus data acquisition system. All the outputs of the test were collected by means of a suitable virtual instrument developed in LabView 2020 environment.

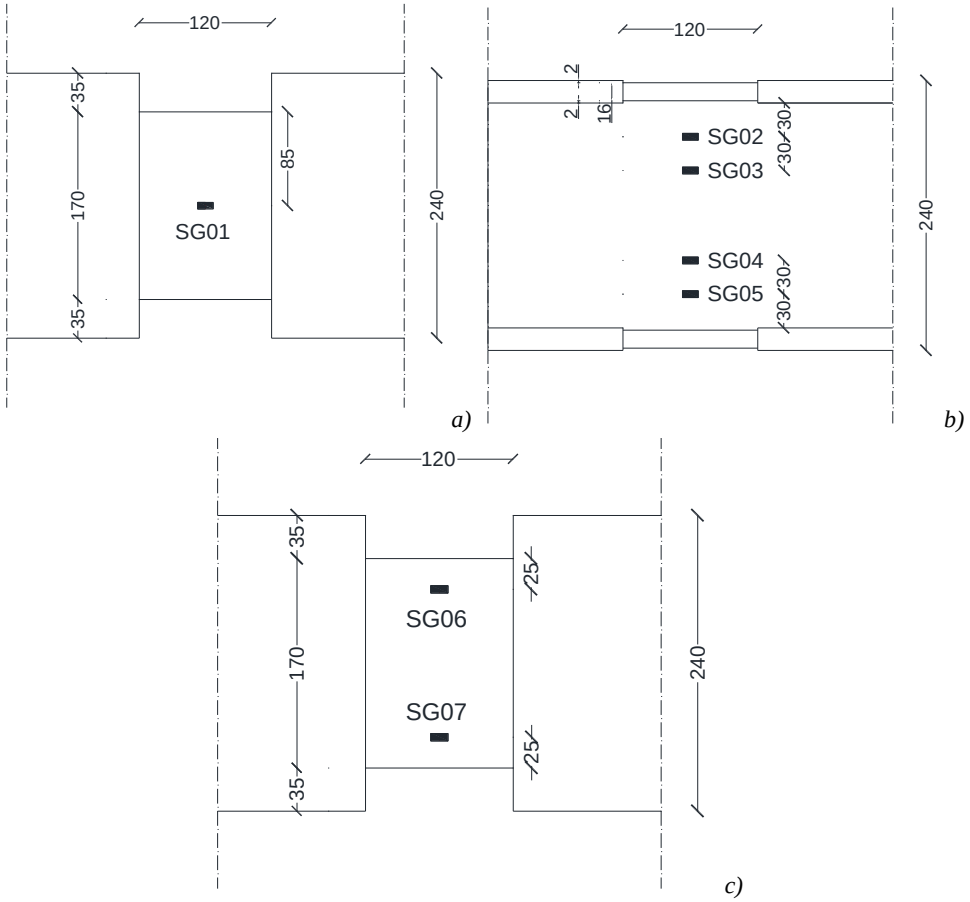

Figure 5.3 - Positioning of the strain gages: a) upper flange; b) web; c) lower flange.

The experimental results were compared with a suitable FEM model developed in ABAQUS environment. This FEM model is shown in Figure 5.4, and the modelling was conducted analogously to what discussed in Chapter 4.

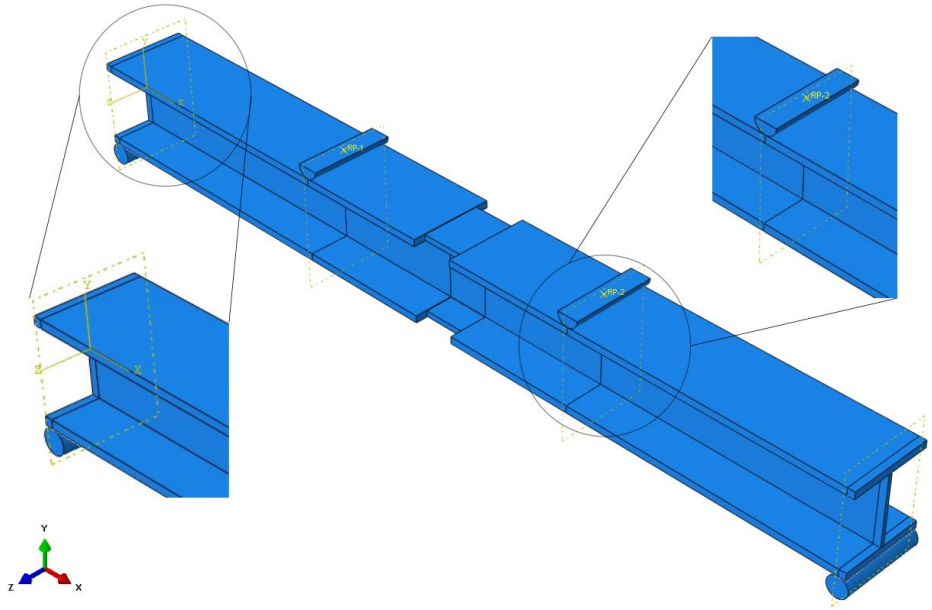

Figure 5.4 – FEM model of the setup sketched in Figure 50.

The model has been discretized with tetrahedral elements with a mesh size of maximum 4 mm. The mechanical characteristics of the material are reported in Table XIII assuming a perfectly elastic plastic model. The semi-cylinders and the supports were modelled as rigid and a friction coefficient of 0.125 has been assumed. The semi-cylinders are fully fixed (no degrees of freedom were allowed) and the beam is placed on them using Abaqus "hard contact" setting, which is simply the interaction between two surfaces that are allowed to relatively translate. The semi-cilinder of the upper part of the sample has been modelled analogously to the supports, and the load was applied on them through the definition of two reference points respectively.

The stresses σ_x acting on the selected measuring points have been obtained by the corresponding strains acquired during the testing of the Young's modulus of the material and sketched in Figure 5.5. The numerical stresses at the same points obtained by the FEM model are also reported in Figure 5.5. An examination of this figure shows that the experimental and numerical

results are in very good agreement confirming that the LRPD behaves as theoretically expected.

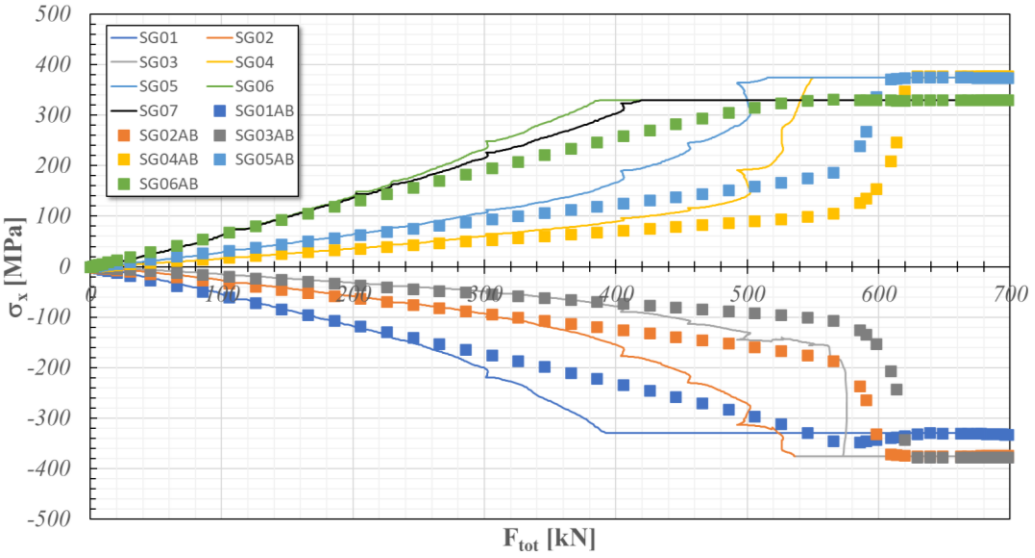

Figure 5.5 – Stresses vs. load; the dotted curves represent the Abaqus simulations output, while the continuous curves represent the experimental output obtained by the strain gages.

To complete the analysis of the experimental behaviour of the beam the relative displacement between the mid-span section and the boundary sections of LRPD has been defined as follows

$$\Delta_{LRPD} = v_3 - mean(v_2; v_4) \tag{68}$$

Where v_2, v_3 and v_4 are the vertical displacements of the monitoring points DI2, DI3 and DI4 shown in Figure 5.1. It is worth noting that the LRPD has been designed for a HEB240 profile and, therefore, it must behave elastically as a HEB240 beam of length equal to that of LRPD. In Figure 5.6 the experimental Δ_{LRPD} is reported and compared with the theoretical (obtained by simple elastic beam theory calculations) and numerical results. An examination of this figure confirms that the LRPD behaves kinematically as expected.

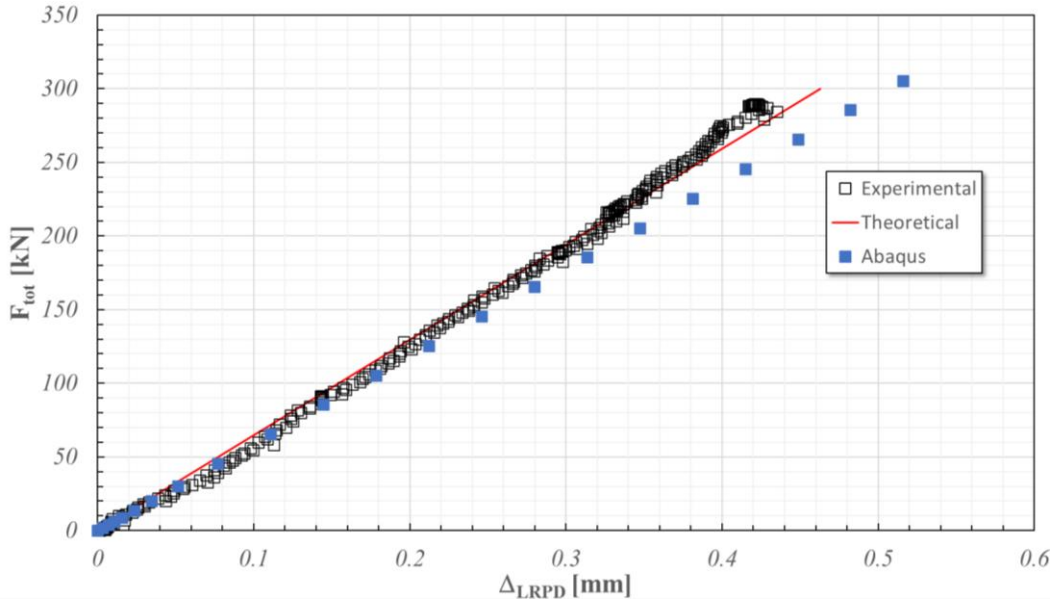

Figure 5.6 –Load vs. relative displacements.

CONCLUSIONS

This thesis focused on an innovative connection device for steel structures, covered by national and international patents to be adopted mainly in moment resisting frames. The device is named Limited Resistance Plastic Device (LRPD), and its features allow the possibility of independently setting its limit resistance and its flexural stiffness, thus allowing the full onset of plastic deformations along its internal portion.

Firstly, the range of applications in which the proposed device can be adopted was investigated. Particular attention was paid to the types of structure involved, and both the national and international codes which apply to these structures were considered. Furthermore, alternative devices to the LRPD were presented and briefly discussed, and comparisons have been performed to evaluate the reliability of the proposed device.

The LRPD was described and deeply discussed. Its geometrical and technological characteristics were clearly defined as was the design process. Then, the geometrical characteristics of the device were also presented using the optimal problem formulation. The optimization is based on a non-linear programming approach developed through the use of suitable geometrical and mechanical constraints and boundaries. These constraints can be linear, as is generally the case for geometrical purposes, or non-linear, when the mechanical and kinematical aspects are considered. These constraints must then be satisfied simultaneously while minimizing a suitably chosen objective function (usually the volume of the device). The LRPD was tested under the simplest conditions possible (e.g. investigating the rotational features with a constant bending moment) and then, also in practical conditions.

In this regard, the validity of the LRPD was investigated in multistorey and multispan moment resisting steel frames. By developing static and

dynamic analyses, and by collecting the response of different frames equipped with the LRPD, its feasibility was tested in real applications.

A very important topic presented in this thesis was the investigation of the possible role played in the reinforcement of masonry structures by means of steel frames equipped with an LRPD. This hypothesis regarded the complete substitution of a masonry panel with a suitably designed steel frame. The goal was to recreate the specific capacity curve of the substituted panel. The optimization problem was adapted to this special application by including new parameters and new assumptions in the dimensioning of the devices. This test demonstrated that, thanks to the contribution of the device, an assigned capacity curve can be recreated with a good approximation, thus obtaining the lateral stiffness restoration for the frame. Moreover the limit resistance of the frame was regulated by controlling its post-elastic phase.

In summary, it can be stated that:

- thanks to the numerical simulations the proposed device was shown to be highly reliable when subjected to a constant and linear bending moment;
- frames equipped with an LRPD can be suitably designed with an assigned capacity curve;
- the optimization problem was deeply investigated and improved;
- the experimental analyses provide a real scale application of the device, also confirming the reliability and the efficacy of the LRPD;
- the possibility to adopt a simplified procedure to design the device was provided, permitting reliable solutions to the optimization problem to be obtained, significantly simplifying the computational efforts and the complications associated with the design process.

The future developments of the work presented in this thesis can be listed as follows:

- the connection strategy between the LRPD and the other parts of the frame requires a deeper characterization and a standardization.;
- the torsional behaviour of the device should be studied in greater detail, since in practical applications and in tridimensional buildings its presence cannot be neglected;
- the dissipative behaviour of the device is another topic that would benefit from further studies considering its possible role as a disposable fuse.

REFERENCES

EN 1993-1-8:2006, Eurocode 3: Design of Steel Structures Part 1-8: Design of Joints, 2006.

Italian Ministry of Infrastructure and Transport, National Standard NTC 2018, DM 17/01/2018.

FEMA-350, Recommended Seismic Design Criteria for New Steel Moment-Frame Buildings, 2000.

ANSI/AISC 360-16, Specification for Structural Steel Buildings, 2016

D.K. Miller (1998), *Lessons learned from the Northridge earthquake*. Engineering Structures, 20 (4–6), 249-260.

E.P. Popov, T.S. Yang, S.P. Chang (1998), *Design of steel MRF connections before and after 1994 Northridge earthquake.* Engineering Structures, 20, 1030–1038.

A. Plumier (1997), *The dogbone: back to the future*. Engineering Journal, 34(2), 61-67.

N.R. Iwankiw, C.J. Carter (1996), *The dogbone: a new idea to chew on*. Mod. Steel Constr. 36 (4), 18-23.

J. Shen, T. Kitjasateanphun, W. Srivanich (2000). *Seismic performance of steel moment frames with reduced beam sections*. Engineering Structures; 22(8):968-83.

M.D. Engelhardt, T. Winneberger, A.J. Zekany, T.J. Potyray (1998). *Experimental investigation of dogbone moment connections*. Eng. J. 35, 128–139.

G. Dougka, D. Dimakogianni, I. Vayas (2014). *Innovative energy dissipation systems (FUSEIS 1-1) - Experimental analysis*. Journal of Constructional Steel Research, 96: 69-80.

G. Dougka, D. Dimakogianni, I. Vayas (2014). *Seismic behavior of frames with innovative energy dissipation systems (FUSEIS 1-1)*. Earthquake and Structures, 6(5), 561-580.

M. Valente, C.A. Castiglioni, A. Kanyilmaz (2017). *Numerical investigations of repairable dissipative bolted fuses for earthquake resistant composite steel frames*. Engineering Structures, 131, 275–292.

M. A. Morshedi, K. M. Dolatshahi, S. Maleki (2017). *Double reduced beam section connection*. Journal of Constructional Steel Research, 138, 283-297.

H. Farrokhi, F. Danesh, S.A. Eshghi (2009). *Modified moment resisting connection for ductile steel frames (numerical and experimental investigation)*, Journal of Constructional Steel Research, 65 (10–11) 2040–2049.

A. Atashzaban, I. Hajirasouliha, R. A. Jazany, M. Izadinia (2015). *Optimum drilled flange moment resisting connections for seismic regions*, Journal of Constructional Steel Research, 112, 325-338.

M. Morrison, D. Schweizer, T. Hassan (2015). *An innovative seismic performance enhancement technique for steel building moment resisting connections*. Journal of Constructional Steel Research, 109, 34-46.

S.R. Mirghaderi, T. Shahabeddin, A. Imanpour (2010). *Seismic performance of the accordion-web RBS connection.* Journal of Constructional Steel Research, 66, pp. 277-288.

A. Saleh, S.R. Mirghaderi, S.M. Zahrai (2016), *Cyclic testing of tubular web RBS connections in deep beams*. Journal of Constructional Steel Research, 117, 214–226.

L. Calado, J. M. Proenca, M. Espinha, C. A. Castiglioni (2013). *Hysteretic behaviour of dissipative bolted fuses for earthquake resistant steel frames*. Journal of Constructional Steel Research, 85, 151-162.

L. Calado, J. M. Proenca, M. Espinha, C. A. Castiglioni (2013). *Hysteretic behavior of dissipative welded fuses for earthquake resistant composite steel and concrete frames*. Steel and Composite Structures, Vol. 14, No. 6, 547-569.

B. Pantò, D. Rapicavoli, S. Caddemi, I. Caliò (2017). *A smart displacement based (SDB) beam element with distributed plasticity*, App. Math. Model., 44, 336-356.

B. Pantò, D. Rapicavoli, S. Caddemi, I. Caliò (2019). *A Fibre Smart Displacement Based (FSDB) beam element for the nonlinear analysis of reinforced concrete members*, International Journal of Non-Linear Mechanics, 117, 103222.

I. Caliò, M. Marletta, B. Pantò (2012). *A new discrete element model for the evaluation of the seismic behaviour of unreinforced masonry buildings*, Engineering Structures, 40, 327-338.

Benfratello, C. Cucchiara, L. Palizzolo, P. Tabbuso (2017). *Fixed strength and stiffness hinges for steel frames*. AIMETA 2017 – Proc. 23rd Conf. Italian Ass. Theor. Appl. Mech., 1, 1287-1296.

S. Benfratello, L. Palizzolo, P. Tabbuso (2019). *Optimal design of new steel connections*. EngOpt 2018 Proceedings of the 6th International Conference on Engineering Optimization, 644–656.

S. Benfratello, S. Caddemi, L. Palizzolo, B. Pantò, D. Rapicavoli, S. Vazzano (2020), *Smart beam element approach for LRPH device*, Lecture Notes in Mechanical Engineering, 197-213.

L. Palizzolo, S. Benfratello, P. Tabbuso, S. Vazzano (2019), *Numerical validation of LRPH behaviour by fem analysis*, Adv. Eng. Mat., Struct. Syst.: Inn., Mech. Appl. – Proc. 7th Int. Conf. Struct. Eng., Mech. Comp., 1224-1229.

S. Benfratello, S. Vazzano (2021). *On the limit behaviour of moment resisting connections under uncertainties*, OP Conf. Ser.: Mater. Sci. Eng., 1203 032081.

L. Palizzolo, S. Vazzano (2021). *Iterative optimal design of special moment resisting devices for steel frames*, OP Conf. Ser.: Mater. Sci. Eng., 1203 032079.

S. Benfratello, L. Palizzolo (2017). *Limited resistance rigid perfectly plastic hinges for steel frames*, Int. Rev. Civ. Eng., 8(6), 286-298.

S. Benfratello, L. Palizzolo, P. Tabbuso, S. Vazzano (2019). *On the post-elastic behaviour of LRPH connections*. Int. Rev. Mod. Sim., 12(6), 341-353.

S. Benfratello, L. Palizzolo, P. Tabbuso, S. Vazzano (2020). *LRPH device optimization for axial and shear stresses*. Int. Rev. Civ. Eng., 11(4).

S. Benfratello, S. Caddemi, L. Palizzolo, B. Pantò, D. Rapicavoli, S. Vazzano (2021). *Targeted steel frames by means of innovative moment resisting connections*. Journal of Constructional Steel Research, 183, 106695.

S. Benfratello, L. Palizzolo, S. Vazzano (2022). *A new design problem in the formulation of a special moment resisting connection device for preventing local buckling*, Applied Science, 12/202.

Hibbitt, Karlsson, and Sorensen (2010). “ABAQUS/Standard user’s manual”.

ACKNOWLEDGEMENTS

Gli anni di dottorato sono stati intensi e gratificanti. Innumerevoli persone hanno contribuito alla mia crescita personale e professionale in modi a me inaspettati e meravigliosi. Pertanto, a tutta l'Università degli Studi di Palermo, dagli studenti ai professori, dai tecnici agli amministrativi, dai preziosi colleghi ai vecchi e nuovi amici, sento di rivolgere la mia più profonda gratitudine e il mio più profondo affetto.

Alcuni, però, meritano una menzione e un ringraziamento particolare in virtù dell'importanza che hanno rivestito nel raggiungimento di questo importante e agognato traguardo.

Al Professore Palizzolo, che mi ha accolto con affetto e professionalità, e che mi ha guidato negli anni sempre con pazienza, dedizione e sapienza.

Al Professore Benfratello, che con la sua gentilezza, precisione e passione, è stato un perenne punto di riferimento nel percorso, disponibile e preciso fino alla fine.

Ai colleghi Chiara M., Marco, Silvia, Marianna, Emma, Nino, Maria, Salvatore P., Salvatore R., Chiara B., Dario. I momenti di svago e di pausa sono tra i più felici e belli che ricorderò. Grazie per l'affetto che mi avete donato.

A Pietro, Giorgia, Giulia, Francesco, Antonino, Giuliana, che con la loro simpatia e la loro intelligenza hanno rappresentato una piacevolissima compagnia nei lunghi e proficui periodi di studio.

Al team ERA di Monaco di Baviera, in particolare ad Antonis, i quali mi hanno accolto calorosamente fin dall'inizio nonostante il particolare periodo storico, e che insieme a Mirza, Jens, Denise, Antonio, Erica e Alessandro hanno riscaldato e reso speciale il freddo inverno della Baviera.

Alla Tecnozinco, e in particolare a Paolo e Antonino, grandi colleghi e lavoratori, che con la loro esperienza ed amicizia hanno contribuito ad arricchire il percorso.

A Erasmo, Gaetano, Giovanni e tutti gli altri tecnici e amici del laboratorio, per l'umana bellezza, per la loro disponibilità e per la loro instancabile operosità.

A tutti i nuovi amici e colleghi del Corpo Nazionale dei Vigili del Fuoco, in particolare a Marcello, Giovanni e agli altri 'appestati'. Per l'irruento affetto che ci lega e per essere, ed essere stati, porto sicuro personale e professionale.

Ai miei amici più sinceri. A Cristiana, Francesco, Luca, Antonio, Marianna, ai Fuorilogos. La vostra compagnia e amicizia è stata fonte di incalcolabili momenti felici, e hanno contribuito a rendere ciò possibile.

A Romina, che mi ha sempre accompagnato e che è sempre stata per me fidata compagna e consigliera. Non esistono parole adatte e sufficienti ad esprimere quanto sia grato di aver condiviso con lei parte del cammino.

Ai miei genitori, ai miei fratelli e al resto della mia famiglia. Hanno sempre fermamente e saldamente creduto in me (più di me), spronandomi e sostenendomi incondizionatamente con sacrificio e affetto. Senza di loro non sarei la persona che sono oggi. A loro, quindi, il più profondo e incondizionato ringraziamento.